UNIVERSITY OF NOTTINGHAM

INSTITUTE OF ENGINEERING SURVEYING
AND SPACE GEODESY

PRECISE ORBIT DETERMINATION
FOR GPS SATELLITES

by
Stephen Whalley, B.Eng.

Contents

i

iii

Abstract

The NAVSTAR Global Positioning System (GPS) has been under development by the US Department of Defense since 1973. Although GPS was developed for precise instantaneous position and velocity determination, it can be used for high precision relative positioning, with numerous applications for both surveyors and geodesists. The high resolution of the satellite's carrier phase has enabled relative positioning accuracies of the order of one part per million to be routinely obtained, from only one or two hours of data. These accuracies are obtained using the broadcast ephemeris, which is the orbit data that is broadcast in the satellite's radio transmission. However, the broadcast ephemeris is estimated to be in error by up to twenty five metres and this error is one of the principle limitations for precise relative positioning with GPS.

An alternative to the broadcast ephemeris, is to determine the satellite orbits using the carrier phase measurements, obtained from a network of GPS tracking stations. This thesis describes the algorithms and processing techniques used for the determination of GPS satellite orbits using double differenced carrier phase measurements. The data from three different GPS campaigns have been analysed, which demonstrate a GPS orbital accuracy of between two and four metres, giving baseline accuracies of the order of one or two parts in ten million.

Acknowledgements

This thesis represents the culmination of three years of research on orbit determination for the Global Positioning System satellites. The work was carried out with the support of the Director of the Institute of Engineering Surveying and Space Geodesy (IESSG), Professor V. Ashkenazi and the head of the Department of Civil Engineering, Professor P. Pell. The project was funded through a studentship given by Shell (UK) Exploration and Production.

The author would like to express his gratitude to his supervisor Professor V. Ashkenazi for his continual advise and encouragement and for the help from his joint supervisor Dr. A.H. Dodson throughout the research project.

The author would also like to thank all the members of the IESSG, in particular the help and advise given by Dr. T. Moore and Dr. C. Hill on all aspects of orbit determination and for the many fruitful discussions on the Global Positioning System, Mr. G.A. Basker, Dr. C. de la Fuente, Mr. G.H. Ffoulkes-Jones, Mr. P.J. Summerfield and Miss. J. Westrop.

Finally, the author would like to thank his parents for their support and encouragement throughout all his years spent at Nottingham University.

List of Figures

viii

List of Tables

xi

Chapter 1.
Introduction

CHAPTER 1

Introduction

Satellite geodesy is a science which uses measurements made to both natural and artificial satellites, for a variety of geodetic and geophysical applications. The first measurements made from an artificial satellite were those from Sputnik I, which was launched in 1957. The Doppler shift of the satellite's radio transmissions were measured and these were used in conjunction with the coordinates of the tracking station to determine the position of the satellite in its orbit. The reverse computation was also possible, whereby the coordinates of the satellite could be used with the doppler shift measurements to derive the coordinates of the tracking station. These discoveries led to the development of the United States (US) Navy Navigation Satellite (Transit), which was first launched in 1961. These navigation satellites are still in use today, but acquiring a position fix can take up to an hour. In the US armed services, there was a requirement for an instantaneous, high precision, worldwide positioning system.

The Global Positioning System (GPS) was developed to fulfill this role. The project was a result of previous research by the US Navy on the TIMA-TION program and the US Air Force 621B project, both of which were aimed at producing a passive radio-navigation system. Although GPS was primarily developed for the military, the system is currently freely available to civilian users. The system can be used to solve a variety of real time navigation problems on land, at sea and in the air, by the simultaneous measurement of *pseudoranges* from four or more satellites. For geodetic applications, the system can be used in a relative positioning mode, using measurements of the satellites *carrier frequency* to obtain much higher positioning accuracies.

1

Fundamental to both absolute and relative positioning with GPS, is a knowledge of the satellite's position at every measurement epoch. Generally, the *broadcast ephemeris* is used, which is computed by the US Department of Defense and is broadcast by each GPS satellite. Typically, this has been shown to give relative positioning accuracies of the order of one part per million. Clearly, the accuracy of the system has made a significant impact on both the surveying and geodetic communities, challenging the traditional terrestrial measuring techniques. However, certain applications require an even higher order of accuracy, for example, the monitoring of tectonic plate motions over continental sized networks requires an accuracy often exceeding one part in 10^7.

Two other space geodetic techniques are in use, which achieve this level of accuracy, Satellite Laser Ranging (SLR) and Very Long Baseline Interferometry (VLBI). SLR measures the range between a ground based laser telescope and a satellite using the return flight time of a short pulse of laser light. These ranges can be used in a dynamical analysis to determine the coordinates of the laser tracking stations and the coordinates of the satellite. Generally, the data is collected over a period of several days or even months from several sites, to produce the coordinates the tracking stations, accurate to within a few centimetres. VLBI uses two or more radio antennas, which measure the difference in arrival time of the signal wavefronts from extra galactic radio sources (such as quasars). Several radio sources are observed in a session and the measurements are used to obtain the baseline vector components between the radio antennas.

Whilst SLR and VLBI are highly precise measuring systems, they both require very large and expensive items of equipment, which are usually located at permanent tracking sites. Both SLR and VLBI have been developed into *mobile* systems, but these are still relatively immobile. However, with the advent of GPS, a highly mobile and inexpensive measurement system is available. In order to achieve accuracies comparable with SLR and VLBI, a thorough modelling of the GPS error sources is necessary. One of the principle limitations in determining long baselines with GPS, is the accuracy of

the broadcast ephemeris.

A more accurate satellite orbit can be determined using a dynamical method of analysis, where a force model is used to represent all the known forces acting upon the satellite. The numerical integration of this force (acceleration) model, twice with respect to time, will give the satellites position at discrete intervals in time (predicted orbit). The numerical integration is started from an initial position and velocity vector (state vector). Measurements made between a network of tracking stations and the GPS satellite can be used to improve this predicted orbit, by solving for corrections to the satellite state vector and to any required force model components, using a least squares method of adjustment. For GPS orbit determination, the coordinates of a number of the tracking stations are held fixed in the adjustment, to values determined from previous VLBI or SLR campaigns.

Precise GPS orbits are important not just for the determination of ground station coordinates, but they also have applications in satellite to satellite tracking. Low earth orbiting satellites require a particularly complex force model in comparison with the high altitude GPS satellites. Hence, the coordinates of a low earth satellite equipped with a GPS receiver, can be determined in a similar manner to those of a terrestrial GPS receiver, without the need to use a complex force model. In 1992, the US intend to launch the TOPEX/POSEIDON oceanographic satellite. This satellite carries a GPS receiver, with the intention of obtaining a ten centimetre orbital accuracy.

The basic concepts of the Global Positioning System and the processing techniques used for relative positioning are described in chapter 2 of this thesis. Chapter 3 describes the determination of GPS satellite orbits using the dynamical method of analysis. The software which has been used and developed for GPS satellite orbit determination is described in chapter 4. Three separate data sets have been analysed in this thesis, to test the GPS orbit determination procedure and to test the integrity of the programs. The first two data sets are based upon European networks and these are discussed in chapters 5 and 6. A *standard GPS data set* is being distributed by the Special Study Group 1.104 of the International Association of Geodesy and

3

this data set is analysed in chapter 7. The thesis is concluded in chapter 8.

Chapter 2.
The Global Positioning System : Overview and Processing Algorithms

CHAPTER 2

The Global Positioning System : Overview and Processing Algorithms

2.1 Introduction

The NAVSTAR (NAVigation Satellite Timing And Ranging) Global Positioning System (GPS) program started in 1973. The aim was to develop a system for highly precise position and velocity determination, and for the precise transfer of time. The system must also support an unlimited number of users, at any time, all over the world.

The program is managed by the Joint Program Office (JPO), combining the resources of United States, Department of Defense armed services. The JPO established three development phases.

- Phase I, which was the concept validation and development of the prototype Block I satellites.

- Phase II, the full scale engineering development, included the development of the Block II satellites, and the testing of prototype satellite receivers.

- Phase III is the production and deployment of the operational system. The program has just entered Phase III with the launch of the first Block II satellite in February 1989.

During the 1990s, the Navy Navigation Satellite (TRANSIT) will be phased out for both the civilian and military users and reliance will be placed upon the use of GPS for navigation and positioning. Other ground based radio-navigation systems will be superseded by GPS for the military users

5

by the mid 1990s, but civilian usage will be permitted until the end of the century.

The GPS description can be divided into three segments, called the Space, Control and User Segments.

2.1.1 Space Segment

When GPS is fully operational, the space segment will consist of 18 Block II satellites (with three orbital spares), placed in six equally spaced orbital planes. The orbital planes will have an inclination of 55°, with adjacent planes offset by 40° in argument of latitude. The satellites have a nominal altitude of 20183 km, with a period of 11 hours and 58 minutes. It is this configuration that will enable the user to track a minimum of four satellites, for real time positioning, anywhere in the world. However, some areas may experience several minutes of degraded accuracy, when poor satellite geometry occurs(Section 2.3.4). In addition to these 21 satellites, a further seven satellites will be maintained on the ground in case of satellite malfunctions.

Each Block II satellite, produced by Rockwell International Incorporated, will contain two rubidium and two caesium beam atomic clocks. The clocks are powered by an array of solar panels, with batteries to power the satellite when it is eclipsed by the earth. The proposed launch schedule for the rest of the Block II satellites is given in table (2.1).

Currently, there are seven research and development Block I satellites, placed in two orbital planes, at an inclination of 63° . This configuration was designed to maximise the daily coverage over the Army Proving Grounds in Yuma, Arizona. In Europe, four satellite coverage is provided for approximately four hours each day.

The atomic clocks contained in the satellites, oscillate at a fundamental frequency of 10.23 MHz. It is from this frequency, that all components of the satellite signal are generated.

Satellite Signal

The satellite signals are transmitted on two L band carrier frequencies of 1575.42 MHz (L1) and 1227.60 MHz (L2). The L1 carrier frequency is mod-

ulated with two mutually orthogonal, pseudo-random noise (PRN) codes, called the C/A (Coarse/Acquisition) code and the P (Precise) code. The L2 carrier frequency is modulated with the P code only.

The PRN codes are formed with a sequence of the binary digits, 0 and 1, which are generated mathematically, using a specified algorithm. The C/A code is a one milli second long sequence and it is modulated onto the carrier at a chipping rate of 1.023 MHz. The P code is a 267 day long binary sequence, with a chipping rate of 10.23 MHz. Each satellite uses a unique, week long section of the P code. The satellites may be identified by the particular seven day section of the P code that they are using. This is referred to as the satellite PRN number. The current Block I satellites are designated PRN numbers 3, 6, 8, 9, 11, 12 and 13.

The PRN code is modulated onto the carrier frequency using binary biphase modulations. These simply multiply the phase by +1 for the binary state 0, and -1 for the binary state 1. Hence a change in binary state, will lead to a 180° change in phase (figure 2.1).

In addition to these codes, both the carrier frequencies are modulated with a satellite data message, at a rate of 50 bits per second. The message is 1500 bits long and is divided into five subframes. It is modulated onto both the C/A and P codes and lasts for 30 seconds.

Subframe 1 contains the satellite clock correction parameters and timing information.

Subframes 2 and 3 contain the broadcast ephemeris, using a Keplerian type representation (section 3.2). Six of these parameters describe a mean orbital ellipse, with nine correction terms to allow for deviations from this mean orbit. The ephemeris is computed in an earth-fixed earth-centered reference system and it is valid for a period of one and a half hours from a given reference time. The Keplerian representation has the advantage that the ephemeris will degrade gracefully with time after this period.

Subframe 4 contains coefficients to estimate the ionospheric delay for single frequency receivers (section 2.5.2). A data message (OPSCAP), containing information from the control segment, is to be implemented at a later

7

carrier frequency

modulations

modulated carrier
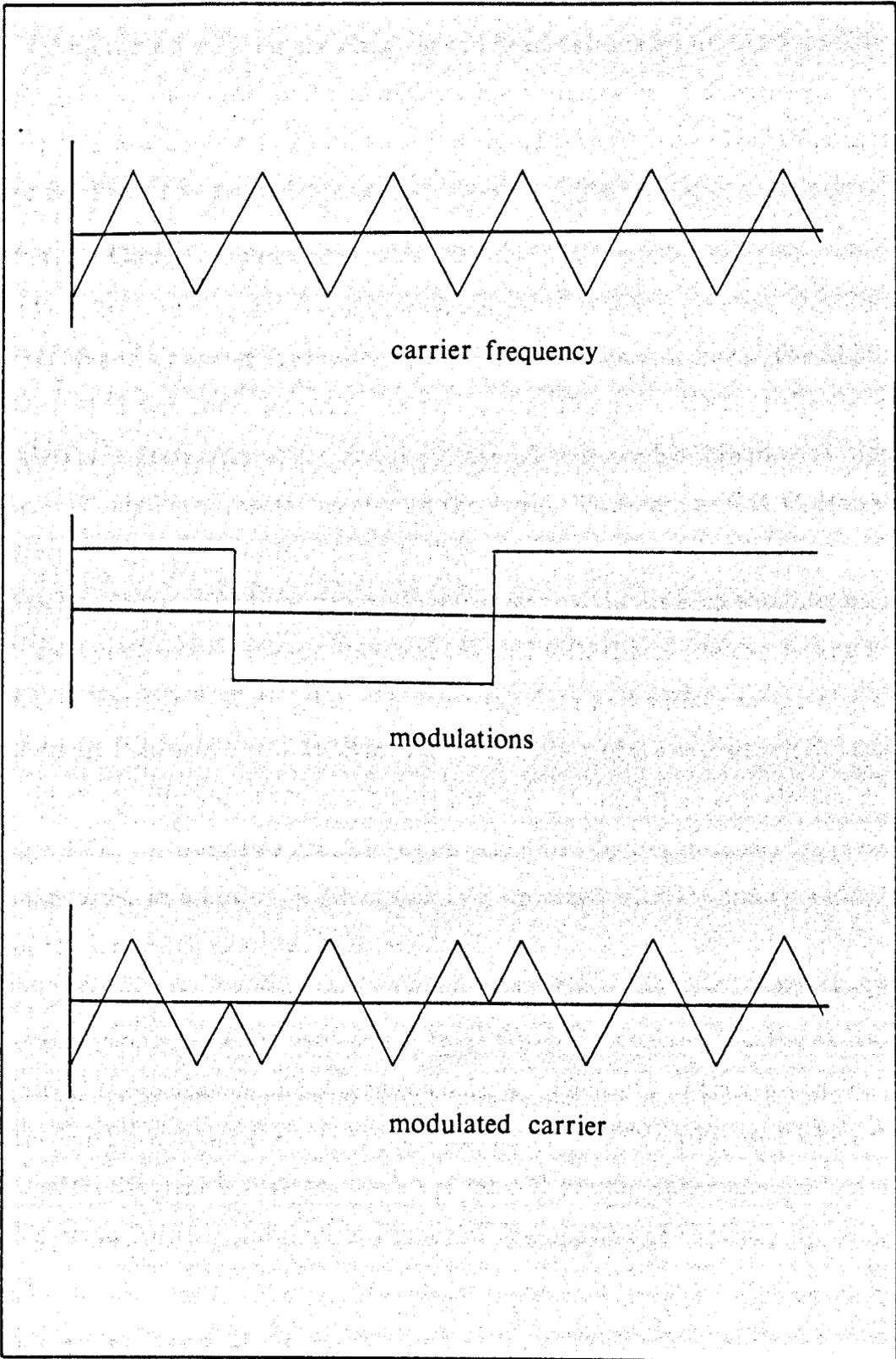
Figure 2.1: Binary code modulations

date [Barber, 1989].

Subframe 5 contains the almanac and health status for up to 25 satellites. Each subframe contains the almanac (approximate orbit description) and health status for one satellite. Hence, it would take twelve and a half minutes to acquire a complete almanac.

2.1.2 Control Segment

The fully operational Control Segment consists of a Master Control Station (MCS) and a number of Monitor Stations and Ground Antennas. The MCS is located at the Consolidated Space Operations Centre (CSOC) at the Falcon Air Force Station, near Colorado Springs. There are five Monitor Stations at precisely known locations around the world. These are at CSOC, Hawaii, Kwajalein, Ascension Islands and Diego Garcia (Figure 2.2).

The Monitor Stations record dual frequency data for each satellite, using a caesium beam frequency standard. Each Block II satellite can be tracked for at least 90 % of its orbit. The tracking data and surface meteorological data are then sent to the MCS for the computation of the satellite clock biases and the prediction of the satellite ephemeris. Precise time is maintained at the MCS by using two caesium beam and three hydrogen maser frequency standards. In addition, a direct link is maintained with the time standards, of the United States Naval Observatory.

The broadcast ephemeris, satellite clock corrections and satellite health information are then relayed to the three Ground Antennas, located at Kwajalein, Diego Garcia and Ascension Island. The data is then uploaded to the satellites on an eight hourly cycle. To allow GPS to be used when the Control Segment is disabled, each upload will contain ephemeris predictions for up to fourteen days, with a graceful degradation of accuracy up to 200 m.

2.1.3 User Segment

The User Segment covers all the receivers, that are capable of processing the GPS satellite signals. The receiver passively tracks the signal, which allows the system to support an unlimited number of users. The receiver type

9

will be determined by the user's requirements, taking into account the size, weight, durability and the level of processing required. For navigation, the receiver must be capable of determining real time positions, using pseudo-range measurements on the P or C/A codes. For geodetic work, the receiver must be able to measure and store... the carrier phase and store the data for post processing.

The position obtained will be made relative to a standard referencing surface by the receiver... for a civilian user... The GPS is based upon the dual frequency P code... code available to authorized military users. The GPS... the single frequency C/A code... will be made available to the civilian user...

For real time positioning the accuracy of the fix is 16 metres (m)... and 76 metres (m) for SPS. The... is the spherical error... to the point in space where 50% of all position fixes... metres, can be obtained by using the P... code, to determine... accuracy... [Wells and Blanchard, 1982]...

For relative positioning, a higher order of accuracy can be achieved... the measurements are made on the satellite carrier frequency. The... fix can be performed... using the algorithms described in section [2.3]... The relative determination... would lead to accuracies better than one part per million...

... for Geodetic Surveys

... one can obtain the coordinates... the most common...

Figure 2.2: DMA Operational tracking network

will be determined by the user's requirements, taking into account the size, weight, durability and the level of processing required. For navigation, the receiver must be capable of determining real time positions, using *pseudorange* measurements on the P or C/A codes. For geodetic work, the receiver must be able to measure and time tag the carrier phase and store the data for post processing.

Two positioning services will be made available, the Standard Positioning Service (SPS) and the Precise Positioning Service (PPS). The PPS is based upon the dual frequency P code and will only be made available to authorised military users. The SPS uses the single frequency C/A code and will be made available to the civilian user.

For real time positioning the accuracy of the PPS is 16 metres (m) SEP and 76.3 m SEP for the SPS. The SEP is the spherical error probable, defined as the radius of a sphere, which contains 50% of all position fixes. Higher accuracies may be obtained by using GPS in the differential mode, to determine coordinate differences from a known receiver position [Blanchard, 1989].

For relative geodetic positioning, a higher order of accuracy can be achieved by making measurements on the satellite's carrier frequency. This data can be post processed, using the algorithms described in section (2.4). Processing data in this way can yield baseline accuracies better than one part per million.

Signal Acquisition for Geodetic Receivers

The receiver can obtain the satellite signals in different ways, the most commonly used method is called code correlation.

A code correlation receiver must be able to generate a replica C/A code from its internal oscillator. The incoming satellite code is then electronically aligned with the replica code, by shifting this replica code in time. This time shift is termed the pseudorange, and it represents the signal propagation time , biased by the satellite and receiver clock errors.

The C/A code can then be removed from the carrier by mixing it with the replica code. The satellite data message can now be accessed, which

contains the broadcast ephemeris and satellite clock correction parameters. A handover word (HOW) is also contained within the message, which allows the receiver to generate the correct portion of the week long P code.

The P code can now be accessed in the same way as the C/A code, providing the receiver has knowledge of the P code formulation.

The TI 4100 NAVSTAR NAVIGATOR is an example of a code correlating receiver. It is capable of obtaining pseudorange measurements on both the C/A and P codes and can record the L1 and L2 frequency carrier phase observables for up to four satellites. The receiver is designed for both real time navigation work and for precise geodetic relative positioning. Data can be recorded on a dual cassette recorder, with each cassette storing about thirty minutes of data, if a three second measurement interval is selected. Alternatively, a personal computer can be used to record data onto three and a half inch floppy discs. The dual frequency capability of the receiver has meant its extensive use, particularly for the measurement of long baselines, where the two frequencies are used to eliminate the effects of the ionosphere (section 2.5.2). All the data described in this thesis was recorded using TI 4000 receivers.

Some receivers do not use the C/A or P code to access the carrier frequency. One receiver of this type, the Macrometer [Ashkenazi, 1987], demodulates the carrier by using a squaring technique. The -1 and + 1 modulation will be removed, leaving a carrier at twice the original frequency. A disadvantage of this technique is the removal of both the PRN codes and the satellite data message. This type of receiver will then require an external ephemeris, making real time positioning very impractical.

There are many commercially available receivers, capable of recording both the carrier phase and the code data, details can be found in other texts [Wells, 1986].

2.2 Future Prospects for GPS

Originally it was intended to place the Block II satellites in orbit, by using the Space Shuttle. Unfortunately, with the Challenger disaster in 1986, a

new launch plan was required. Now, all the Block II satellites are to be launched from the expendable Delta II, Medium Launch Vehicles (MLV). This has necessitated the redesign of some satellites to allow for the MLV launch, and the revised launch schedule is given in table (2.1).

The first Block II satellite was launched on the 14th of February 1989. It's orbital position was designed to cover a gap in the observing window, over the Yuma Proving Ground, Arizona. The three launches proposed for later this year are designed to optimise worldwide two dimensional coverage.

It is intended to augment the 18 satellite constellation by using the 3 on-orbit spares as active satellites. This optimised 21 satellite coverage would reduce the areas in the world, where the poor satellite geometry adversely affects the positioning accuracy of GPS. These occurrences are called outages. Also, approval was given to increase this constellation to 24 satellites, but this is not envisaged until the mid 1990s.

It was realised by the Department of Defense that uncontrolled access to the GPS signals may compromise national security. To alleviate this, it has been proposed to degrade the potential accuracy of the system by two methods.

Selective Availability (SA) would be used to deny access to the Precise Positioning Service (PPS). This would be implemented by altering the satellite data message (epsilon) or by manipulating the satellite clock (dither). Full system accuracy could be obtained from encrypted corrections given in the data message. The SA would be applied to all Block II satellites, as soon as they are declared operational.

The second proposal, *Anti-Spoofing* (A-S), would be the use of a new unpublished P code, called a Y code, which is only available to users with the proper cryptography. This would protect against hostile imitations of the PPS signal.

There is much speculation in the civilian sector as to the effect of SA, but it is hoped that the carrier phase data used for geodetic applications will not be significantly affected.

Number to launch	Period	Comments
4	1989	PRN 14 Launched on February 14th
5	1990	
5	1991	2 Dimensional capability
5	1992	
4	1993	3 Dimensional capability
2	1994	Spare satellites
	1995	20 Block IIR (replenishment) satellites to be deployed

Table 2.1: Proposed Block II launch schedule

2.3 Point Positioning

2.3.1 Introduction

The concept of point positioning, using GPS satellites, is based upon the measurement of range, between receiver and satellite. If the ranges to three satellites of known coordinates can be measured, then the receiver coordinates can be determined. This assumes that the receiver and satellites do not lie in the same plane. The basic GPS range observable, the pseudorange, is proportional to the signal transmission time, between the satellite and receiver. Therefore for precise positioning, it is essential to use a stable time scale, to which all measurements can be referenced. The time scale adopted for GPS is known as GPS System Time.

2.3.2 GPS System Time

The astronomical time scales (UT) would be unsuitable for GPS because of the daily variations in the earth's rotation rate. For GPS it is necessary to use a linear time scale.

One of the most stable time scales in the world, is the Universal Time Coordinated (UTC), determined by the United States Naval Observatory (USNO). This is a constant atomic time scale, based upon 25 different caesium beam frequency standards. UTC(USNO) is corrected by discrete leap second jumps to keep it close to the astronomical time scale UT1. The GPS System Time maintained by the Master Control Station, is physically kept within one microsecond of UTC (USNO). However, the leap second adjustments made to UTC (USNO) would disrupt the continuous navigational capacity of GPS and are consequently not applied. GPS System time is currently (April 1989) running five seconds ahead of UTC (USNO).

GPS System Time is measured modulo 604800 seconds starting from Saturday night/Sunday morning each week. Each week increment is counted in GPS weeks, from midnight 5/6 January 1980.

A series of polynomial coefficients are broadcast in the navigation message, giving the offset between UTC(USNO) and GPS System Time, to within 100 nanoseconds. In addition, a further set of coefficients are pro-

vided, to calculate the offset of the satellite clock from GPS System Time.

2.3.3   The Pseudorange Solution

The range between the GPS satellite and the receiver is measured by scaling the signal propagation time by the speed of light. To establish the true propagation time, the satellite and receiver clock offsets must be determined. The satellite clock offset is contained within the navigation message, given by the three terms a_0, a_1 and a_2. These represent the coefficients of a second order polynomial.

The receiver clock offset is unpredictable and must be determined as part of the pseudorange solution. Assuming the measurements contain no other error sources, the pseudorange can be expressed as

$$PR = \rho/c + (\Delta T_s - \Delta T_A) \qquad (2.1)$$

Where

PR = pseudorange measurement (s)

ρ = geometrical satellite to receiver range (m)

c = speed of light (m/s)

ΔT_s = satellite clock offset (s)

ΔT_A = receiver clock offset (s)

The earth's atmosphere will cause the satellite signal to bend and slow down, delaying its arrival at the receiver. The ionosphere and the troposphere will both cause significant, but different delays. These effects can be estimated and different models are considered in section (2.5.2).

Neglecting the atmospheric effects, four pseudorange measurements to four different satellites are required. These are to solve for the three unknown receiver coordinates and the receiver clock offset. Equation (2.1) can be linearised about the approximate values of the receiver coordinates and the estimated receiver clock offset.

$$\frac{\partial \rho}{\partial X_A}\Delta X_A + \frac{\partial \rho}{\partial Y_A}\Delta Y_A + \frac{\partial \rho}{\partial Z_A}\Delta Z_A + \frac{\partial \rho}{\partial T_A}\Delta T_A = (O_{PR} - C_{PR}) + \nu \qquad (2.2)$$

16

Where

X_A, Y_A, Z_A = approximate coordinates of receiver at station A

$\Delta X_A, \Delta Y_A, \Delta Z_A$ = corrections to approximate coordinates

T_A = initial estimate of the receiver clock bias

ΔT_A = correction to receiver clock bias

O_{PR} = observed pseudorange (m)

C_{PR} = computed pseudorange (m)

ν = residual value

The computed pseudorange, is determined from the satellite ephemeris and from the approximate coordinates of the receiver. The satellite clock offset T_s and the estimated receiver clock offset are added to produce the computed pseudorange C_{PR}.

$$C_{PR} = \rho_c + c(T_A - T_s) \qquad (2.3)$$

The partial differential coefficients $\partial\rho/\partial X$ can be calculated from the expression for range,

$$\rho = \sqrt{(X^S - X_A)^2 + (Y^S - Y_A)^2 + (Z^S - Z_A)^2} \qquad (2.4)$$

Where

X^S, Y^S, Z^S = satellite coordinates

X_A, Y_A, Z_A = approximate coordinates of receiver
at station A

Hence,

$$\frac{\partial\rho}{\partial X_A} = \frac{(X^S - X_A)}{\rho} \qquad (2.5)$$

The partial derivative of range with respect to the receiver clock offset is given as,

$$\frac{\partial\rho}{\partial T_A} = c \qquad (2.6)$$

Where c is the speed of light.

To solve for the receivers position at a given epoch in time, four simultaneous pseudoranges are required. These four pseudorange observables will lead to a unique solution of the position and the receiver clock bias. If five or more satellites can be observed, redundant observations are introduced

and a least squares approach can be adopted to determine the most probable solution.

If real time positioning is not required, then pseudorange measurements can be recorded over many epochs. This will lead to a more precise solution and the receiver clock can then be modelled as a polynomial (Section 2.5.3).

The pseudorange can be measured using the C/A code or the P code. The C/A code has a repeat period of one millisecond, which corresponds to approximately 300 km in range. This manifests itself as an ambiguity, which can be resolved by most receivers if several satellites are observed. The P code with its week long sequence is totally unambiguous and has the advantage that the range can be resolved more precisely. The approximate range resolutions for the P and C/A codes are 0.3 m and 3.0 m respectively.

2.3.4 System Accuracies

The accuracy of a point position fix is dependent upon several factors. Errors in the range measurements and a poor geometrical configuration of the satellites will cause significant positional errors. The range measurement errors are caused by atmospheric delays, satellite and receiver clock biases, satellite ephemeris errors and measurement noise. The modelling of these errors is considered in section (2.5).

The Geometrical Dilution Of Precision (GDOP) is used to express the satellite geometry. The GDOP is a function of the dilution of precision of both the position (PDOP) and receiver clock biases (TDOP). Where,

$$GDOP = \sqrt{(PDOP)^2 + (TDOP)^2} \qquad (2.7)$$

The numerical value of GDOP can be determined from the covariance matrix of the pseudorange solution. If the covariance matrix (section 2.4.6) is given by,

$$\begin{pmatrix} \sigma_{xx}^2 & \sigma_{xy}^2 & \sigma_{xz}^2 & \sigma_{xt}^2 \\ \sigma_{yx}^2 & \sigma_{yy}^2 & \sigma_{yz}^2 & \sigma_{yt}^2 \\ \sigma_{zx}^2 & \sigma_{zy}^2 & \sigma_{zz}^2 & \sigma_{zt}^2 \\ \sigma_{tx}^2 & \sigma_{ty}^2 & \sigma_{tz}^2 & \sigma_{tt}^2 \end{pmatrix} \qquad (2.8)$$

Then,

$$GDOP = \sqrt{\sigma_{xx}^2 + \sigma_{yy}^2 + \sigma_{zz}^2 + \sigma_{tt}^2} \qquad (2.9)$$

The error in the user position can be estimated by multiplying the range measurement error by the corresponding DOP values. For example, with a range error of five meters, and a PDOP of four meters, the radial error in the user position would be 20 meters.

For a low GDOP, the ideal four satellite configuration would be three satellites placed equally around the horizon, with one satellite directly overhead (See figure 2.3). A high GDOP would be with all four satellites in one part of the sky (See figure 2.4).

2.4 Relative Positioning with GPS

2.4.1 Introduction

The removal of the PRN codes from the carrier frequency, will leave an unmodulated wave, often referred to as the reconstructed carrier. Geodetic receivers should be capable of measuring this carrier phase to about one per cent of its wavelength, giving a possible resolution of 2mm, for the 19cm L1 wavelength. This ignores other errors in the system, but it gives an indication of the accuracies that can be achieved.

The various algorithms used for the processing of carrier phase observables are given here, but further details are given in other texts [Yau, 1986], [de la Fuente, 1988].

2.4.2 Basic Phase Observables

The measurement of the reconstructed carrier phase must be made with respect to time. Hence, it is normal to measure the satellite phase, relative to the phase generated by the receiver oscillator. Assuming that the satellite clock and receiver clocks are synchronised to GPS System Time, the difference in phase or the beat frequency measurement is given as,

$$\Phi_A^i(\tau) = \Phi^i(t) - \Phi_A(\tau) \qquad (2.10)$$

19
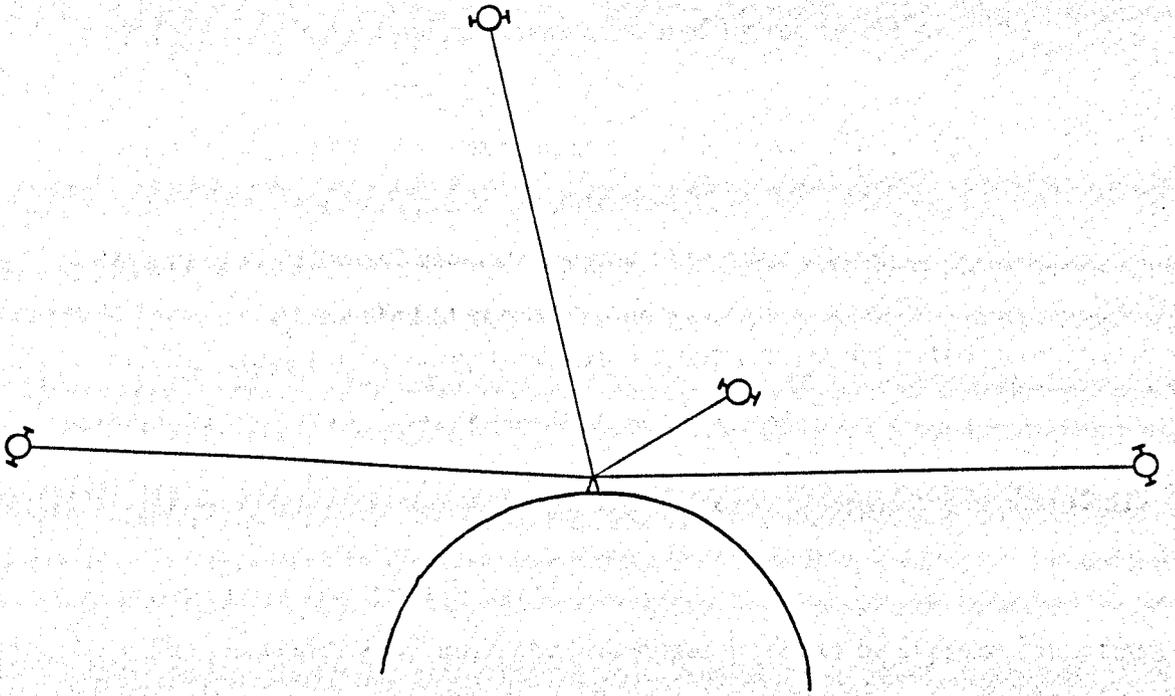
Figure 2.3: Typical satellite configuration for low GDOP
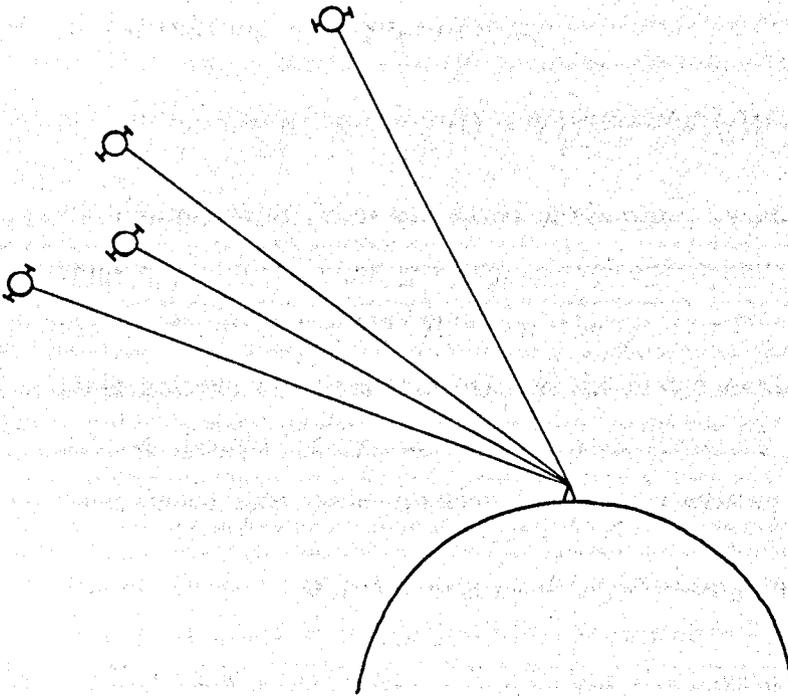
Figure 2.4: Typical satellite configuration for high GDOP

Where

$\Phi_A^i(\tau)$ = instantaneous phase measured by receiver A at

received time τ

$\Phi^i(t)$ = phase of the incoming signal from satellite i

transmitted at satellite time t

$\Phi_A(\tau)$ = phase of generated signal of receiver A,

measured at received time τ

The signal propagation time can be determined from the geometrical range ρ_A^i between satellite i and receiver A. Hence,

$$\tau - t = \rho_A^i(t)/c \qquad (2.11)$$

Where c = the speed of light.

The phase of the incoming satellite signal $\Phi^i(t)$ can be expressed in terms of the received time τ and the range ρ , giving

$$\Phi^i(t) = \Phi^i(\tau - \rho_A^i(t)/c) \qquad (2.12)$$

This expression can be expanded using Taylors theorem, ignoring terms higher than the first order to give,

$$\Phi^i(t) = \Phi^i(\tau) - \frac{f}{c}(\rho_A^i(t)) \qquad (2.13)$$

The phase $\Phi_A^i(\tau)$ is measured modulo one cycle, and the receiver maintains count of the number of whole cycles that have been received since the first measurement epoch. However, the receiver has no knowledge of the integer number of cycles that exist at the first epoch. This integer ambiguity can be allowed for by adding an integer term N_A^i to equation(2.10). The basic phase observable equation can now be written as,

$$\Phi_A^i(\tau) = \Phi^i(\tau) - \frac{f}{c}(\rho_A^i(t)) - \Phi_A(\tau) + N_A^i \qquad (2.14)$$

The basic phase observable contains the constant integer term N_A^i and the range term $\rho_A^i(t)$, which relates to the receiver coordinates. In order to eliminate the time varying satellite phase $\Phi^i(\tau)$ and receiver phase $\Phi_A(\tau)$ linear differences can be formed, between satellites and stations.

21

2.4.3 Single Differences

A single difference is the instantaneous phase difference, between two receivers and one satellite. It is also possible to define single differences between two satellites and one receiver [Wells, 1986]. Using the former definition, the phase difference between two receivers A and B, and satellite i is,

$$
\begin{aligned}
\Phi^i_{AB}(\tau) &= \Phi^i_B(\tau) - \Phi^i_A(\tau) \\
&= \Phi_A(\tau) - \Phi_B(\tau) + \frac{f}{c}(\rho^i_A(t) - \rho^i_B(t)) + N^i_{AB} \qquad (2.15)
\end{aligned}
$$

Where $N^i_{AB} = N^i_B - N^i_A$

The single difference will eliminate the satellite phase $\Phi^i(\tau)$, and the two integers N^i_B and N^i_A are combined into one integer N^i_{AB}.

2.4.4 Double Differences

A double difference is formed from subtracting two single differences, measured to two satellites i and j (figure 2.5). Hence,

$$
\begin{aligned}
\Phi^{ij}_{AB}(\tau) &= \Phi^j_{AB}(\tau) - \Phi^i_{AB}(\tau) \\
&= \frac{f}{c}(\rho^j_A(t) - \rho^j_B(t) - \rho^i_A(t) + \rho^i_B(t)) + N^{ij}_{AB} \qquad (2.16)
\end{aligned}
$$

Where $N^{ij}_{AB} = N^j_{AB} - N^i_{AB}$

It can be seen from equation (2.16) that all the time dependent unknowns have been eliminated. The only unknowns are the constant lock-on double difference phase ambiguity N^{ij}_{AB} and the range value ρ^{ij}_{AB}. It is this range term that contains the unknown receiver coordinates. For short baselines, the value of the integer ambiguity N^{ij}_{AB} can be estimated as part of the solution and it can be constrained to its integer value in a subsequent solution. The process of constraining the integers generally improves the accuracy of the solution [Yau, 1986].

2.4.5 Triple Differences

A triple difference is formed from two double differences, measured at two different epochs τ_n and τ_{n+1}. The triple difference observable is then written
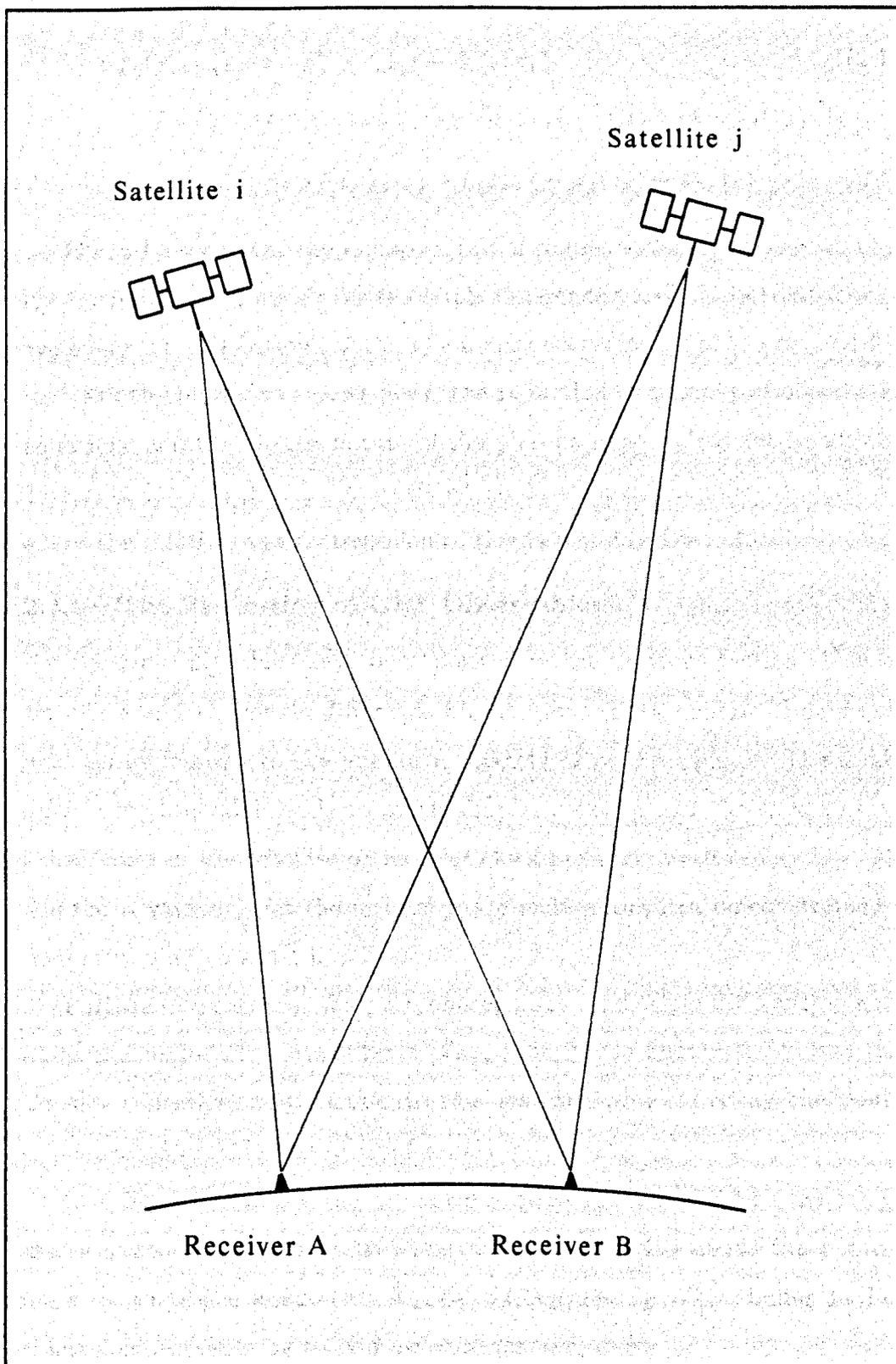
Figure 2.5: Double difference phase method

as,

$$\Phi_{AB}^{ij}(\tau_{n+1,n}) = \Phi_{AB}^{ij}(\tau_{n+1}) - \Phi_{AB}^{ij}(\tau_n) \qquad (2.17)$$

$$= \frac{f}{c}(\rho_A^j(\tau_{n+1}) - \rho_B^j(\tau_{n+1}) - \rho_A^i(\tau_{n+1}) + \rho_B^i(\tau_{n+1}))$$

$$-\frac{f}{c}(\rho_A^j(\tau_n) - \rho_B^j(\tau_n) - \rho_A^i(\tau_n) + \rho_B^i(\tau_n)) \qquad (2.18)$$

It can be seen that the unknown initial double difference phase ambiguity is eliminated. This makes the triple difference particularly robust, when cycle slips occur (section 2.5.1). The main disadvantages of the triple difference are the increase in noise level, the reduction in number of observation equations and the integer nature of the phase ambiguity cannot be utilised. The selection of the time interval, which to form differences over will also affect the solution and a discussion of this is found in [Yau, 1986].

2.4.6 The Processing of GPS Observables

Four phase observables have been derived in the previous section. The basic phase and the single difference observations, both contain time dependent terms relating to the unknown satellite or receiver phase. The double difference observable leads to much simpler solution and the effects of any instabilities in the satellite or receiver clock are very much reduced. It also has the advantage that the integer phase ambiguities can be constrained to integer values, for short baselines.

Further discussion of the pure phase, single and triple difference observables can be found in other texts [Yau, 1986] [de la Fuente, 1988] and they are not considered any further in this research project. Only the double difference observable will be used for the processing.

In order to solve for the unknown station coordinates and the integer ambiguities, it is necessary to linearise equation (2.16) about the approximate values of the unknowns, $X_A, Y_A, Z_A, X_B, Y_B, Z_B, N_{AB}^{ij}$. Using Taylor's expansion and ignoring second order terms and above,

$$\frac{f}{c}\left[\left(\frac{\partial \rho_A^i}{\partial X_A} - \frac{\partial \rho_A^j}{\partial X_A}\right)\Delta X_A + \left(\frac{\partial \rho_A^i}{\partial Y_A} - \frac{\partial \rho_A^j}{\partial Y_A}\right)\Delta Y_A + \left(\frac{\partial \rho_A^i}{\partial Z_A} - \frac{\partial \rho_A^j}{\partial Z_A}\right)\Delta Z_A\right]$$

$$-\frac{f}{c}\left[\left(\frac{\partial \rho_B^i}{\partial X_B} - \frac{\partial \rho_B^j}{\partial X_B}\right)\Delta X_B + \left(\frac{\partial \rho_B^i}{\partial Y_B} - \frac{\partial \rho_B^j}{\partial Y_B}\right)\Delta Y_B + \left(\frac{\partial \rho_B^i}{\partial Z_B} - \frac{\partial \rho_B^j}{\partial Z_B}\right)\Delta Z_B\right]$$

$$+ \frac{\partial \Phi^{ij}_{AB}}{\partial N^{ij}_{AB}} \Delta N^{ij}_{AB} = (O_\Phi - C_\Phi) + \nu \tag{2.19}$$

where,

$$\eth \frac{\partial \rho^i_A}{X_A} = \frac{X^i - X_A}{\rho^i_A} \tag{2.20}$$

and,

$$\frac{\partial \Phi^{ij}_{AB}}{\partial N^{ij}_{AB}} = 1 \tag{2.21}$$

The observed double difference phase O_Φ is obtained directly from the values recorded at the two receivers, giving

$$O_\Phi = \Phi^i_A(\tau) - \Phi^j_A(\tau) - \Phi^i_B(\tau) + \Phi^j_B(\tau) \tag{2.22}$$

The computed phase $\Phi^i_A(\tau)_C$ for one satellite and one receiver is determined from the geometrical range, corrected for atmospheric delays,

$$\Phi^i_A(\tau)_C = \frac{f}{c}(\rho^i_A) + \Phi_{ion} + \Phi_{trop} \tag{2.23}$$

The double difference computed phase C_Φ is obtained from differencing equation (2.23) in the same way as equation (2.22).

The observation equation (2.19) refers to two satellites and two receivers. The introduction of extra stations (receivers) or satellites will require particular differencing techniques.

Consider the use of four satellites, i, j, k, l and two stations. At one epoch double differences can be formed by differencing between adjacent satellites (i-j), (j-k), (k-l) or by using a base satellite concept and differencing to one satellite, (i-j), (i-k), (i-l).

The differences formed in this way will be highly correlated, because the observations share some common phase measurements. Hence it is necessary to model these correlations to avoid biasing the observations to a particular satellite. The same problem will occur when using more than two stations.

The Correlation of Double Difference Observables

A geometrical correlation matrix C is used to relate the double difference observables Φ_{DD} to the raw phase measurements Φ_{raw}, such that

$$\Phi_{DD} = C \times \Phi_{raw} \tag{2.24}$$

25

In general, the correlation matrix can be expressed using the notation given by *Beutler et al* [1986a],

$$C = \begin{pmatrix} \lambda_{11} C' & \lambda_{12} C' & \lambda_{13} C' \\ \lambda_{21} C' & \lambda_{22} C' & \lambda_{23} C' \end{pmatrix} \tag{2.25}$$

If the base satellite concept is used, the matrix C' for m satellites would have (m-1) rows and m columns.

$$C' = \begin{pmatrix} -1 & 1 & 0 & 0 & 0 & 0 \\ -1 & 0 & 1 & 0 & 0 & 0 \\ -1 & 0 & 0 & 1 & 0 & 0 \\ -1 & 0 & 0 & 0 & 1 & 0 \\ -1 & 0 & 0 & 0 & 0 & 1 \end{pmatrix} \tag{2.26}$$

The submatrix λ for n stations will have n-1 rows and n columns. The definition of the submatrix will depend upon the baseline configuration selected for the processing. Using a *base station* concept the λ matrix can be given as,

$$\lambda = \begin{pmatrix} -1 & 1 & 0 & 0 & 0 & 0 \\ -1 & 0 & 1 & 0 & 0 & 0 \\ -1 & 0 & 0 & 1 & 0 & 0 \\ -1 & 0 & 0 & 0 & 1 & 0 \\ -1 & 0 & 0 & 0 & 0 & 1 \end{pmatrix} \tag{2.27}$$

An efficient way of computing the correlation matrix, is to use the Kronecker matrix product [de la Fuente, 1988]. The Kronecker matrix product of λ and C' is given as,

$$C = \lambda \otimes C' \tag{2.28}$$

The correlation matrix W, by which the double difference must be multiplied, is given as,

$$W = (CC^T)^{-1} \tag{2.29}$$

Using the rules of Kronecker matrix products, the weight matrix W can be written as,

$$W = (\lambda \lambda^T)^{-1} \otimes (C' C'^T)^{-1} \tag{2.30}$$

Hence W can be easily computed without having to invert the whole correlation matrix product (CC^T).

An adjustment can now be carried out, by using a least squares procedure. The weighted observation equations are in the form,

$$W^{\frac{1}{2}}Ax = W^{\frac{1}{2}}b + W^{\frac{1}{2}}\nu \qquad (2.31)$$

where

W = weight or correlation matrix

A = observation equation coefficients

x = vector of unknowns

b = observed minus computed double differenced phase

ν = residual

The most probable solution to equation (2.31) is obtained from minimising the sum of the squares of the weighted residuals. The series of equations that satisfy this condition, are called the normal equations,

$$(A^T W A)x = A^T W b \qquad (2.32)$$

The normal equations are symmetric and can be solved by using Choleski's triangular decomposition method [Spencer et al, 1977]. The solution vector x contains the corrections to the unknown parameters. The residuals ν may be determined from substituting the vector x into equation (2.31).

An estimation of the precision of the unknown quantities can be obtained by forming the covariance matrix. The mean square error of an observation of unit weight [Ashkenazi, 1970] is given as,

$$\sigma_0^2 = \frac{(\nu^T W \nu)}{n - k} \qquad (2.33)$$

where,

n = number of observation equations

k = number of unknowns

The covariance matrix σ_{xx} can then be obtain from,

$$\sigma_{xx} = \sigma_0^2 (A^T W A)^{-1} \qquad (2.34)$$

27

The standard error of any unknown quantity can then be obtained from the respective diagonal element of the covariance matrix.

It is possible to constrain some of these unknowns to predefined values. For example for the solution of a network, using the double difference observable, it is normal to fix the coordinates of one of the stations and determine coordinate differences relative to that station. The coordinates are held fixed by using an observation equation of the form,

$$\Delta x = (x_o - x_c) + \nu \qquad (2.35)$$

x_o = observed value of the station coordinate

x_c = computed value of the station coordinate

The value of x_o will be the same as x_c if the station coordinates are to be constrained to the approximate coordinates. The equation (2.35) can then be multiplied by a suitably high weight and added to the normal equations. Similar equations are then formed for the y and z coordinates of the station.

2.5 Description of Error Sources in the GPS Observables

Errors in geodetic networks can be divided into two basic types; measurement errors and errors in the position of the satellite (ephemeris errors). The measurement errors are caused by,

- Cycle Slips.

- Atmospheric Delays.

- Satellite and Receiver clock biases.

- Relativistic Effects.

The methods used to reduce the effects of these errors are given in the following sections.

2.5.1 Cycle Slips

A common problem encountered when using carrier phase observables, is the occurrence of cycle slips. This is when the receiver *loses lock* on the satellite signal. When the signal is reacquired, the integer count of the number of cycles will be lost. The magnitude of the slip can vary between one cycle and several thousand cycles. The fractional part of the phase is still measured correctly, therefore it is important that cycle slips are corrected by integer values.

The loss of lock can be due to faults in the receiver hardware, by the obstruction of the antenna, or by a temporary power failure. For dynamic applications of GPS, sudden accelerations of the antenna can cause a loss of lock.

When considering a method of cycle slip reparation, the data can be repaired either from a single station or from a number of stations, using the residuals from a solution to check for the cycle slips.

Many methods of single station cycle slip repair have been suggested. Dual frequency data can be used to correct for small cycle slips at a single station [Goad, 1986]. At each epoch, the difference in carrier phase observables can be written as,

$$\delta_t = \Phi_A^i(t)_{L1} - \frac{f_{L1}}{f_{L2}} \Phi_A^i(t)_{L2} \qquad (2.36)$$

Where

$\Phi_A^i(t)_{L1}$	= Observed L1 carrier frequency at epoch t
$\Phi_A^i(t)_{L2}$	= Observed L2 carrier frequency at epoch t
f_{L1}	= L1 frequency (1575.42 MHz)
f_{L2}	= L2 frequency (1227.60 MHz)

Changes in the difference δ_t over time will caused by the ionosphere. The coefficients in equation (2.36) are 1.0 and -1.28 for the L1 and L2 frequencies respectively. Hence a slip of one cycle on L1 would cause δ_t to change by 1.0, and a slip of one cycle on L2 would cause δ_t to change by -1.28. Providing the magnitude of δ_t is small enough, it is then possible to identify the occurrence and size of a slip, and then correct the raw carrier phase data.

Another method of single station cycle slip reparation, is to fit a polynomial expression to the raw carrier phase data using a least squares method [de la Fuente, 1988]. A prediction of the next phase observable can be made by extrapolating the polynomial onto the next epoch. A check can then be made between the predicted and observed phase, to check for the occurrence and size of any cycle slips. In practice this method has been found to work, but it is computationally a very time consuming process.

Both these methods are only useful for data where the epoch separation is small. When a gap occurs in the data, it is not easy to predict the value of the cycle slip over this gap.

An alternative to fixing cycle slips at one station, is to use a phase difference solution, and check the value of the residuals. Using a triple difference algorithm, a cycle slip will show up as a spike in the residuals (Figure 2.6). The deletion of the phase data at the epoch of the slip will remove the spike, and a solution free of cycle slips will remain. It is the robust nature of the triple difference that makes it suitable for preprocessing carrier phase data.

With a double difference solution, cycle slips will show up as a jump in the residuals (figure 2.7). This means that for a double difference solution, it is necessary to correct the raw phase data, from the epoch of the slip, until the end of the data. Consider the residuals from a double differenced phase solution given in table (2.2), using satellite 12 as the base satellite.

It appears that a slip of 2 cycles has occurred in satellite 6 at epoch 7. It is also possible that a slip of -2 has occurred in satellites 9, 11 and 12. This is because at an epoch, common cycle slips between the satellites that are being differenced, will be eliminated in the double differenced solution. Hence, the phase data from epoch 7 can be corrected by 2 cycles for satellite 6, or by -2 cycles for satellites 9, 11 and 12.

When a large gap occurs in a data set, it is not always possible to determine the value of a slip exactly. One method is to solve for a new integer term in equation (2.19). This has the disadvantage that the integer nature of the slip is ignored and with a lot of cycle slips, a large number of unknowns will have to be estimated.
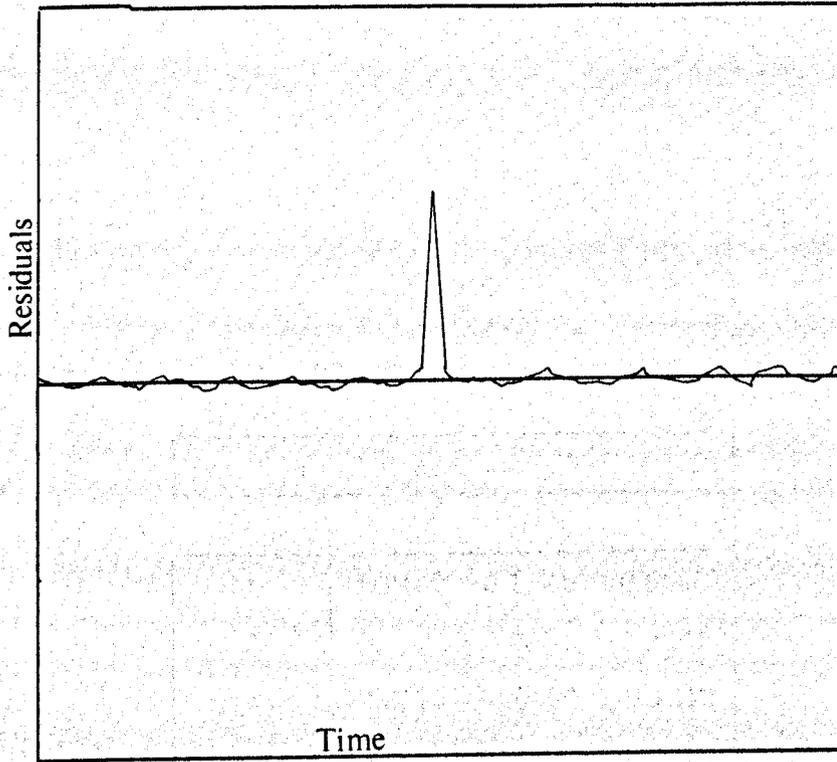
Figure 2.6: Triple difference phase residuals
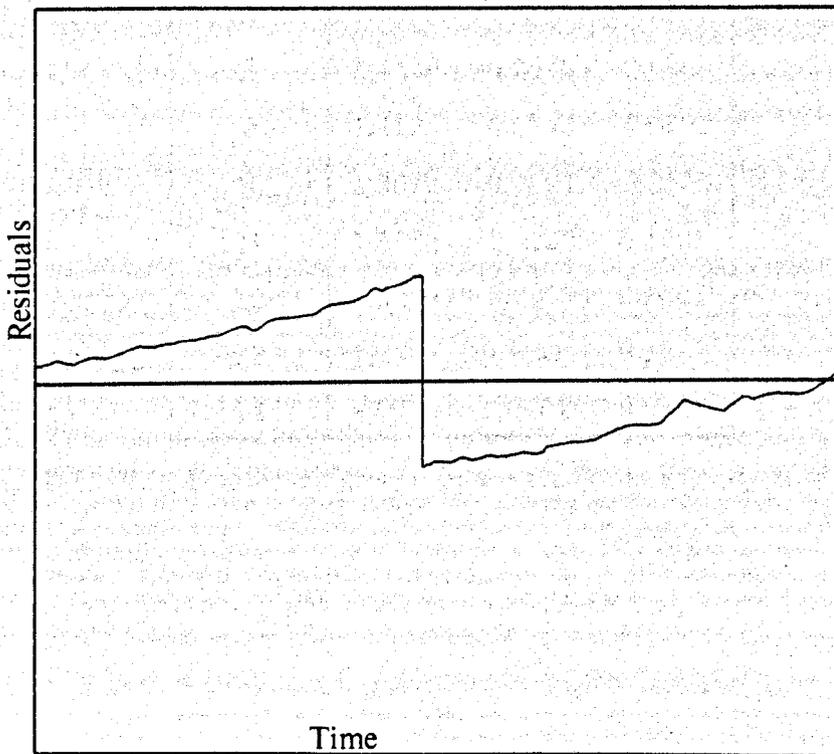
Figure 2.7: Double difference phase residuals

31

Satellites	6 & 12	9 & 12	11 & 12
epoch			
1	-0.2167	0.1571	0.0560
2	-0.2324	0.0053	0.0361
3	-0.3175	-0.0106	-0.1212
4	-0.4087	-0.0690	-0.1312
5	-0.5194	-0.0405	-0.1028
6	-0.5146	0.1422	-0.2035
7	1.4673	0.2552	-0.0726
8	1.4439	-0.0576	-0.0669
9	1.4126	-0.0843	-0.0629
10	1.3679	-0.0694	-0.0636
11	1.3762	-0.0222	0.1381
12	1.3280	-0.0033	0.1401
13	1.2384	0.1229	0.1287
14	1.0932	0.0451	0.0843

Table 2.2: Double difference phase residuals with cycle slips

2.5.2   Atmospheric Refraction

The earths atmosphere will cause the GPS signal to bend and slow down. The excess path length due to the signal bending is small for satellite elevation angles greater than 10° [Dodson, 1989], and this effect is normally ignored. The excess path length at the zenith, due to the propagation delay can be obtained from integrating the refractivity N, from the base, to the top of the ionosphere.

$$\Delta S = 10^{-6} \times \int_b^t N \, \delta S \qquad (2.37)$$

Where

ΔS = excess path length due to the propagation delay

N = refractivity of the atmosphere

t = top of the atmosphere

b = base of the atmosphere

The refractivity changes throughout the earth's atmosphere, and for GPS observables, the different effects of the ionosphere and the troposphere must be considered. The troposphere extends from the ground up to height of about 50 km, and the ionosphere extends from the top of the troposphere up to a height of about 500 km.

Troposphere

The troposphere is a non dispersive medium and will affect the L1 and L2 frequencies similarly. The atmospheric refractivity N [Dodson, 1986] is generally given as,

$$N = 77.6 \left(\frac{P}{T}\right) + 3.73 \times 10^5 \left(\frac{e}{T^2}\right) \qquad (2.38)$$

Where

e = partial water vapour pressure (millibar)

T = atmospheric temperature (Kelvin)

P = atmospheric pressure (millibar)

The first term of equation (2.38) is the dry component of the troposphere and it accounts for about 90% of the tropospheric delay. The second term is the wet component, which depends upon the partial water vapour pressure.

The inhomogenous distribution of the water vapour pressure throughout the atmosphere makes it very difficult to model. The only instrument capable of measuring the water vapour pressure, in the direction of the satellite is a microwave radiometer. However, the expense and inconvenience of the instrument, render it impractical for general GPS observations. A typical zenithal delay due to the troposphere is about 2 m, increasing to about 26 m at a zenith angle of 85°. Various models have been suggested to account for the tropospheric delay, and they are generally based upon surface weather measurements, made at each receiver.

One model proposed by Hopfield, was derived from data collected from meteorological balloons. The excess path length at zenith, is expressed in terms of the heights of the wet and dry troposperes [Hopfield, 1971]. These delays are then mapped down to the required zenith angle.

Saastamoinen used a model which assumes a constant drop in temperature up to a height of about 10 km, with a constant temperature above this point. The range correction in meters ΔS_0 is given as,

$$\Delta S_0 = 0.002277 \sec z[P + \left(\frac{1255}{T} + 0.05\right) exp^{-B\tan^2 z}] + D_R \qquad (2.39)$$

where

z =   apparent zenith angle

P =   total barometric pressure (millibars)

e =   partial water vapour pressure (millibars)

T =   absolute temperature (Kelvin)

B and D_R are corrections tabulated in [Saastamoinen, 1973]. The apparent zenith angle z may be calculated from the true zenith distance Z,

$$z = Z - \Delta z" \qquad (2.40)$$

where,

$$\Delta z" = \frac{16.0\tan Z}{T}\left(P + \frac{4800e}{T}\right) - 0".07(\tan^3 Z + \tan Z)\frac{P}{1000} \qquad (2.41)$$

A standard model for the variation of water vapour pressure is used, based upon the relative humidity r.

$$e = 6.108r \, exp^{\left[\frac{(17.15T-4684)}{T-38.45}\right]}$$ (2.42)

In a similar way to Hopfield, the zenithal delay is mapped down to the required zenith angle. Both models have been tested on the GPS software at Nottingham, and for the long baselines (greater than 100 km) processed in this thesis, the Saastamoinen model was found to be the most reliable.

In the absence of any surface meteorological data, a standard atmosphere model can be used. One such model [Curley, 1988], is used in the *MAGNET* processing software, developed for the TI 4100 receiver by Mr. R. Hatch. The pressure is estimated by,

$$P = (1015 - 1.75 \cos \Phi) exp^{-hx}$$ (2.43)

where

P = pressure (millibars)

h = height (km)

Φ = latitude

The term x is given as,

$$x = 0.113 + 0.001h + 0.017 \sin \Phi (1 + 0.382 \cos(0.0174(J - 30)))$$ (2.44)

where J is the day number from the start of the year.

The delay in meters of the signal at the zenith is then given as,

$$DR_Z = 0.002276P$$ (2.45)

This delay can then be mapped down to the required satellite elevation angle E by the function,

$$DR = \frac{DR_Z}{\sin E} + \frac{0.00143 \cos E}{\sin E} + 0.0445 \cos E$$ (2.46)

The use of uncalibrated meteorological equipment can introduce significant height errors in a baseline. It has been shown [Beutler et al, 1987] that

a 1mm error in calculating the zenithal delay can introduce a height bias of up to 2.9 mm. Indeed over small networks, the use of uncalibrated meteorological equipment and any localised surface weather conditions, may not truly represent the troposphere above. In these situations, it is usually better to use a standard atmosphere model, than to use surface weather data.

It has also been shown that ignoring the atmospheric delay will introduce a scale increase of about one part per million (ppm) [Beutler et al, 1987]. If a suitable model is used, the dry part (90%) of the delay can be satisfactorily calculated, resulting in a scale error of the order of 0.1 ppm.

Ionosphere

The ionosphere is a dispersive medium and will affect the L1 and L2 frequencies differently. Also, the ionosphere affects the signal modulations by delaying them (group delay), but the carrier phase is advanced (phase delay) by an equal amount. The refractivity N is related to the frequency by the following,

$$N = k \times \left(\frac{E}{f^2} \right) \tag{2.47}$$

Where

E = free electron density

f = frequency

k = constant term

The free electron density will depend upon the solar activity. Factors affecting the number of free electrons in the ionosphere include the daily and seasonal variations in the sun and the eleven year sun spot cycle, which is expected to reach a maximum in 1990/91. Typical zenithal delays vary from 10 meters around midday, to around 2 meters at night.

The phase advance due to the ionosphere [Ashkenazi et al, 1977] can be shown to be,

$$\Phi_A = \Phi_{vac} - \Phi_{obs} = \frac{a_1}{f} + \frac{a_2}{f^2} + higher\ order\ terms \tag{2.48}$$

Where

36

Φ_A = phase advance

Φ_{vac} = carrier phase measured in a vacuum

Φ_{obs} = carrier phase observed

a_1, a_2 = constants which include the total electron count

f = frequency

Using two frequencies and ignoring second order terms and higher,

$$\Phi_{vac}^{L1} - \Phi_{obs}^{L1} = \frac{a_1}{f_{L1}} \qquad (2.49)$$

$$\Phi_{vac}^{L2} - \Phi_{obs}^{L2} = \frac{a_1}{f_{L2}} \qquad (2.50)$$

Hence from equation (2.50),

$$\frac{f_{L2}}{f_{L1}}\Phi_{vac}^{L1} - \Phi_{obs}^{L2} = \frac{a_1}{f_{L2}} \qquad (2.51)$$

Combining equations (2.49) and (2.51), the phase measured in a vacuum Φ_{vac}^{L1} is given as,

$$\Phi_{vac}^{L1} = \frac{f_{L1}^2\Phi_{obs}^{L1} - f_{L1}f_{L2}\Phi_{obs}^{L2}}{f_{L1}^2 - f_{L2}^2} \qquad (2.52)$$

A similar expression can be derived for the L2 frequency,

$$\Phi_{vac}^{L2} = \frac{f_{L1}f_{L2}\Phi_{obs}^{L1} - f_{L2}^2\Phi_{obs}^{L2}}{f_{L1}^2 - f_{L2}^2} \qquad (2.53)$$

Hence with dual frequency measurements, a first order correction for the ionospheric delay can be obtained directly. For single frequency receivers, the parameters broadcast in the satellite navigation message, can be used [Rockwell, 1981]. The parameters are expected to remove up to 50% of the ionospheric delay. Further discussion of the ionospheric correction for single frequency receivers is beyond the scope of this research project, but it has been considered by other authors [Georgiadou and Kleusberg, 1987].

The effect of neglecting the ionospheric delay, is a contraction in scale of a baseline. A typical scale error of the order of 0.7 ppm has been shown with no ionospheric modelling [Beutler et al, 1987].

The use of dual frequency measurements for short baselines is not recommended, because the increased noise level of the combined L1/L2 solution

may exceed the differential dispersive delay. The increase in noise level using the dual frequency observation can be estimated from the propagation of error law and it can be shown to be approximately four times the magnitude of the single frequency observation [Kleusberg et al, 1985]. Generally, the L1 solution is used for baselines of up to 10 or 20 km. Above this value the ionosphere will generally cause significant errors and a combined L1/L2 solution should be adopted.

2.5.3 Satellite and Receiver Clock Errors

In order to take accurate code and phase measurements, it is necessary to synchronise the satellite and receiver clocks to GPS System Time. The satellite clock offset can be calculated from the parameters given in the satellite data message.

The receiver clock offset must be determined by the user and the pseudorange solution can be used for this. Providing four satellite coverage is maintained, a value for the receiver clock offset can be determined every epoch. Alternatively, if a relatively stable receiver clock is used, a polynomial can be used to model the clock offset.

$$T_A(t_i) = \alpha + \beta(t_i - t_0) + \gamma(t_i - t_0)^2 \qquad (2.54)$$

Where

$T_A(t_i)$ = receiver clock offset at epoch t_i

α, β, γ = constants representing the receiver clock offset, drift and ageing terms.

t_0 = reference epoch

Hence, equation (2.2) can be written as,

$$\frac{\partial \rho}{\partial X_A}\Delta X_A + \frac{\partial \rho}{\partial Y_A}\Delta Y_A + \frac{\partial \rho}{\partial Z_A}\Delta Z_A + \frac{\partial \rho}{\partial T_A}\Delta T_A = (O_{PR} - C_{PR}) + \nu \quad (2.55)$$

Where

$$\frac{\partial \rho}{\partial T_A}\Delta T_A = c(\alpha + \beta(t_i - t_0) + \gamma(t_i - t_0)^2) \qquad (2.56)$$

The double difference solution is relatively insensitive to receiver clock errors and it is normally sufficient to use a second order polynomial to model the clock.

Δr(m)	ppm
orbital error	baseline error
100	5
20	1
2	0.1
0.2	0.001

Table 2.3: Baseline errors for given orbital errors

2.5.4 Orbital Error

One of the major error sources affecting precise positioning, is the orbital error. For a point positioning solution, errors in the satellite ephemeris will propagate directly into the position of the receiver. For relative positioning, the baseline error can be estimated from the following expression [Wells, 1986],

$$\frac{\Delta b}{b} = \frac{\Delta r}{r} \tag{2.57}$$

Where

Δb = baseline error

b = baseline length

Δr = orbital error

r = orbital radius

If an orbital radius of 20000 km is assumed, the effect of various orbital errors are given in table (2.3), expressed in parts per million of the baseline length.

The current broadcast ephemeris is estimated to be accurate to about 20 m, suggesting possible baseline accuracies of the order of one part per million. Typical baseline errors when using the broadcast ephemeris ate given in table (2.4),

The implication from table (2.4) is that for short baselines (less than 10 km), baseline accuracies of less than one centimetre can be achieved with the broadcast ephemeris. For larger baselines and networks (greater than 10 km), the broadcast ephemeris is often inadequate, and a more precise orbit

39

Baseline (km)	Error
1	1 mm
10	1 cm
100	10 cm
1000	1 m

Table 2.4: Baseline error for the broadcast ephemeris

will have to be used.

An alternative to using the broadcast ephemeris, is to use a post mission precise ephemeris, such as that produced by the Naval Surface Warfare Centre[1] (NSWC). This is estimated to be accurate to within five meters and is available to certain bona fide users (section 3.3).

The University of Texas produce a precise ephemeris and this is available to the general user upon request. Litton Aero Services Ltd. also produce an ephemeris, specifically for use with their codeless *Macrometer* geodetic receivers.

It is also possible to determine the satellite orbit as part of a network adjustment, using the GPS observables. An orbit determination process is described in chapter 3 of this thesis, and a further discussion on orbital errors is given there.

2.5.5 Relativistic Effects

The frequency of the received signal will differ from that transmitted, due to the effects of general and special relativity. These are caused by the difference in potential between the satellite and receiver and by the difference in their velocities. An average correction is made by the Control Segment by setting the satellite clock frequency low by a factor of 4.45×10^{-10}. This will mean that the transmitted signal is now 10.22999999545 MHz [Spilker, 1978].

2.5.6 Miscellaneous Error Sources

It is not possible to describe all the known error sources, which affect the precision of GPS observables, but two other problems must be mentioned.

---

[1]Formerly the Naval Surface Weapons Centre

Multipath is an error caused by the satellite signal being reflected from a surface, before reaching the antenna. The delayed signal will interfere with the direct signal on its arrival at the antenna. The effect of multipath will only last for a limited period in time, until the satellite-antenna geometry has changed sufficiently. Multipath is more problematic for receivers used in a highly reflective environment, such as an oil rig. Careful design and siting of the antenna can alleviate the problem.

The phase centre of an antenna is the point where the incoming phase measurements are made. The position of the phase centre can move depending upon the azimuth and elevation angles of the incoming phase signal [Sims, 1985]. The effect can be minimised by orientating all the antennas used in a survey in a common direction, usually towards the north. Further care must be taken when establishing the height of the phase centre of the antenna, which is different for the L1 and L2 frequencies on the TI 4100 antenna (figure 2.8).

2.6   Data Preprocessing

There are two main preprocessing stages that are required before the GPS data can be used in a least squares network adjustment. These are necessary to reduce the quantity of data and to correct the phase data for the receiver clock offset.

2.6.1   Compression of Data

Typically, geodetic receivers are capable of measuring the pseudorange and phase data at intervals of between three seconds and minute. When recording data from several satellites, at different stations, a large amount of data is collected. To reduce the data processing time and storage requirements, a form of data compression is required.

A simple solution is to fit a low order polynomial to a number of these measurements, using a least squares technique. A normal point can then be produced for this span of data, which represents all the data points . It is necessary to chose the epoch of the normal point carefully, so that each measurement is given equal weight in the determination of the normalised

41
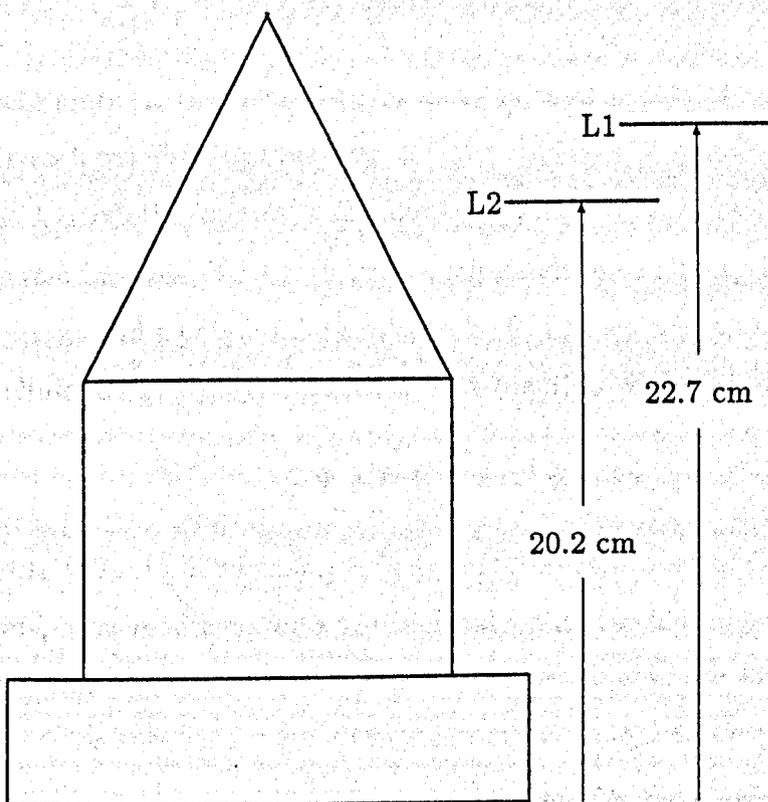
Figure 2.8: Position of the L1 and L2 phase centres on the TI 4100 antenna

Baseline	Δx	Δy	Δz	Length
Normal pointed data at sixty second epochs				
A to B	-6508.925	15760.968	5396.580	17885.673
A to C	-30718.403	32537.806	24304.935	50922.087
Raw data at three second epochs				
A to B	-6508.927	15760.968	5396.581	17885.674
A to C	-30718.400	32537.805	24304.934	50922.084

Table 2.5: Normal pointed data results

data point. In general, for the GPS phase data, the epoch nearest to the mean epoch has been chosen for the normal point. For phase difference techniques, it is essential to produce normal points at simultaneous epochs for each satellite and receiver.

A geodetic receiver will record the phase data at nominally constant intervals in time. The data from each satellite can be split into equal length sections and a polynomial can then be fit to each section using a least squares technique. The polynomial will be a function of time t, of the form,

$$\Phi = a + bt + ct^2 + dt^3 + \cdots \qquad (2.58)$$

In the simplified example in figure (2.9), the normal points each represent five phase readings, with the normal point calculated at the mid epoch of the data span. The data recorded from each satellite must be sectioned at the same epochs, for simultaneous normal points to be produced. This will necessitate the rejection of some observations when satellites rise and fall, but the normal points will then be uncorrelated.

A further use of normal pointing is to combine data from different receiver types, where the recording interval may differ (Chapter 6).

An important requirement for any data compression technique, is that the final solution will not be unduly affected by using the compressed data set. Table (2.5) shows a comparison between two baselines (A to B) and (A to C) computed using three second data and then using data normal pointed to one minute intervals.
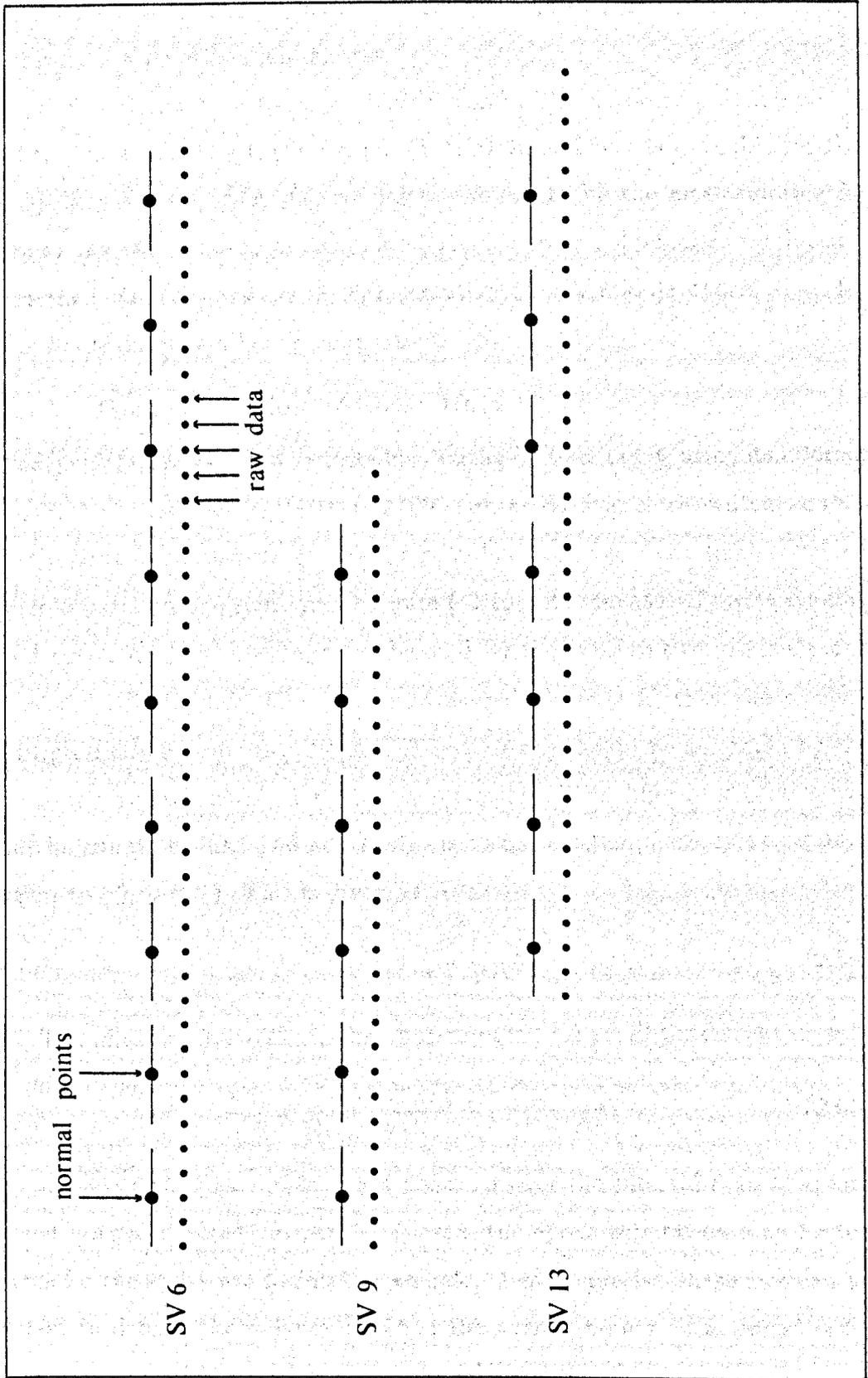
Figure 2.9: Production of normal points for the phase data

44

The maximum difference between the two solutions for any of the baseline components was three millimetres.

Comparisons have been conducted using different order polynomials to fit the data. For the three second TI 4100 data that was available for this project, a second order polynomial was found to be the most suitable for producing one minute normal points. Higher order polynomials produced a normal point that was more representative for the middle epoch, than for the whole data span being compressed.

2.6.2 Time Correction of Phase Data

The geodetic receiver will record phase data and time tag it, using its internal clock. Any offset from GPS System Time of the receiver clock, will mean that the time tags are incorrect. The magnitude of this error can be determined from a pseudorange solution. In figure (2.10), the measured phase reading and corresponding time tags are denoted by the subscript m. At an epoch i, if the GPS System Time of the measured phase is t_i, then the receiver will produce the time tag $t_i + \Delta t_i$. The time tags could be corrected by the receiver clock offset Δt_i, but then observations from different receivers will not be simultaneous. The alternative is to correct the phase by an amount equal to $(\Phi_i - \Phi_{i_m})$. This is given as,

$$\Phi_i = \Phi_{i_m} + \frac{\partial \Phi}{\partial t} \Delta t \qquad (2.59)$$

The phase rate $\partial \Phi / \partial t$ can be approximated for small time intervals by,

$$\frac{\partial \Phi}{\partial t} = \frac{\Phi_{(i+1)_m} - \Phi_{i_m}}{(t_{i+1} + \Delta t_{i+1})_m - (t_i + \Delta t_i)_m} \qquad (2.60)$$

However, the phase rate is not constant over the interval t_i to t_{i+1}, and when normal pointed data is being used, the epoch separation may be too large for the above approximation to hold. A more precise phase rate can be determined from the polynomial fit of the normal points. If a second order polynomial has been used to fit a span of data, the phase at time t_i from a given reference time t_0 is given as,

$$\Phi(t_i) = a + b(t_i - t_0) + c(t_i - t_0)^2 \qquad (2.61)$$

45
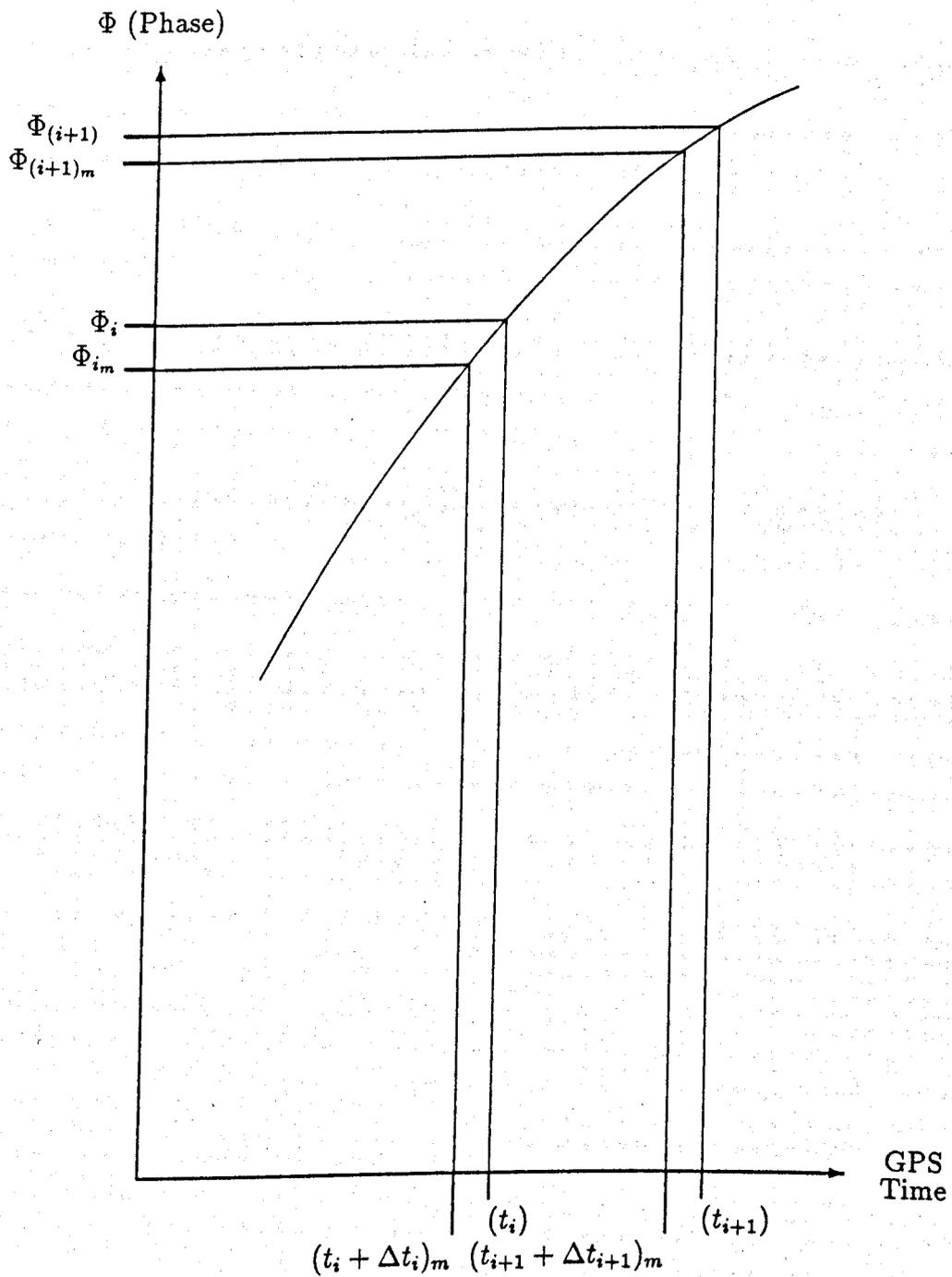
Figure 2.10: Time correction of the phase data

where a, b and c are constants.

The phase rate is then obtained from differentiating with respect to t,

$$\frac{\partial \Phi}{\partial t} = b + 2c(t_i - t_0) \tag{2.62}$$

The corrected phase value is now obtained from,

$$\Phi_i = \Phi_{i_m} + (b + 2c(t_i - t_0))\Delta t_i \tag{2.63}$$

Chapter 3.
Orbit Determination

Orbit Determination

3.1 Introduction

The carrier phase observable can be used to determine baseline lengths to an accuracy of about one part per million, when using the broadcast ephemeris. If large baselines are to be measured, the magnitude of this error may become unacceptable. An alternative is to use the NSWC precise ephemeris, which should be suitable for baseline determination up to an accuracy of half a part per million. However, for higher precision work, it is necessary to model the satellite orbit, by solving for selected orbital parameters as part of the least squares network adjustment.

To determine elements of the orbit by any method, it is necessary to use a network of tracking stations. For the production of the broadcast and precise ephemerides, a global tracking network is used. However, when using a phase difference technique to determine the orbit, simultaneous measurements are required between the satellites and stations. This necessitates the use of a regional or continental network.

The following two sections describe the production of the broadcast and precise ephemerides. Section (3.4) gives details of the orbit determination approach used in this research project for regional networks.

3.2 Broadcast Ephemeris Prediction

The prediction of the satellite ephemeris by the Master Control Station (MCS) is a two stage process.

Initially, a reference orbit is computed by the Naval Surface Warfare Cen-

tre (NSWC), using the *CELEST*[1] computer program [O'Toole, 1976]. This reference orbit, is a 40 day prediction, based upon one week of pseudorange data, collected from the GPS Monitor Stations (MS). Every two weeks, a new reference orbit is sent to the MCS. The orbit is estimated to have a maximum error in the along track direction of between five and twenty meters [Varnum and Chaffee, 1982].

The second stage of the process uses a Kalman filter to determine the current satellite states from satellite observations. These are then used in the filter to predict the future states of the satellite for the broadcast ephemeris. Measurements of pseudorange and delta pseudorange are made at each MS, every six seconds. These measurements are made with a caesium beam frequency standard and the time tag of each measurement is corrected to GPS System Time at the time of signal transmission. The pseudorange measurements are smoothed to produce one value every fifteen minutes and the delta pseudorange measurements are sampled every fifteen minutes. The reference orbit is now subtracted from the smoothed measurements to produce measurement residuals. These are corrected for the effects of the ionosphere, troposphere, relativity, earth rotation and the antenna offsets. These measurements are then used as the input to the Kalman filter, to produce estimates of the satellite's position and the satellite clock offset. The predicted satellite coordinates, which are determined in cartesian coordinates, are converted into keplerian type elements, then uploaded to the satellites by the Ground Antennas.

The first six Keplerian elements given in table (3.1) describe the satellite's motion at the reference time t_0. Corrections terms are given to allow for perturbations from this smooth orbit. The term Ω_0 is not the right ascension, but is the difference between the right ascension at the ephemeris reference time Ω_{oe} and the Greenwich Apparent Sidereal Time ($GAST_{week}$) at the start of the GPS week.

---

[1]Recently a new multi-satellite program has been developed for computing the GPS reference orbit called *OMNIS*. This has been developed by the NSWC to replace the *CELEST* program

Element	Description
M_0	mean motion
e	eccentricity
$\sqrt{a}$	square root of the semi-major axis
Ω_0	$\Omega_{oe} - GAST_{week}$ (see text)
i_0	inclination at time t_0
ω	argument of perigee
Δn	mean motion difference
$\dot{\Omega}$	rate of right ascension
$\dot{i}$	rate of inclination
C_{uc}, C_{us}	cosine and sine corrections to argument of latitude
C_{rc}, C_{rs}	cosine and sine corrections to orbital radius
C_{ic}, C_{is}	cosine and sine corrections to inclination
t_0	ephemeris reference time
af_0	satellite clock offset
af_1	satellite clock drift term
af_2	satellite clock ageing term

Table 3.1: Broadcast ephemeris representation

The satellite clock offset terms are also given in the ephemeris message. These three terms give the clock offset with respect to the reference time, and are perturbed by a function which describes general relativity, so that the user may ignore the effect.

The calculation of the satellite coordinates from the broadcast ephemeris is done in two stages [Ashkenazi and Moore, 1986]. Initially, the cartesian coordinates of the satellite are computed in the orbital plane. These are then rotated through the inclination angle, to make the z axis coincident with the terrestrial z axis. Finally, the coordinates are rotated about the z axis by the angle Ω, to make the x axis coincident with the Greenwich Meridian.

The accuracy of the broadcast ephemeris is estimated to be in the region of 20 metres with possible degradation up to 50 metres in certain areas. Once GPS is fully operational, the errors are not expected to exceed one metre radially, seven metres along track and three metres across track [Wells, 1986].

3.3 Precise Ephemeris Prediction

More precise satellite coordinates can be obtained by using one of the several post-computed ephemerides that are available.

The 'official' precise ephemeris is computed by the Naval Surface Warfare Centre (NSWC) and is based upon measurements from the five Monitor Stations, augmented with data collected in Australia, England, Argentina, Bahrain and Ecuador (figure 3.1). The ephemeris is computed for spans of eight days, covering the GPS week from Sunday to Saturday. A half day extension at each end of the week, provides a full day overlap between successive weeks. Comparisons have been made between these end of week overlaps, to check the consistency of the orbit data. The agreement has been shown to be better than five meters [Gouldman et al, 1989]. Authorised civilian users can obtain the ephemeris through the U.S. National Geodetic Survey, after a period of about four weeks. The ephemeris is given in earth-fixed cartesian coordinates, describing the satellite's position and velocity in kilometres and kilometres/second every fifteen minutes. An interpolation method can be used to determine the coordinates at the required epoch.
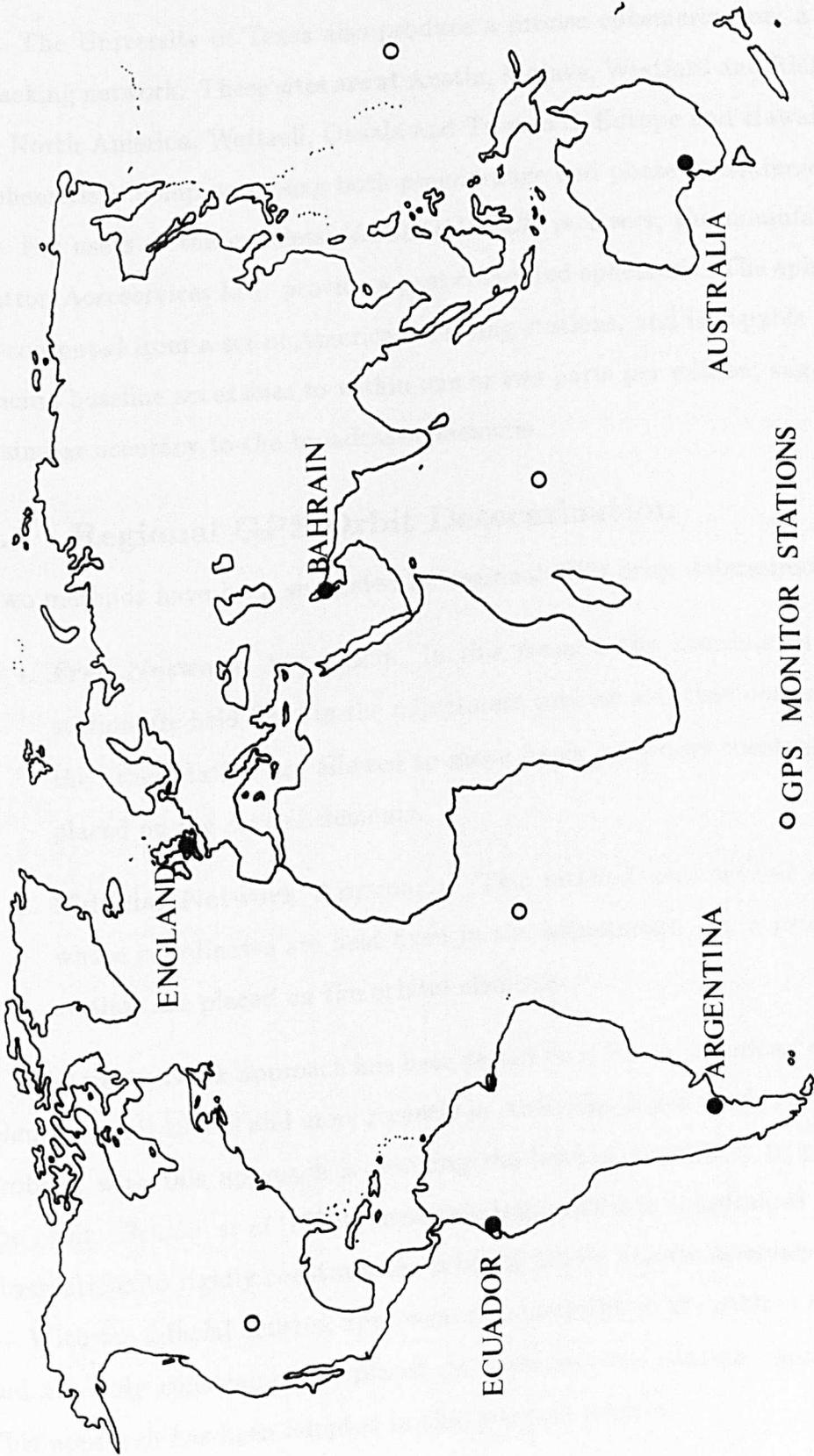
Figure 3.1: Precise ephemeris tracking network

The University of Texas also produce a precise ephemeris from a global tracking network. These sites are at Austin, Mojave, Westford and Richmond in North America, Wettzell, Onsala and Tromso in Europe and Hawaii. The ephemeris is computed using both pseudorange and phase measurements.

For users of the codeless *MACROMETER* receivers, the manufacturer, Litton Aeroservices Ltd. provide a post computed ephemeris. The ephemeris is computed from a set of American tracking stations, and is capable of producing baseline accuracies to within one or two parts per million, suggesting a similar accuracy to the broadcast ephemeris.

3.4 Regional GPS Orbit Determination

Two methods have been suggested for regional GPS orbit determination.

1. **Free Network Approach.** In this method the coordinates of one station are held fixed in the adjustment process and the coordinates of the other station are allowed to move freely. *A priori* constraints are placed on the orbital elements.

2. **Fiducial Network Approach.** This method uses several stations whose coordinates are held fixed in the adjustment. No *a priori* constraints are placed on the orbital elements.

The free network approach has been tested on a North American network [Beutler et al, 1986b] and more recently in Australia [Rizos et al, 1989]. One problem with this approach is deciding the level of constraint to place on the orbit. *Beutler et al* [1986b] used tabulated satellite coordinates as false observations to rigidly constrain the orbit at fifteen minute intervals.

With the fiducial network approach, no constraint on the orbit is required and the only constraints are placed on some selected station coordinates. This approach has been adopted in this research project.

3.4.1 Fiducial Network Concept

The fiducial network concept for GPS orbit determination is based on several GPS receivers, which are placed at sites, whose coordinates are precisely

known (fiducial sites). The necessity to use precisely known coordinates limits the choice of network, which must be located near sites where VLBI or SLR facilities have been used. In Europe and North America this presents no problem, but in the southern hemisphere, where there is a lack of these facilities, a free network approach may have to be adopted.

The receivers, which are placed at these fiducial sites, are then used to track the satellites. Simultaneous measurements are also recorded by receivers located at sites whose coordinates are unknown (figure 3.2). This network of receivers at the fiducial sites can then be used in an orbit improvement process to determine more precise satellite orbits. This improvement in the orbital accuracy will result in a more precise determination of the unknown receiver coordinates.

To process the data from the network efficiently, a simultaneous adjustment of the satellite orbit parameters and unknown station coordinates is required, with the coordinates of the fiducial sites held fixed. Two methods can be used for the orbit adjustment process,

1. Orbit Determination. An adjustment of the satellite orbit, which has been obtained from integrating the satellite force model. (Sections 3.5 and 3.6)

2. Orbit Relaxation. An adjustment of some of the elements of the broadcast ephemeris. (Section 3.9)

The choice of station geometry for the fiducial network is particularly important. Three or more receivers are required, to be located at well distributed sites in a region extending for several hundred kilometres. The fiducial sites should not be colinear and all the unknown receiver sites should lie within or very close to the fiducial network. Experiments have shown that the best fiducial networks cover the maximum possible east-west and north-south directions and have all the unknown sites located close to the fiducial sites [Lichten et al, 1989].

In the example shown in figure (3.3), the fiducial sites W, Y and Z in network A, occupy a long narrow network and the unknown site X is located

GPS satellites

radio signals
from quasar

VLBI

VLBI

VLBI
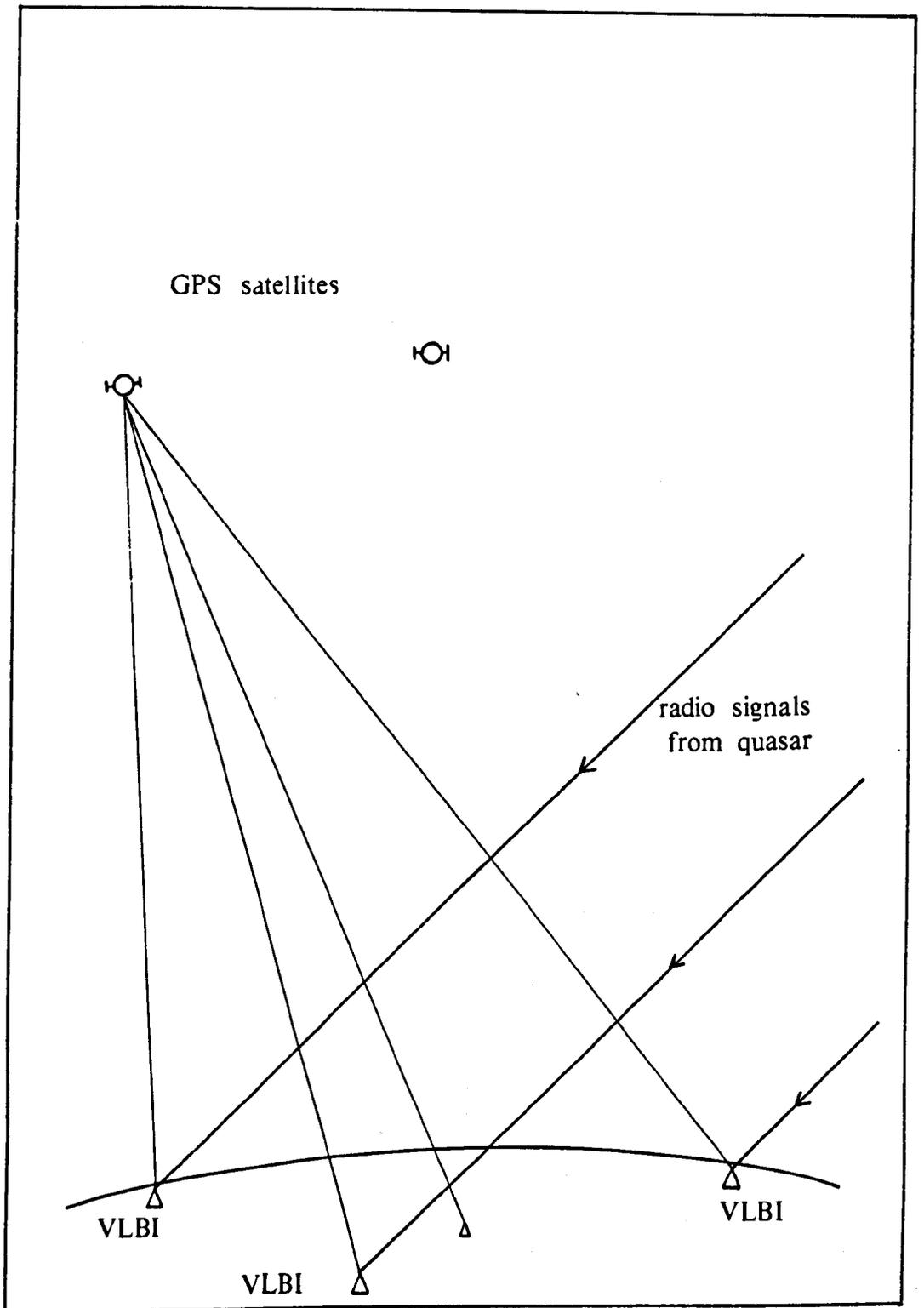
Figure 3.2: Fiducial network concept
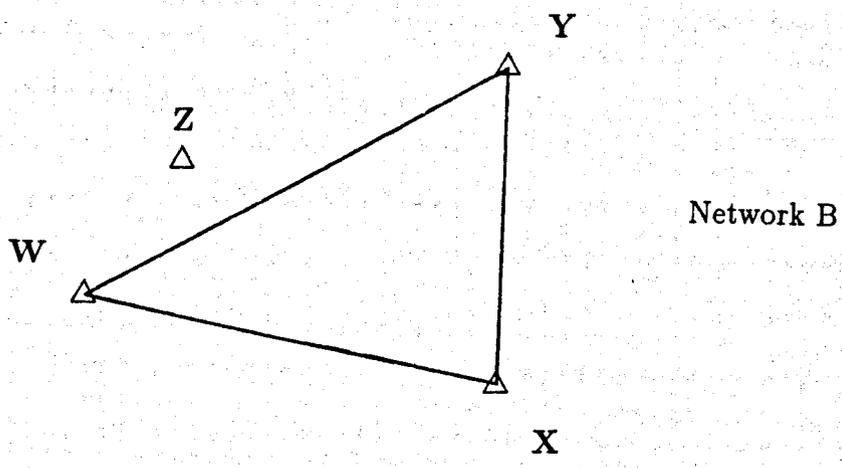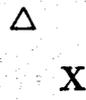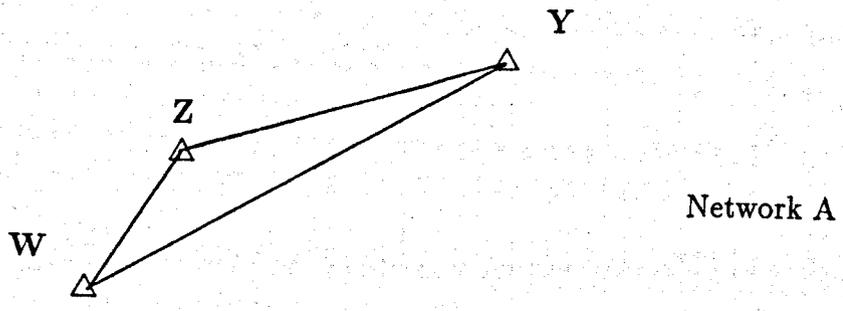
Network A

Network B

Figure 3.3: Fiducial network configurations

a long way outside the network. This configuration would be expected to produce a poor determination of the receiver coordinates at site X.

Network B uses the largest possible fiducial network, with the sites located in an optimal triangular pattern. The location of receiver Z, close to the fiducial network should enable a good estimation to be made of it's coordinates.

The fiducial network concept uses the precision of the VLBI or SLR determined coordinates to strengthen the GPS network. It is therefore necessary to exercise particular care when measuring and calculating the eccentricities between the VLBI or SLR reference marks and the GPS antenna phase centres.

The use of VLBI/SLR coordinates for the fiducial sites will tie the GPS network to the absolute reference frame of the VLBI/SLR solution. This will enable an easy comparison to be made between the VLBI/SLR and GPS baseline vector components.

CIGNET : A Global GPS Tracking Network

CIGNET, the Cooperative International GPS NETwork is a global network which is continually tracking the GPS satellites. The data is recorded from nine sites, which send the tracking data on a weekly basis to the U.S. National Geodetic Survey, where is reformatted and archived. The data is available on request for the determination of satellite orbits and other research purposes. The sites use a combination of TI 4100 and Mini Mac 2861 AT satellite receivers. The Mini Mac is a receiver capable of tracking up to ten satellites and currently the Mini Mac receivers at the CIGNET sites track all the available satellites, including the Block II satellite 14. The TI 4100 receivers track a specified satellite constellation, including satellite 14, details of which are given in the GPS Bulletin of the CSTG. The sites occupied are,

Site location	Receiver type	
Tsukuba/Kashima, Japan		Mini Mac
Kokee Park, Hawaii	TI 4100	
Yellowknife, Canada	TI 4100	
Mojave, California	TI 4100	Mini Mac
Westford, Massachusetts	TI 4100	Mini Mac
Richmond, Florida	TI 4100	Mini Mac
Tromso, Norway	TI 4100	
Onsala, Sweden	TI 4100	
Wettzell, West Germany	TI 4100	

The data from two of these sites has been used for the computation of the satellite orbits in chapter 6. The data is provided in a standard format, with separate files containing the measurement records (time-tagged pseudorange and carrier phase), satellite broadcast ephemeris and meteorological data.

3.5   The Principles of Orbit Determination

The purpose of any orbit determination procedure is to produce precise satellite coordinates, at given epochs in time. The satellite's position in space can be determined from a model, which represents all the known forces acting upon the satellite. This force model can be integrated with respect to time, once to obtain velocity, and twice to obtain position. The model will include the gravitational and surface forces acting upon the satellite.

Errors in this reference orbit (integrated orbit) can be corrected by tracking the satellite from a series of well distributed sites. These tracking observations can then be used in least squares adjustment to solve for various orbital parameters using either the free network or the fiducial network approach. The receiver site coordinates and parts of the force model are expressed in an earth fixed (rotating) reference frame, but the integration must be carried

out in an inertial (non rotating[2]) reference frame. Hence, it is necessary to define a set of reference frames and the relationship between them.

3.5.1 Inertial Reference Frames

The fundamental astronomical reference frame adopted by the International Astronomical Union (IAU) in 1976 is called FK5. FK5 describes the apparent places of over 5000 stars and extragalactic radio sources at the epoch of January 1.5, year 2000.

The inertial reference frame used in this thesis, is a geocentric cartesian system based upon the FK5 frame. The origin is located at the earth's centre, with the x axis directed towards the mean equinox of J2000.0, the z axis is normal to the equatorial plane of J2000.0, and the y axis completes the right handed coordinate system.

A similar reference frame is used to describe the planetary ephemeris, produced by the Jet Propulsion Laboratory, Pasadena. This is given in heliocentric coordinates and is called DE200/LE200.

3.5.2 Earth Fixed Reference Frames

An earth fixed coordinate system has its axes fixed with respect to positions on the earths surface. The conventional terrestrial system has its origin at the earth's centre, with the x axis directed towards the Bureau International de l'Heure (BIH) zero meridian. The z axis passes through the Conventional International Origin (CIO) pole and the y axis completes the right handed coordinate system. The CIO pole is defined by the mean axis of rotation of the earth, between the years 1900 and 1905.

The coordinates of the receiver sites are given in an earth fixed geocentric reference frame and the coefficients of the gravitational potential are given in a earth fixed spherical reference frame. Many different reference frames have been adopted by the geodetic community, but for GPS, the World Geodetic System 1984 (WGS84) has been used since January 1987 and this is based on the conventional terrestrial system.

---

[2]The inertial reference frame is non rotating with respect to a framework of points fixed in space

3.5.3 Transformation from Inertial to Earth Fixed Coordinates

Earth fixed coordinates r_{ef} of a point can be obtained from inertial coordinates r_{in} by using the theories of nutation and precession, and accounting for the earth rotation and polar motion effects. The complete transformation is given by the following expression.

$$r_{ef} = P.E.N.Pr\ r_{in} \qquad (3.1)$$

Where

$P =$ rotation matrix for polar motion

$E =$ rotation matrix for earth rotation

$N =$ rotation matrix for nutation

$Pr =$ rotation matrix for precession

The reverse transformation is given by the expression using the transpose of the matrices.

$$r_{in} = Pr^T.N^T.E^T.P^T\ r_{ef} \qquad (3.2)$$

A description of the rotation matrices is given in the following sections, further details can be found in several texts [Agrotis, 1984] [Moore, 1986].

Precession

If the effect of the planets is ignored, the mass centre of the earth and moon, would move in a plane around the sun, called the ecliptic. The great circle, formed by the ecliptic on the celestial sphere, will have a pole called the pole of the ecliptic. The effect of the sun, moon and the earth's equatorial bulge, will cause the axis of rotation of the earth, to move around the pole of the ecliptic, in a complete circle, every 25800 years. This is known as luni-solar precession, and has an amplitude of approximately 23.5°.

The attraction of the planets, will cause the pole of the ecliptic to move by about 0.47 seconds each year and the equinox will move eastwards by about 0.12 seconds each year. This motion is called planetary precession, and the combination with luni-solar precession is known as general precession.

The general precession can be calculated from three equatorial precession parameters, ζ_A, z_A, θ_A [Agrotis, 1984]. The precession matrix Pr is given as,

$$Pr = R_3(-z_A)\,R_2(\theta_A)\,R_3(-\zeta_A) \qquad (3.3)$$

The rotation matrices R_2 and R_3 are defined in appendix B. The mean of date coordinates r_m of a point, are obtained from the inertial coordinates r_{in} such that,

$$r_m = Pr\,r_{in} \qquad (3.4)$$

The mean of date coordinates are given at epochs of Barycentric Dynamical Time (TDB), which is the time scale for the equations of motion, relative to the solar system's barycentre.

Nutation

In addition to the general precession, the moon causes two other periodic motions; long period and short period nutation. The former has a period of 18.6 years, with an amplitude of about 9 seconds. The short period nutation has a period of two weeks, with an amplitude less than 0.5 seconds.

Nutation is described in terms of two angles, the nutation in longitude $\Delta\psi$ and the nutation in obliquity $\Delta\epsilon$. These relate the mean of date coordinates to the true of date coordinates r_t (defined by the true equator and equinox of date) such that,

$$r_t = N\,r_m \qquad (3.5)$$

The rotation matrix N is given as,

$$N = R_1(-\epsilon - \Delta\epsilon)\,R_3(-\Delta\psi)\,R_1(\epsilon) \qquad (3.6)$$

The values of $\Delta\epsilon$ and $\Delta\psi$ are given by the summation of a 106 term series.

Earth Rotation

To obtain instantaneous terrestrial coordinates r_i, the true equinox of date must be rotated through the hour angle GAST (Greenwich Apparent Sidereal Time). The angle GAST is defined in terms of UT1, the hour angle measured from the Greenwich meridian to the mean sun. Values of UT1 minus UTC are published monthly in Circular D, of the BIH. The instantaneous

terrestrial coordinates are given by,

$$r_i = E \, r_t \tag{3.7}$$

Where $E = R_3(GAST)$.

Polar Motion

The pole of the instantaneous terrestrial system is not fixed with respect to the earth. The movement of the pole can be ascribed to three motions,

1. An annual motion around the mean position, with an amplitude between 0.06 and 0.10 seconds.

2. A similar motion with a fourteen month period, with an amplitude of between 0.08 and 0.18 seconds.

3. A movement of the mean pole position by about 0.0033 seconds per year, along the 70° westward meridian.

The position of the true pole with respect to the mean CIO pole, is given in terms of two angles, x_P and y_P. The CIO pole is defined to be the mean axis of rotation over the years 1900 to 1905. Values of x_P and y_P are published by the BIH in Circular D. The rotation matrix for polar motion is then given as

$$P = R_2(-x_P)R_1(-y_P) \tag{3.8}$$

Then the earth fixed coordinates r_{ef} of the point are given by,

$$r_{ef} = P \, r_i \tag{3.9}$$

3.5.4 Force Model Components

The forces acting upon any satellite can be divided into two basic groups. The gravitational forces include the earths gravitational attraction, lunar, solar and planetary attractions and tidal effects. The other type of forces are the surface forces, which depend upon the altitude and physical properties of the satellite, and these include the solar radiation pressure and atmospheric drag.

For GPS satellites, at an altitude of 20000 km, the atmospheric drag can be considered negligible [Wells, 1986], and it is usually ignored in the force model. The more significant components of the force model are described in more detail in the following sections.

Gravitational Attraction of the Earth

The force due to the gravitational field is a function of the satellite's position in an earth fixed reference frame. The acceleration vector $\ddot{r}_{ef}$ at a point, due to the gravitational attraction, is obtained from the gradient of the potential field ∇U.

The potential U at a point above the earth, is normally expressed in terms of a spherical harmonic expansion, where

$$U = \frac{GM}{R}\left[1 + \sum_{n=2}^{\infty}\sum_{m=0}^{n}\left(\frac{a}{R}\right)^n P_n^m(\sin\Phi)(C_n^m\cos m\lambda + S_n^m\sin m\lambda)\right] \quad (3.10)$$

Where

G	=	universal gravitational constant
M	=	mass of the earth
a	=	earths equatorial radius
R, λ, Φ	=	earth fixed spherical polar coordinates of the point
n, m	=	degree and order of the spherical harmonic expansion
$P_n^m(\sin\Phi)$	=	Legendre polynomial
C_n^m, S_n^m	=	spherical harmonic coefficients

The expansion of equation (3.10) is the summation of an infinite number of terms. As the altitude of a satellite increases, the effect of the higher order terms is reduced and the expansion is truncated after a finite number of terms. The coefficients C_n^m and S_n^m are defined by various models.

The model recommended for use with the GPS satellites, is the WGS 84 Earth Gravitational Model (EGM). This is an expansion to degree and order 180. However, only the coefficients up to degree and order 18 have been declassified for civilian use. The coefficients of the EGM have been

63

obtained from numerous observations of Doppler, Satellite Laser Ranging, Surface Gravity, Satellite Altimetry, GPS and data pertaining to lumped gravitational coefficients [D.O.D., 1986]. For this model the value of the product GM is taken to be $3896005.0 \times 10^8 \, m^3 \, s^{-2}$.

The GEM T1 geopotential model has also been used for some of the results obtained in this thesis. This model has been derived purely from the tracking data obtained from seventeen different satellites, which had a large range of inclination angles and altitudes [Marsh et al, 1988]. The value of the product GM is taken as $3896004.36 \times 10^8 \, m^3 \, s^{-2}$. The GEM T1 model takes the axis of maximum momentum as its axis, which is defined by the coordinates of the poles between the years 1979 and 1984. The differences $\overline{x}$ and $\overline{y}$ between this pole and the BIH pole are 1.2 m (0."0382) and 8.7 m (0."2803) respectively. Hence, to use this model, the station coordinates should be rotated through $\overline{y}$ about the x axis and through $\overline{x}$ about the y axis. The polar motion values used for the reference frame transformations should also be decreased by $\overline{x}$ and $\overline{y}$.

The gravitational attraction of the earth decreases rapidly with increasing altitude. For GPS satellites at an altitude of 20,000 km, only the first few terms of the geopotential expansion are required. Figure (3.3) shows the difference between a GPS orbit computed using the GEM-T1 geopotential model up to degree and order twenty and one computed using the GEM-T1 geopotential model up to degree and order eight. After 100 hours, the maximum difference between the orbits is less than 2.5 centimetres in the along track component. The maximum orbit lengths used in this research project spanned four days of GPS data, equivalent to about 75 hours, for which the (8×8) geopotential expansion was considered sufficient.

The coefficients C_n^m and S_n^m are given in a normalised form $\overline{C}$ and $\overline{S}$ in most models, including the WGS84 (EGM). The coefficients are

$$C_n^m = N_n^m \overline{C} \qquad (3.11)$$

and

$$S_n^m = N_n^m \overline{S} \qquad (3.12)$$

Orbit component differences for GEM T1

100 hour
orbit integration
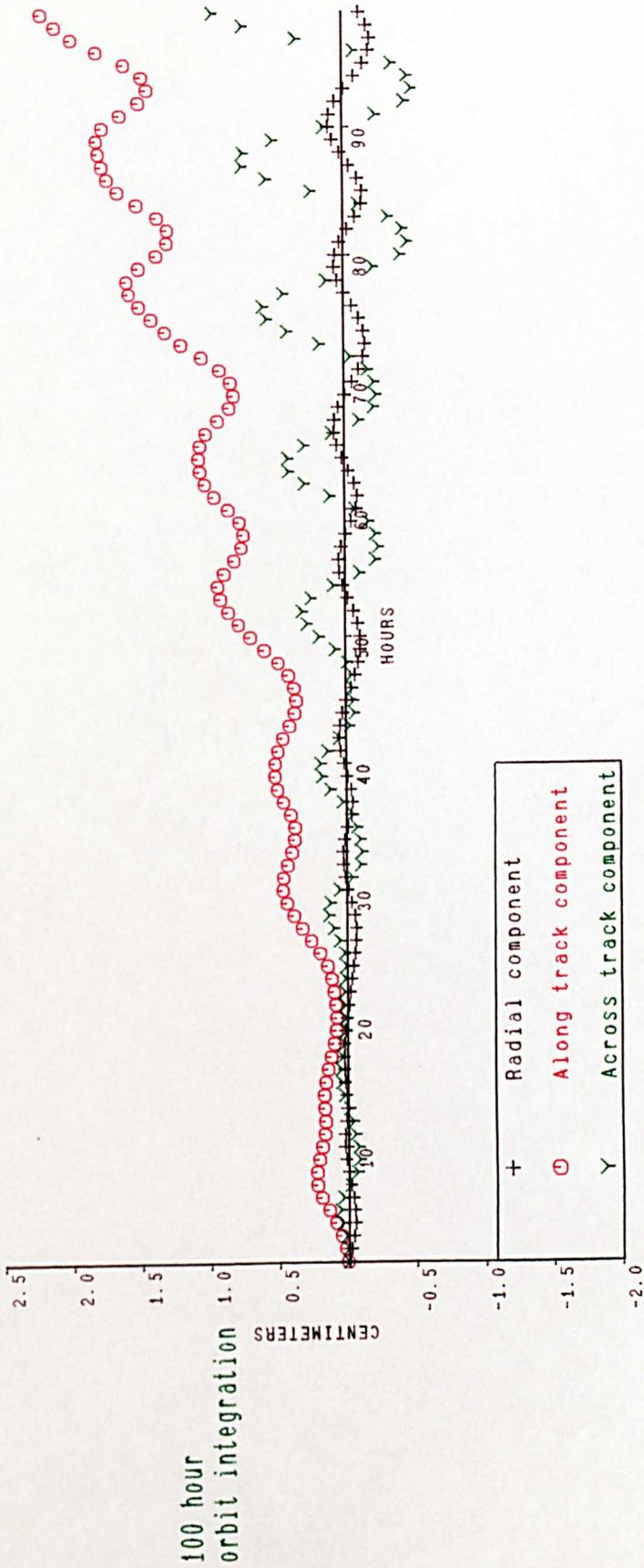
Figure 3.4: Differences between orbits computed using a (20×20) geopotential model and a (8×8) geopotential model.

65

Where N_n^m is the normalising factor,

$$N_n^m = \left[\frac{(n-m)!(2n+1)(2-\delta om)}{(n+m)!} \right]^{\frac{1}{2}} \qquad (3.13)$$

δom is the Kronecker delta which takes values,

$$\delta om = \begin{cases} 0 & \text{if } m \neq 0 \\ 1 & \text{if } m = 0 \end{cases} \qquad (3.14)$$

The earth fixed acceleration vector $\ddot{r}_{ef}$ is given by

$$\ddot{r}_{ef} = \nabla U = \frac{\partial U}{\partial r_{ef}} \qquad (3.15)$$

Where r_{ef} and $\ddot{r}_{ef}$ represent the earth fixed positions and accelerations $x, y, z, \ddot{x}, \ddot{y}, \ddot{z}$. The potential U is expressed in terms of the spherical polar coordinates R, Φ and λ, and use of the chain rule will lead to,

$$\ddot{r}_{ef} = \frac{\partial U}{\partial R} \left(\frac{\partial R}{\partial r_{ef}} \right) + \frac{\partial U}{\partial \Phi} \left(\frac{\partial \Phi}{\partial r_{ef}} \right) + \frac{\partial U}{\partial \lambda} \left(\frac{\partial \lambda}{\partial r_{ef}} \right) \qquad (3.16)$$

The inertial frame acceleration due to the earths gravitational attraction can now be obtained from this,

$$\ddot{r}_{in} = Pr^T N^T E^T P^T \ddot{r}_{ef} \qquad (3.17)$$

Moon, Sun and Planetary Attractions

The gravitational attraction of the sun, the moon and the planets (third bodies) will exert a force on both the satellite and the earth. The inertial frame acceleration of the satellite due to a third body, relative to the earth is given as,

$$\ddot{r} = \ddot{r}_s - \ddot{r}_e \qquad (3.18)$$

Where

$\ddot{r}_s$ = acceleration of satellite towards the third body

$\ddot{r}_e$ = acceleration of earth towards the third body

Hence, the acceleration of the satellite with respect to the earth can be given as [Agrotis, 1984],

$$\ddot{r} = GM_j \left[\frac{r_j - r}{|r_j - r|^3} - \frac{r_j}{|r_j|^3} \right] \qquad (3.19)$$

Where

M_j = mass of the third body j

r_j = inertial frame coordinates of the third body

r = inertial frame coordinates of the satellite

The heliocentric coordinates of the moon and the planets are given in the Jet Propulsion Laboratories ephemeris DE200/LE200. These are inertial (J2000.0) coordinates, given at 0.0 hours TDB each day. Values for the required epoch can be obtained by interpolation.

For GPS satellites, the moon and the sun cause the most significant perturbations to the orbit. Table (3.2) gives the approximate magnitudes of the effects, for a 24 hour orbital arc [Landau and Hein, 1986].

Force	Acceleration(ms^{-2})	Perturbation(m)
Lunar	5×10^{-6}	3000
Solar	2×10^{-6}	800

Table 3.2: Third body effects on GPS orbits

The magnitude of the effect of the planetary attraction is negligible compared to the effects listed in table (3.2), and can be ignored in most computations.

Solid Earth and Ocean Tides

The gravitational attractions of the sun and the moon cause the non-rigid earth to deform. These deformations will affect the earths gravitational attraction and must be accounted for in precise orbit determination. The oceans are also attracted towards the sun and the moon, and the earth responds to this variable ocean loading by deforming. This deformation will also affect the gravitational attraction of the earth, but to a lesser extent than the earth tides. The various models used to account for the solid earth and ocean tides are discussed in [Agrotis, 1984] and [Moore, 1986]. For GPS satellites, the magnitude of these perturbations are given in table (3.3) for a one day arc. [Landau and Hein, 1986]. It can be seen that for arc lengths of up to a few days, the effect of the ocean tides will be relatively small.

Force	Acceleration(ms^{-2})	Perturbation(m)
Solid Earth	1×10^{-9}	0.3
Ocean	0.5×10^{-9}	0.04

Table 3.3: Tidal effects on GPS orbits

Solar Radiation Pressure

One of the most uncertain force model components is the solar radiation pressure. The photons emitted from the sun, collide with the satellite, and this change in momentum, will create a force in the direction away from the sun. The intensity of the radiation obeys the inverse square law, and the radiation pressure is then given as,

$$P = \frac{I_0}{c} \left[\frac{A}{|r - r_j|} \right]^2 \qquad (3.20)$$

Where

A	= Astronomical unit $(1.4959787 \times 10^{11})$
r	= Inertial frame satellite position vector
r_j	= Inertial frame sun position vector
c	= Speed of light
I_0	= Intensity of the radiation at a distance A $(= 1367.2\,Wm^{-2})$

The intensity of the radiation I_0 is not constant, but it varies according to the solar activity. These variations are not expected to exceed about 7 % [Rizos and Stolz, 1985]. The inertial frame acceleration caused by the solar radiation pressure in the direction away from the sun, is obtained by multiplying P, by the area to mass ratio.

$$\ddot{r} = C_R \left(\frac{I_0}{c} \right) \left(\frac{A}{|r - r_j|} \right)^2 \left(\frac{a}{m} \right) \vec{e}_{ss} \qquad (3.21)$$

Where $\vec{e}_{ss}$ is the unit vector in the direction of the satellite from the sun.

The coefficient C_R is a solar radiation reflectance coefficient, which will absorb certain deficiencies in the model, such as a changing area to mass ratio. The value of C_R can be determined as part of the orbit determination process (section 3.7)

Spherical satellites such as LAGEOS can be satisfactorily modelled by using equation (3.21). However, the GPS satellite has a complex shape, with two large solar panels attached to either side, necessitating a more detailed model.

One model which represents the shape and reflective properties of the Block I satellites is the ROCK IV model, which has been developed by the satellite manufacturers [Fliegel et al, 1985]. A local satellite coordinate system is used, which has the z axis directed towards the centre of the earth and the y axis directed along the axis of the solar panels. The x axis forms a right handed system with these (figure 3.5). It is assumed that the momentum reaction wheels on the satellite, align the y axis normal to the plane containing the satellite, sun and earth. Stepping motors then rotate the solar panels to maximise the surface area facing the sun. For the Block II satellites a new solar radiation pressure model has been developed by the satellite manufacturer called the ROCK IV 2 model [Fliegel and Gallini, 1989].

The ROCK IV model uses thirteen distinct surfaces, which are described as either flat or cylindrical. Associated with each surface, is a reflectivity coefficient and a specularity coefficient. The model is used by the NSWC to support long arc orbit computations (40 days). For shorter arcs, a more simplified model can be considered.

One particular effect of the solar radiation pressure on the GPS satellite is a *y bias force*. This is a force acting along the axis of the solar panels (i.e. the y axis). Several reasons have been suggested to account for this force [Fliegel et al, 1985]

1. Misalignment of the solar panel axis with the normal to the plane containing the earth, sun and satellite. This may be due to structural misalignments or misalignments in the satellite attitude sensing mechanism.

2. Thermal re-radiation effects. This is caused by the heat absorbed by the satellite being re-radiated through louvres in the sides of the satellite. These louvres are normal to the y axis and any asymmetric radiation
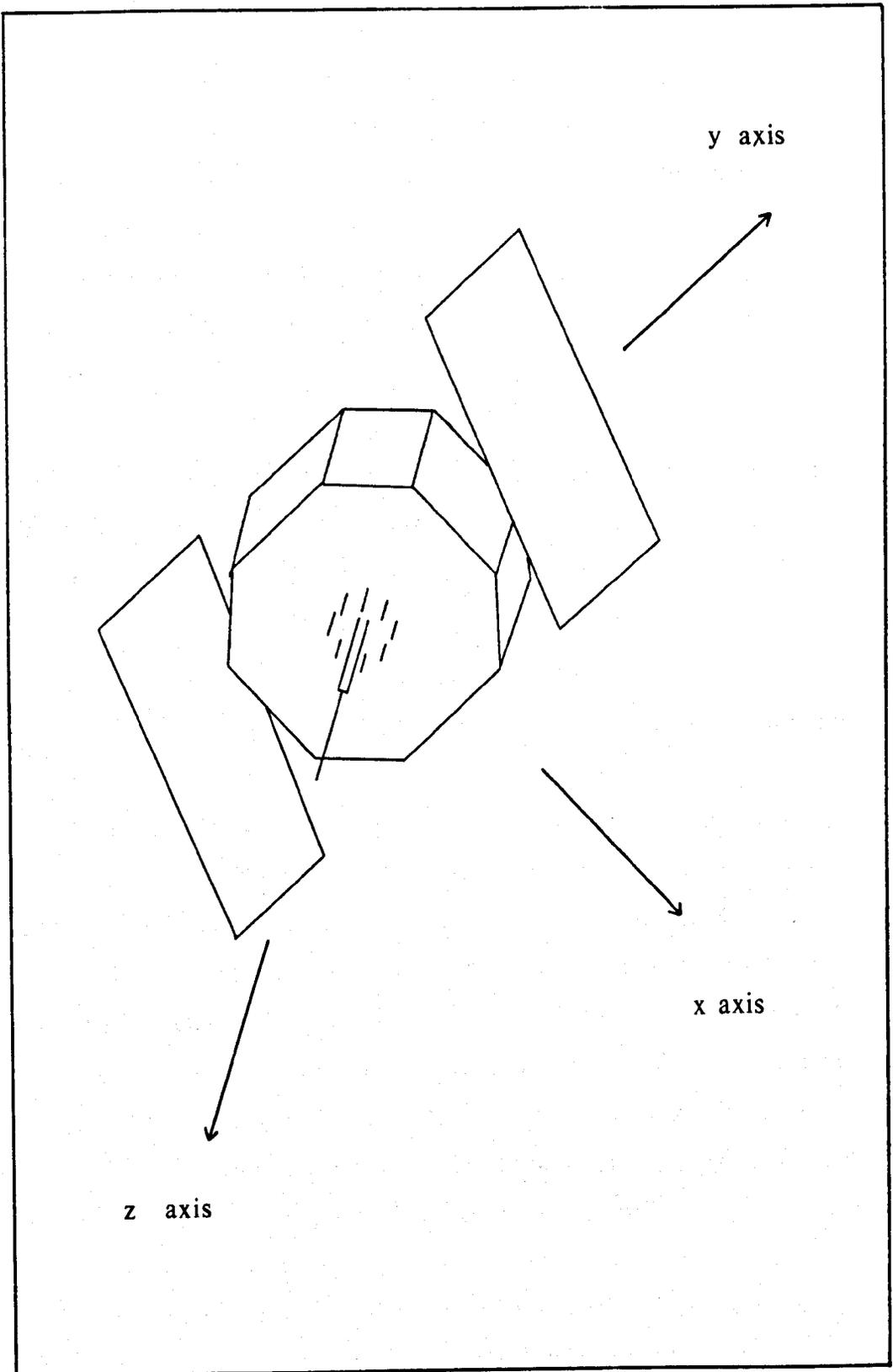
Figure 3.5: Definition of the space vehicle coordinate system

effects will produce a force along the y axis.

The y axis force changes very slowly with time and can be treated as a constant for orbital arcs of a few days. The magnitude of the force can be determined by solving for an acceleration in the y axis direction, as part of the orbit determination process.

The acceleration can be considered as a constant C_y, multiplied by the unit vector $\vec{e}_y$, normal to the satellite, sun and earth plane (figure 3.6).

$$\ddot{r}_{ybias} = C_y \vec{e}_y \tag{3.22}$$

The unit vectors to the sun $(\vec{e}_{ss})$ and the earth $(\vec{e}_{se})$ can be computed directly from the satellite coordinates and the planetary ephemeris. The unit vector normal to these $(\vec{e}_y)$ is given as the vector product,

$$\vec{e}_y = \vec{e}_{ss} \wedge \vec{e}_{se} \tag{3.23}$$

Hence, the constant y bias force C_y can be introduced as part of the orbit determination process.

The high altitude orbit of the GPS satellite means that the satellite's are virtually in constant sunlight. Twice a year, each satellite is eclipsed by the earth and the direct solar radiation pressure will be reduced. Initially, the satellite just touches the area of penumbra (partial shadow), but each revolution increasing the period of eclipse until a maximum of about forty minutes. During these periods it is necessary to cut off the solar radiation pressure model, using a shadow factor η. Sudden changes in the satellite force model will lead to instabilities in the numerical integration, so it is necessary to introduce a gradual change from full sunlight, $\eta = 1.0$, to full shadow in the umbra, $\eta = 0.0$.

A simple model can be used to reduce the shadow linearly through the penumbra. Referring to figure (3.7), the distance from the earth to the top of the umbra cone z can be determined by using similar triangles,

$$\frac{z}{a_e} = \frac{z + |r_s|}{S_r} \tag{3.24}$$

71
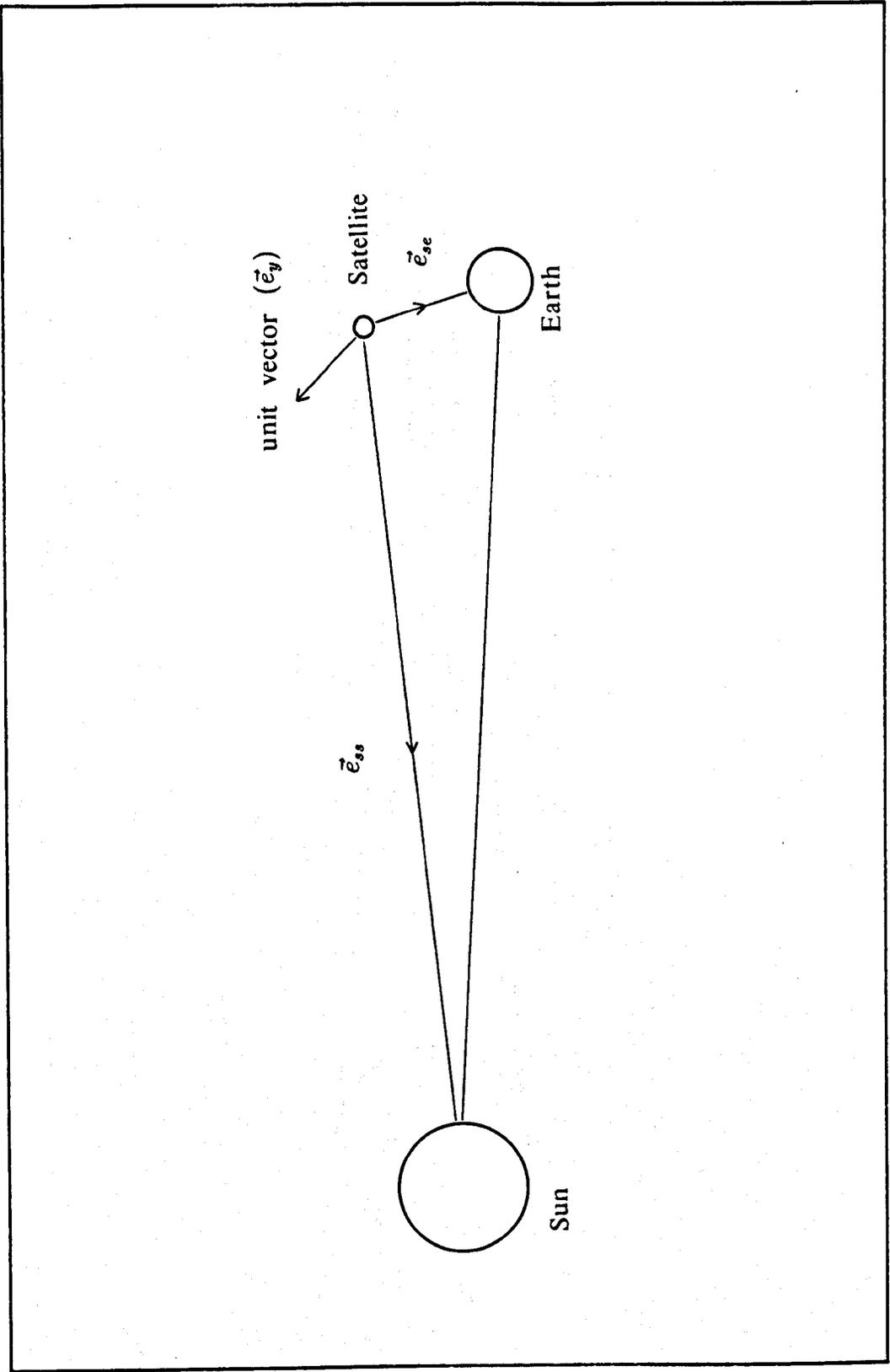
Figure 3.6: Derivation of y bias unit vector
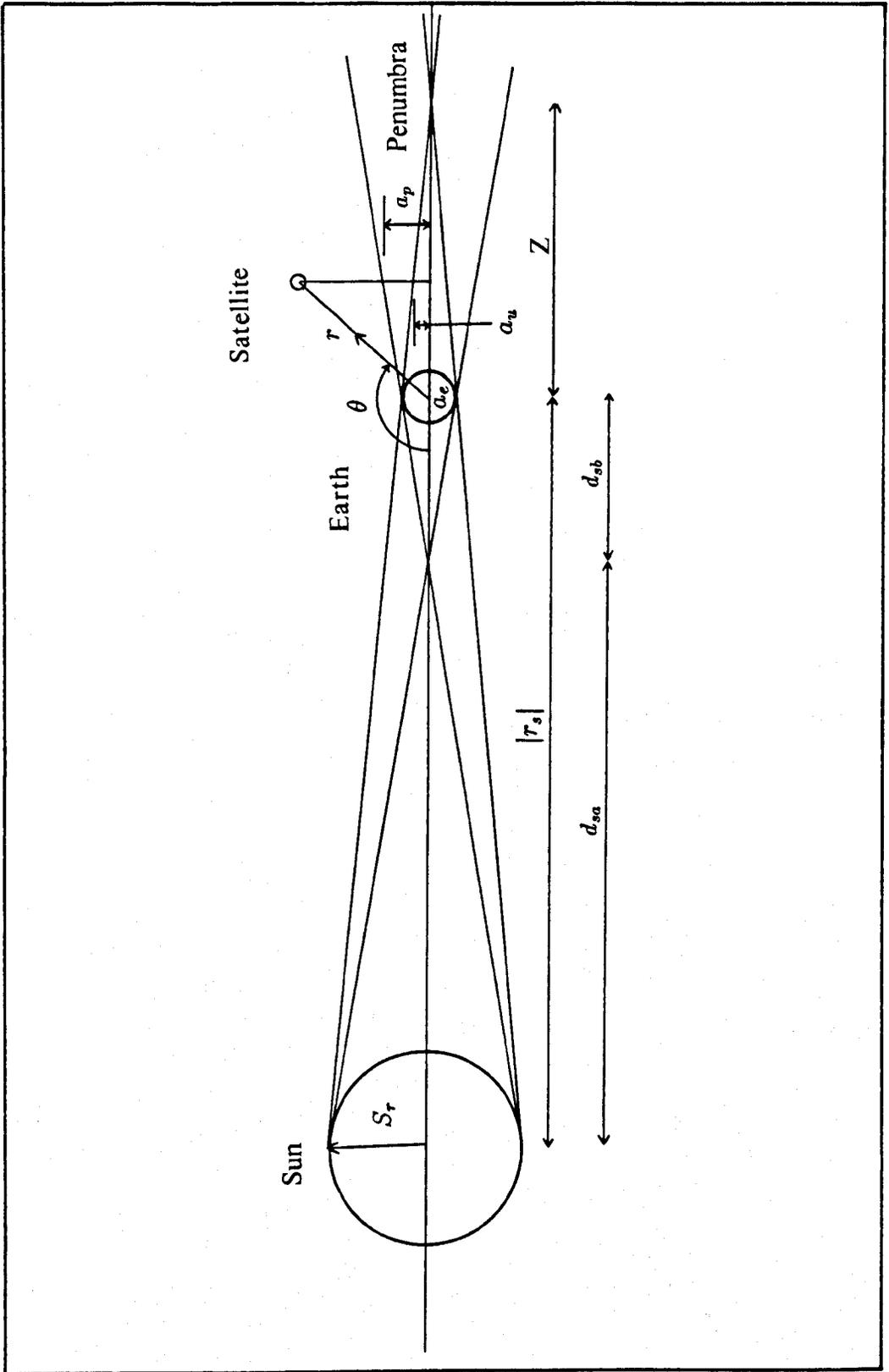
Figure 3.7: Solar radiation shadow model

Hence,

$$z = \frac{a_e |r_s|}{(S_r - a_e)} \tag{3.25}$$

By similar triangles again, it can be seen that,

$$\frac{z - |r \cos \theta|}{a_u} = \frac{z}{a_e} \tag{3.26}$$

and,

$$
\begin{aligned}
a_u &= \left(\frac{a_e}{z}\right)(z - |r \cos \theta|) \\
&= a_e - \left|\frac{r \cos \theta}{r_s}\right|(S_R - a_e) \\
&\approx a_e - \left|\frac{r \cos \theta}{r_s}\right| S_R
\end{aligned}
\tag{3.27}
$$

Where $|r \cos \theta| = \frac{|r.r_s|}{|r_s|}$.

The value of a_u is the radius of the umbra cone, at the position of the satellite. The radius of the penumbra cone a_p, at the satellite position can be determined using similar triangles again in figure (3.7).

$$\frac{a_p - a_e}{|r \cos \theta|} = \frac{a_e}{d_{sb}} \tag{3.28}$$

and,

$$\frac{d_{sa}}{d_{sb}} = \frac{S_R}{a_e} \tag{3.29}$$

Hence equation (3.29) can be written in terms of the distance to the sun $|r_s|$.

$$|r_s| = d_{sb}\left(1 + \frac{S_R}{a_e}\right) \tag{3.30}$$

Combining equations (3.28) and (3.30),

$$
\begin{aligned}
a_p &= a_e + \frac{(a_e + S_R)|r \cos \theta|}{|r_s|} \\
&\approx a_e + \left|\frac{r \cos \theta}{r_s}\right| S_R
\end{aligned}
\tag{3.31}
$$

A value for the shadow factor η can be determined from these values of a_u and a_p. If the value of $\cos \theta$ is greater than zero ($\theta < 90°$), then the satellite is in full sunlight. This is given for $r.r_s > 0$, then $\eta = 1.0$.

If the value of $\cos\theta$ is less than zero, then a further check is required,

$$|r \wedge \vec{e_s}| \geq a_p \quad \eta = 1.0$$

$$|r \wedge \vec{e_s}| \leq a_u \quad \eta = 0.0$$

$$a_p > |r \wedge \vec{e_s}| > a_u \quad \eta = \left(\frac{r \wedge \vec{e_s} - a_u}{a_p - a_u}\right) \tag{3.32}$$

Where $\vec{e_s}$ is the unit vector $\frac{r_s}{|r_s|}$ in the direction of the sun from the earth.

Hence a modified solar radiation model can be used, formed from equations (3.21) (3.22) and the shadow factor η, giving

$$\ddot{r}_{solar} = \eta \left[C_R \left(\frac{A}{|r - r_j|}\right)^2 \left(\frac{I_0}{c}\right) \left(\frac{a}{m}\right) \vec{e_{ss}} + C_y \vec{e_y} \right] \tag{3.33}$$

Where'

$\vec{e_{ss}}$ = unit vector in the sun satellite direction

$\vec{e_y}$ = unit vector in the satellite coordinate system y axis

A further source of solar radiation modelling error is caused by the radiation reflected from the earth's surface (the albedo effect). Modelling the albedo is a very complex process, due to both temporal and spatial variations in the reflected radiation. The magnitude of the albedo pressure is estimated to be in the region of 1 to 2 % of the direct solar radiation pressure, in the radial direction. Consequently, it is usually ignored for orbit computations spanning only a few days. The approximate magnitude of the solar radiation pressure for a one day arc is given in table (3.4).

Force	Acceleration(ms^{-2})	Perturbation(m)
Direct	10^{-7}	200
y bias	10^{-9}	10

Table 3.4: Solar radiation pressure effects

The area to mass ratio will affect the perturbations to the satellite orbit, caused by the solar radiation pressure. For the Block I satellites, the following properties are given [Fliegel et al, 1985],

$A = 5.48m^2$

$m = 440.89$ kg.

For the Block II satellites, the following values are given [Wells, 1986],

$A = 7.25m^2$

$m = 845$ kg.

The mass of the satellite is not constant, but it will decrease as the on-board propellant is used for any required orbital manoeuvres. However, any changes in the area to mass ratio will be absorbed by the scaling coefficient C_R estimated in the least squares solution.

3.6 Equations of Motion

The Newtonian equations of motion of the satellite are given by,

$$\ddot{r} = f(t, r, \dot{r}) \tag{3.34}$$

Where

$\ddot{r}$ = acceleration vector

$\dot{r}$ = velocity vector

r = position vector

t = time

To obtain the velocity at a given time t, equation (3.34) can be integrated with respect to time, from an initial velocity vector $\dot{r}_0$,

$$\dot{r}(t) = \dot{r}_0 + \int_{t_0}^{t} \ddot{r} \delta t \tag{3.35}$$

Integrating equation (3.35) with respect to time, from an initial position vector r_0 will give,

$$r(t) = r_0 + \int_{t_0}^{t} \dot{r} \delta t \tag{3.36}$$

The integration must be carried out in a non rotating (inertial) reference frame, for Newton's Laws to apply. Errors in the state vector $(r_0, \dot{r}_0)$ can be corrected in the least squares adjustment of the orbit (section 3.7).

The integration can be performed by using either analytical or numerical techniques. Analytical techniques lend themselves better to qualitative orbit analysis, whereas a numerical integration technique is more suitable for the quantitative high precision orbit determination that is required here.

76

3.6.1 Numerical Integration

There are two types of numerical integration techniques that can be used, single step and multi-step methods.

When considering a time varying function, the single step method uses the value of the function at time t_i to evaluate the function at time $t_i + h$, where h is the integration step length. For the velocity and acceleration integrals in equations (3.35) and (3.36), this can be written as,

$$\dot{r}(t_i + h) = \dot{r}(t_i) + \int_{t_i}^{t_i+h} \ddot{r} \delta t \tag{3.37}$$

and,

$$r(t_i + h) = r(t_i) + \int_{t_i}^{t_i+h} \dot{r} \delta t \tag{3.38}$$

The integrals of $\ddot{r}$ and $\dot{r}$ may be evaluated by approximating the function over the interval t_i to $(t_i + h)$, by using one of the many single step methods, such as the Runge-Kutta procedure [Spencer et al, 1977]. The error associated with the Runge-Kutta procedure, is not easy to determine. It is estimated that the error is of the order h^m, where m is the order of the Runge-Kutta procedure. Single step methods are particularly time consuming as each integration step will require m function evaluations.

A predictor-corrector scheme is a commonly used multi-step method. An nth order multi-step method, will use the previous $n+1$ values of the function, to predict the $(n+1)^{th}$ value. The corrected value of the function is now determined, using the predicted value along with the previous n values.

The Adams-Bashforth predictor-corrector scheme, uses the Newton backward difference formula to determine the value of the integral. The multi-step technique has the disadvantage that the step length cannot be altered during the integration process, so the step length must be carefully chosen at the start.

An estimate of the error can be obtained from the difference between the predicted and corrected values. The multistep requires only two function evaluations at each epoch (predictor and corrector), and can use a step length eight times larger than the single step method [Ashkenazi et al, 1984]. This makes the multi-step method much more efficient than the single step

method. Normally, the single step method is used to determine the first n values of the function, then an nth order multi-step method is used. The current generation of orbit determination software at Nottingham University uses a 4th order Runge-Kutta starting procedure followed by a 9th order Adams-Bashforth predictor-corrector scheme when enough initial steps have been evaluated. A full description of the use of single step and multi-step methods for orbit determination is given in *Agrotis* [1984].

A test was carried out to determine an efficient step length for the predictor-corrector integration scheme. A compromise has to be reached between the computational speed and the level of accuracy required. A comparison is given in table (3.5) of an orbit computed using different step lengths. The table shows the x, y and z coordinates of the satellite in metres after a 75 hour integration.

Step length (seconds)	x (m)	y(m)	z(m)
120	11913981.633	633699.812	23380570.906
240	11913981.633	633699.812	23380570.906
480	11913981.658	633699.799	23380570.899

Table 3.5: Comparison of different orbit integration step lengths

It can be seen that for a three day arc, the differences between the 120 and 240 second step lengths were below the millimetre level, but much larger differences occurred when a 480 second step length was used. The 240 second step length was selected as a maximum length for the GPS orbit integration.

The numerical integration of the force model, will produce a series of satellite position and velocity vectors in the inertial reference frame, at discrete intervals of time. If the satellite state vector, and the force model were accurately known, this reference orbit could be used directly for the processing of the GPS observables. Errors in this reference orbit can be corrected by using a least squares adjustment, with the GPS observables.

3.7 Least Squares Adjustment of the Orbital Parameters

The satellite state vector r_{on} $(x_0, y_0, z_0, \dot{x}_0, \dot{y}_0, \dot{z}_0)$ required to initialise the integration process need not be known precisely. Corrections can be made to the vector by using observations made between the satellites and the network of tracking sites. The two basic GPS observables, pseudorange and carrier phase, can both be used for this purpose.

The pseudorange has the advantage that it is an unambiguous measurement, but it is less precise than the carrier phase measurement. If the phase integer ambiguity can be satisfactorily resolved, then the carrier phase measurement will give a highly precise observable. The carrier phase can be used for a simultaneous adjustment of the selected receiver coordinates and the satellite state vector. The double difference phase observation equation (2.16) can be linearised about the initial value of r_{on}, to give an expanded form of equation (2.19),

$$
\frac{f}{c}\left[\left(\frac{\partial \rho_A^i}{\partial X_A} - \frac{\partial \rho_A^j}{\partial X_A}\right)\Delta X_A + \left(\frac{\partial \rho_A^i}{\partial Y_A} - \frac{\partial \rho_A^j}{\partial Y_A}\right)\Delta Y_A + \left(\frac{\partial \rho_A^i}{\partial Z_A} - \frac{\partial \rho_A^j}{\partial Z_A}\right)\Delta Z_A\right]
$$

$$
-\frac{f}{c}\left[\left(\frac{\partial \rho_B^i}{\partial X_B} - \frac{\partial \rho_B^j}{\partial X_B}\right)\Delta X_B + \left(\frac{\partial \rho_B^i}{\partial Y_B} - \frac{\partial \rho_B^j}{\partial Y_B}\right)\Delta Y_B + \left(\frac{\partial \rho_B^i}{\partial Z_B} - \frac{\partial \rho_B^j}{\partial Z_B}\right)\Delta Z_B\right]
$$

$$
+\frac{f}{c}\sum_{n=1}^{6}\left[\left(\frac{\partial \rho_A^i}{\partial r_{on}^i} - \frac{\partial \rho_B^i}{\partial r_{on}^i}\right)\Delta r_{on}^i - \left(\frac{\partial \rho_A^j}{\partial r_{on}^j} - \frac{\partial \rho_B^j}{\partial r_{on}^j}\right)\Delta r_{on}^j\right]
$$

$$
+\frac{\partial \Phi_{AB}^{ij}}{\partial N_{AB}^{ij}}\Delta N_{AB}^{ij} = (O_\Phi - C_\Phi) + \nu \tag{3.39}
$$

Where

f =   frequency

c =   speed of light

ρ_A^i =   geometrical range between satellite i at time of signal transmission and receiver A at time of signal reception

X_A, Y_A, Z_A =   approximate coordinates of receiver A

r_{on}^i =   satellite state vector for n $=$ 1 to 6 $(x_0, y_0, z_0, \dot{x}_0, \dot{y}_0, \dot{z}_0)$

O_Φ, C_Φ =   observed and computed values of the double difference phase

N_{AB}^{ij} =   integer phase ambiguity

ν =   double difference phase residual

It is necessary to evaluate the various partial derivatives in equation (3.39). The partial derivatives of the form $\partial \rho_A^i / \partial X_A$ are evaluated as in equation (2.5),

$$\frac{\partial \rho_A^i}{\partial X_A} = \frac{x^i - X_A}{\rho_A^i} \qquad (3.40)$$

Where x^i is the x coordinate of satellite i.

The chain rule can be used to expand the partials of range with respect to satellite vector,

$$\frac{\partial \rho_A^i}{\partial r_{on}^i} = \frac{\partial \rho_A^i}{\partial x^i}\left(\frac{\partial x^i}{\partial r_{on}^i}\right) + \frac{\partial \rho_A^i}{\partial y^i}\left(\frac{\partial y^i}{\partial r_{on}^i}\right) + \frac{\partial \rho_A^i}{\partial z^i}\left(\frac{\partial z^i}{\partial r_{on}^i}\right) \qquad (3.41)$$

The partials of the form $\partial \rho_A^i / \partial x^i$ can be obtained by differentiating equation (2.4) with respect to x^i,

$$\frac{\partial \rho_A^i}{\partial x^i} = \frac{X_A - x^i}{\rho_A^i} \qquad (3.42)$$

Similar expressions can be derived for y^i and z^i.

The partials of the satellite position with respect to the satellite state vector $\partial x^i / \partial r_{on}^i$ cannot be derived analytically, instead they are obtained from the numerical integration. A least squares adjustment will only provide a first order correction to the estimated parameters, so it is only necessary to integrate the most significant component of the force model, when computing

the partial derivatives. The effect of ignoring all the other components except the gravitational potential is discussed in *Agrotis* [1984].

Considering satellite i, the acceleration vector $\ddot{r}^i$ due to the earths gravitational attraction is given as,

$$\ddot{r}^i = \frac{\partial U}{\partial r^i} \tag{3.43}$$

Differentiating with respect to the satellite vector gives,

$$\frac{\partial \ddot{r}^i}{\partial r_{on}^i} = \frac{\partial^2 U}{\partial r_{on}^i \partial r^i} = \frac{d^2}{dt^2}\left(\frac{\partial r^i}{\partial r_{on}^i}\right) \tag{3.44}$$

Where

$$\ddot{r}^i \;=\; \text{satellite acceleration vector } (\ddot{x}^i, \ddot{y}^i, \ddot{z}^i)$$
$$\qquad \text{in the inertial reference frame at time } t$$
$$r^i \;=\; \text{satellite position vector } (x^i, y^i, z^i)$$
$$\qquad \text{in the inertial reference frame at time } t$$

The partial derivative of the acceleration with respect to the satellite state vector can be expanded by the chain rule,

$$\frac{\partial \ddot{r}^i}{\partial r_{on}^i} = \frac{\partial \ddot{r}^i}{\partial x^i}\left(\frac{\partial x^i}{\partial r_{on}^i}\right) + \frac{\partial \ddot{r}^i}{\partial y^i}\left(\frac{\partial y^i}{\partial r_{on}^i}\right) + \frac{\partial \ddot{r}^i}{\partial z^i}\left(\frac{\partial z^i}{\partial r_{on}^i}\right)$$
$$+ \frac{\partial \ddot{r}^i}{\partial \dot{x}^i}\left(\frac{\partial \dot{x}^i}{\partial r_{on}^i}\right) + \frac{\partial \ddot{r}^i}{\partial \dot{y}^i}\left(\frac{\partial \dot{y}^i}{\partial r_{on}^i}\right) + \frac{\partial \ddot{r}^i}{\partial \dot{z}^i}\left(\frac{\partial \dot{z}^i}{\partial r_{on}^i}\right) \tag{3.45}$$

The partials of the satellite's acceleration vector with respect to the position and velocity vectors are evaluated as follows [Agrotis, 1984],

$$\frac{\partial \ddot{x}^i}{\partial x^i} = \frac{\partial^2 U}{\partial x^{i2}}, \quad \frac{\partial \ddot{x}^i}{\partial y^i} = \frac{\partial^2 U}{\partial y^i \partial x^i}, \quad \frac{\partial \ddot{x}^i}{\partial \dot{x}^i} = 0 \tag{3.46}$$

The partial derivatives of the satellite's position and velocity vector with respect to the state vector are given as,

$$\frac{\partial \dot{x}^i}{\partial r_{on}^i} = \left[\frac{\partial \dot{x}^i}{\partial r_{on}^i}\right]_{t_0} + \int_{t_0}^{t} \frac{\partial \ddot{x}^i}{\partial r_{on}^i}\, dt \tag{3.47}$$

and integrating again gives,

$$\frac{\partial x^i}{\partial r_{on}^i} = \left[\frac{\partial x^i}{\partial r_{on}^i}\right]_{t_0} + \int_{t_0}^{t} \frac{\partial \dot{x}^i}{\partial r_{on}^i}\, dt \tag{3.48}$$

The initial values of $\partial r_m^i / \partial r_{on}^i$ at t_0 are easily obtained for $r_m^i = (x^i, y^i, z^i)$ as,

$$\frac{\partial r_m^i}{\partial r_{on}^i} = \begin{cases} 0 & \text{if } m \neq n \\ 1 & \text{if } m = n \end{cases} \tag{3.49}$$

Similar terms can be added to equation (3.39) to solve for any unknown force model components. The equation for the direct solar radiation pressure coefficient C_R would be,

$$\frac{f}{c}\left[\left(\frac{\partial \rho_A^i}{\partial C_R^i} - \frac{\partial \rho_B^i}{\partial C_R^i}\right)\Delta C_R^i - \left(\frac{\partial \rho_A^j}{\partial C_R^j} - \frac{\partial \rho_B^j}{\partial C_R^j}\right)\Delta C_R^j\right] \tag{3.50}$$

The partial derivatives of the form $\partial \rho_A^i / \partial C_R^i$ are expanded in a similar way to equation (3.41),

$$\frac{\partial \rho_A^i}{\partial C_R^i} = \frac{\partial \rho_A^i}{\partial x^i}\left(\frac{\partial x^i}{\partial C_R^i}\right) + \frac{\partial \rho_A^i}{\partial y^i}\left(\frac{\partial y^i}{\partial C_R^i}\right) + \frac{\partial \rho_A^i}{\partial z^i}\left(\frac{\partial z^i}{\partial C_R^i}\right) \tag{3.51}$$

The partials of the satellite position and velocity vector with respect to the solar radiation reflectance coefficient are again obtained by numerical integration,

$$\frac{\partial \dot{x}^i}{\partial C_R^i} = \left[\frac{\partial \dot{x}^i}{\partial C_R^i}\right]_{t_0} + \int_{t_0}^t \frac{\partial \ddot{x}^i}{\partial C_R^i}\, dt \tag{3.52}$$

and integrating again gives,

$$\frac{\partial x^i}{\partial C_R^i} = \left[\frac{\partial x^i}{\partial C_R^i}\right]_{t_0} + \int_{t_0}^t \frac{\partial \dot{x}^i}{\partial C_R^i}\, dt \tag{3.53}$$

Similar expressions are used for the y and z satellite coordinates.

The initial values of $\partial r_m^i / \partial C_R^i$ at t_0 are obtained for $r_m^i = (x^i, y^i, z^i, \dot{x}^i, \dot{y}^i, \dot{z}^i)$ as,

$$\frac{\partial r_m^i}{\partial C_R i} = 0 \tag{3.54}$$

The acceleration partials with respect to the state vector are given by,

$$\begin{aligned}
\frac{\partial \ddot{x}^i}{\partial C_R^i} &= \frac{\partial \ddot{x}^i}{\partial x^i}\left(\frac{\partial x^i}{\partial C_R^i}\right) + \frac{\partial \ddot{x}^i}{\partial y^i}\left(\frac{\partial y^i}{\partial C_R^i}\right) + \frac{\partial \ddot{x}^i}{\partial z^i}\left(\frac{\partial z^i}{\partial C_R^i}\right) \\
&\quad \frac{\partial \ddot{x}^i}{\partial \dot{x}^i}\left(\frac{\partial \dot{x}^i}{\partial C_R^i}\right) + \frac{\partial \ddot{x}^i}{\partial \dot{y}^i}\left(\frac{\partial \dot{y}^i}{\partial C_R^i}\right) + \frac{\partial \ddot{x}^i}{\partial \dot{z}^i}\left(\frac{\partial \dot{z}^i}{\partial C_R^i}\right) \\
&\quad\quad + \frac{\partial \ddot{x}^i}{\partial C_R^i}
\end{aligned} \tag{3.55}$$

The partial $\partial \ddot{x}^i / \partial C_r^i$ is obtained from differentiating equation (3.33).

The constant y bias acceleration C_y can be estimated as part of the least squares adjustment by including the expression,

$$\frac{f}{c}\left[\left(\frac{\partial \rho_A^i}{\partial C_y^i} - \frac{\partial \rho_B^i}{\partial C_y^i}\right)\Delta C_y^i - \left(\frac{\partial \rho_A^j}{\partial C_y^j} - \frac{\partial \rho_B^j}{\partial C_y^j}\right)\Delta C_y^j\right] \qquad (3.56)$$

The partials are evaluated in a similar way to the partials for the solar radiation reflectance coefficient C_R.

Hence, observation equations of a similar form to equation (3.39) can be formed to estimate both the receiver and the satellite dependent unknowns. The normal equations are formed from these observation equations and solved using the methods described in chapter 2. In the least squares adjustment, the coordinates of at least three of the fiducial sites will be held fixed to VLBI or SLR determined coordinates and estimates made for the non fiducial receiver coordinates, initial phase ambiguities, satellite state vectors and any solar radiation pressure parameters required.

3.8   Assessment of Orbital Accuracy

One of the problems encountered in an orbit determination process, is the estimation of the quality of the orbit. Three methods have been used in this research project.

1. **Orbit repeatability**

   Two overlapping, independently determined orbital arcs can be compared against each other to test the repeatability of two orbits. For example, when considering an observation period of six days, the repeatability of the orbits can be assessed by estimating two independent, three day orbits from alternate days of data. This is shown in figure (3.8), described as interleaved arcs. The orbits can then be compared over the common time periods between days 2 and 5.

   The alternative test is to use two adjacent orbits, and extrapolate the first orbit onto the second orbit (figure 3.9). This is a more stringent test of the orbital quality, because any errors in the satellite force model or in the initial state vector, will cause a degradation of the accuracy of the orbit, as it is predicted further away from the observation period.

83
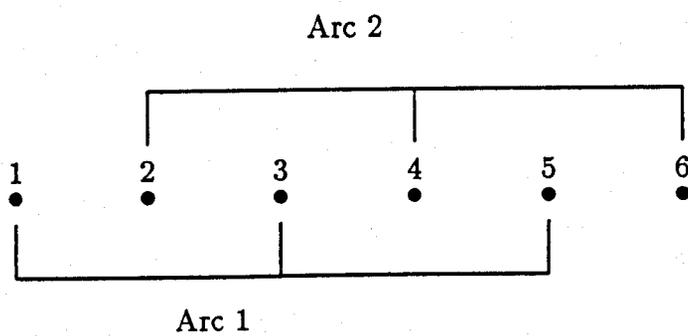
Figure 3.8: Orbit repeatability : interleaved arcs

Arc 2

1   2   3   4   5   6

Arc 1 extrapolated over arc 2
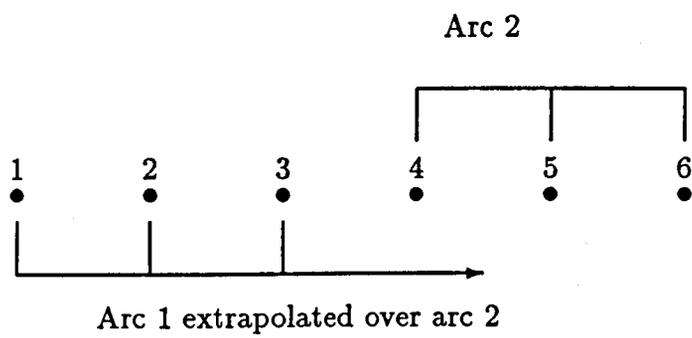
Figure 3.9: Orbit repeatability : extrapolated arcs

If enough data is available, a different network of fiducial sites can be used to compute the orbit, and a comparison can be made from orbits computed using the same period of observations.

The orbit repeatability is not really a test of external accuracy, rather it tests the internal accuracy, as systematic errors may well produce the same biases in the two independent orbital arcs. The external accuracy of the orbit can be estimated by comparison with an orbit computed using an independent data set and software package. The NSWC precise ephemeris can be used for this purpose.

2. **Comparison with a precise ephemeris**

The NSWC precise ephemeris is estimated to be accurate to within five or ten meters. Hence, it is only useful to check the accuracy of an orbit to a similar level of accuracy. One problem with using this method of comparison is determining the differences which may exist between the coordinate reference frames that have been used to compute the orbits. These differences may introduce systematic biases between the two orbits.

3. **Baseline comparison of GPS with other space techniques**

The simplified relationship between the orbital accuracy and baseline error was given in equation (2.57). The baseline error can be best estimated by comparison with VLBI or SLR determined baselines. Hence, an estimate of the orbital accuracy can be derived from this. The estimated baseline lengths will also include the effects of other error sources and this must be considered in any comparison. *Lichten* [1989] suggested that the baseline error ΔL on a line of length L can be expressed as,

$$\Delta L^2 \approx A^2 + B^2 L^2 \qquad (3.57)$$

where A and B describe the contributions to the baseline error from the orbit independent effects and the orbit dependent effects respectively. For short baselines the orbit independent effects such as the

86

measurement noise and any errors in the site eccentricity vectors will be more dominant. However, as the baseline increases in length, the orbit dependent terms become more dominant and the expression simplifies into equation (2.57). Therefore, the longer baselines are more suitable for estimating the accuracy of the orbit than the shorter baselines, which may be affected by the other error sources.

This method of comparing baselines has been used extensively in this thesis for estimating the orbital accuracy, because one of the primary objectives of GPS orbit determination is the computation of high accuracy baselines.

3.9   Orbit Relaxation

A simpler alternative to using the GPS satellite force model to improve the satellite orbit is to use an orbit relaxation technique. For short arcs (up to about three hours of data), selected elements of the orbit are allowed to *relax* as part of the least squares adjustment. Whilst this process will not produce a precise orbit, it has been shown with SLR data to produce precise relative coordinates of the tracking stations [Moore and Ashkenazi, 1987]. This is possible by allowing for systematic translations and accelerations in the orbit (through the estimated orbital parameters), which will absorb certain errors in the satellite observations and the satellite orbit model (broadcast ephemeris). For GPS satellites, corrections can be determined to some of the keplerian elements given in the broadcast ephemeris. Six of these broadcast elements describe a mean orbital ellipse from a given reference time t_0, which are

e - eccentricity

$\sqrt{a}$ - square root of the semi-major axis

i - inclination at time t_0

ω - argument of perigee

Ω_0 - right ascension parameter

at start of GPS week

M_0 - Mean anomaly at time t_0

The partial derivatives of the receiver to satellite range, with respect to the these six orbital parameters can be formed by differentiating the expressions given in [Ashkenazi and Moore, 1986], which give the cartesian coordinates of the satellite in terms of the Keplerian elements. These can then be included in the observation equation given in equation (2.19). These observation equations have been implemented into **PANIC**, the GPS network adjustment package at Nottingham, by a postgraduate student as part of his research project. Details of the derivation of the partial derivatives and the results obtained can be found in his thesis [Aquino, 1989].

In the least squares adjustment process, the argument of perigee term ω is held fixed, because of its high correlation with the mean anomaly term M_0. The coordinates of three or more fiducial sites are held fixed and estimates are made for the non fiducial coordinates, the initial phase ambiguities and the orbital unknowns. Two methods of solution have been attempted in the least squares adjustment,

1. Solving for one set of the five broadcast elements $(e, sqrta, i\Omega_0, M_0)$ for each satellite.

2. Solving for a new set of the five elements every hour for each satellite.

Generally, the second method of orbit relaxation has been shown to give better relative station coordinates, in comparison to the VLBI determined coordinates. This may be because the elements of the broadcast ephemeris are not true keplerian elements and they only represent the satellite orbit for a limited period of time. A comparison between the second method of orbit

relaxation and the orbit determination process (integrated force model) are
given in chapter 7.

Chapter 4.
GPS Orbit Determination Software

GPS Orbit Determination Software

4.1 Introduction

All the software used for orbit determination and GPS processing at Nottingham University has been written in-house by postgraduate students. The programs are written in standard FORTRAN 77, designed to run on the University's ICL 3900 mainframe computer. The majority of the programs are designed to run as batch jobs, which is more efficient for the large programs and data sets, which require a long run time on the computer. It is also more convenient for repetitive computations.

Work on GPS and orbit determination has previously been considered as two separate fields before the start of this research project, with GPS research concentrating on using the broadcast ephemeris. Orbit determination software was primarily written for the LAGEOS satellite, used for Satellite Laser Ranging. The research work has involved the integration of these two distinct software packages and the writing of any necessary software required for the GPS orbit determination. A flow diagram is given in figure (4.1) showing the main programs required for the determination of GPS satellite orbits. These programs are described in further detail in the following sections.

4.2 SODAPOP

SODAPOP (an acronym for Satellite Orbit Determination and Analysis Package Of Programs) has been under development since 1981. Three postgraduate students have been involved in writing the software and details of the current capabilities of the package are given in [Hill, 1989]. Two of the
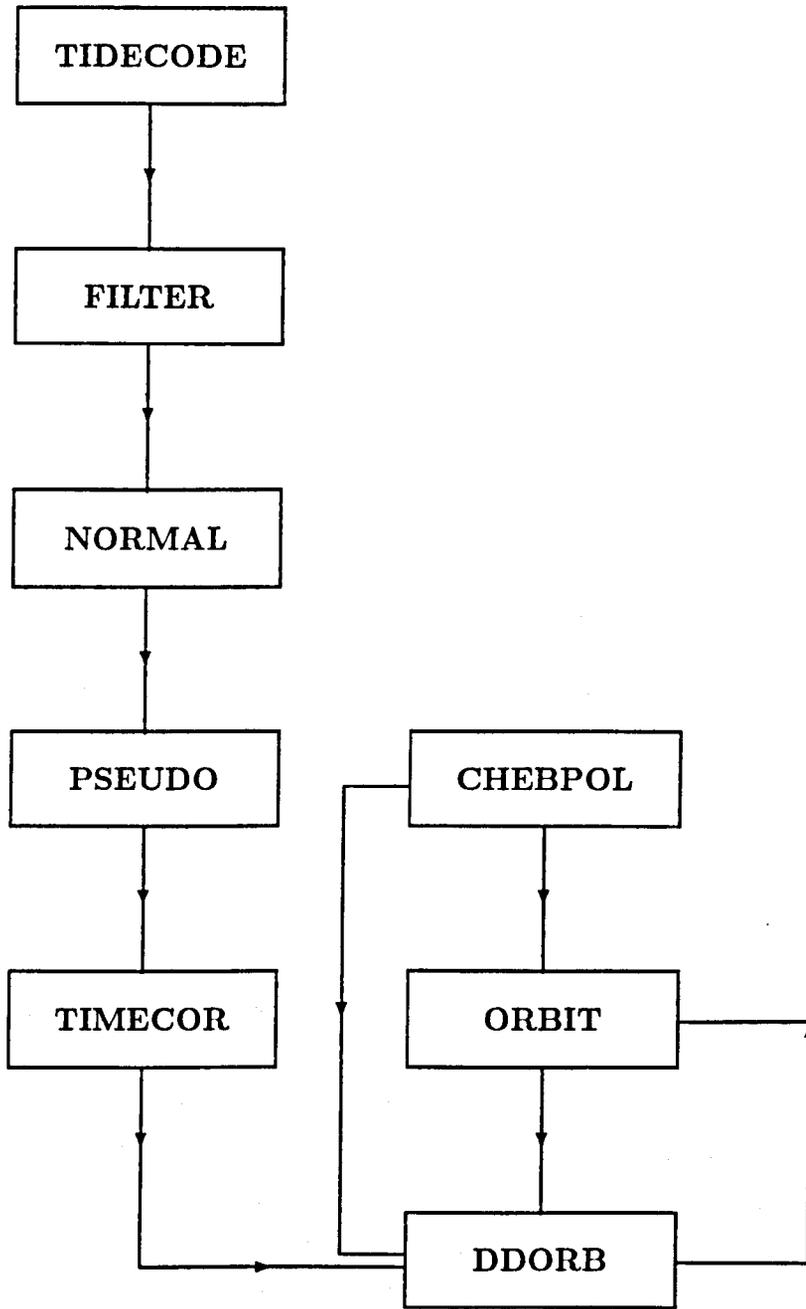
Figure 4.1: Flow diagram for GPS orbit determination

programs in this package have been used for the GPS orbit determination, these are **ORBIT** and **CHEBPOL**.

4.2.1 ORBIT

ORBIT is a precise orbit integration program, initially developed for the LAGEOS satellite [Agrotis, 1984]. The numerical integration is initiated from a given state vector (approximate position and velocity of the satellite) and the position and velocity vectors of the satellite are output at discrete intervals in time.

Very few changes were necessary to allow the program to be used for GPS satellites. These involved implementing the satellite y bias acceleration to the satellite force model and the new shadow factor model. A brief description of the program is given in this section with the necessary parameters required for the GPS satellites.

Input Parameters

The following parameters are required for the program and they are input in a control file.

- Satellite state vector[1] given in an earth fixed or inertial (J2000.0) reference frame. This can be obtained from either the broadcast or precise ephemeris.

- Geopotential model. The degree and order of the geopotential model are selected. The WGS 84 and GEM-T1 models have both been tested for the GPS satellites.

- Centre of mass correction. The distance between the centre of mass of the satellite and the GPS antenna has been estimated as 1.0 m.

- Area to mass ratio. A value of $0.0124 m^2 kg^{-1}$ has been used for the Block I satellites.

- GM. The recommended values of the product GM have been
  GEM-T1 $3986004.36 \times 10^8 m^3 s^{-2}$

---

[1]Given in cartesian coordinates

WGS 84 $3986005.00 \times 10^8 m^3 s^{-2}$

- Direct solar radiation pressure coefficient (C_R). An initial estimate of 1.5 has been used.

- Y bias acceleration (C_y). Initial estimate of 0.0 ms^{-2} used.

- Mean earth rotation rate of 7292115×10^{-11} $rad\,s^{-1}$ (WGS 84 value).

- Ocean tide model. Schwiderski or GEM T1 if using GEM T1 geopotential model.

- Integration step length. 240 seconds for predictor-corrector.

- Number of integration steps required.

- Selection of force model parameters for which the partial derivatives are to be evaluated. These include C_R and C_y. Further partial derivatives can be evaluated for some other parameters, although they are not used for GPS orbit determination.

- Time, date and year in which to start the integration. These correspond to the satellite state vector.

Reference Frame Transformation

It is necessary to convert all the acceleration vectors into the inertial reference frame (J2000.0) prior to the numerical integration. The model used for the transformation includes the IAU 1976 precession and the IAU 1980 nutation models. Earth rotation and polar motion values are obtained from the BIH Circular D at five day intervals. These are input into **ORBIT** in the form of a random access file, generated by the ancillary program **CHEBPOL**. The planetary ephemeris (DE200/LE200) required for the force model is also included in this file.

Force Model

The GPS satellite force model used in the integration is comprised of the following components.

- WGS 84 or GEM T1 geopotential model up to degree and order eight.

- Lunar, Solar and Planetary attractions (Venus, Mars, Saturn and Jupiter).

- Solid earth tides. Simplified Wahr, [Agrotis, 1984], [Moore, 1986].

- Ocean tides. Schwiderski or GEM T1 models.

- Direct solar radiation pressure.

- Y bias acceleration.

Also included is the solar radiation cut-off model, to gradually reduce the solar radiation pressure during an eclipse. The models for the planetary attractions and the ocean tides are not essential for orbital arcs of a few days, but they have been included for possible longer arc computations.

Numerical Integration

The numerical integration is carried out in the J2000.0 inertial reference frame. A 4th order Runge-Kutta (single step) procedure is used to start the integration. Once enough initial steps have been evaluated, a 9th order Adams-Bashforth predictor-corrector scheme is then used.

Output

The main output is contained within two random access files, comprised of,

1. Satellite position and velocity vectors at discrete intervals (same interval as the predictor-corrector integration step length). These are given in the earth fixed or the inertial (J2000.0) coordinate reference frames.

2. Partial derivatives of the satellite position with respect to the state vector and any required force model components (eg. C_R or C_y).

The orbit integration program is designed for a single satellite and it will have to be repeated for all the GPS satellites observed. The satellite ephemeris and partial derivatives are then used as input into the least squares

94

adjustment program **DDORB**, to produce a better estimate for the satellite state vector and the force model components. These updated values can then be input into **ORBIT** again to produce a more accurate orbit.

4.2.2 CHEBPOL

CHEBPOL is a program developed to reduce the computation time required by the orbit integration and the orbit adjustment programs. It computes daily sets of Chebyshev polynomial coefficients to represent the nutation and precession matrices for a period of forty days. This eliminates the need to evaluate the 106 term nutation series at every integration step in **ORBIT** and at every observation epoch in the least squares adjustment program **DDORB**. Also produced in the program are linear interpolation coefficients for the (UT1 - UTC) values and the polar motion values.

Input

The following items are required,

- (UT1 - UTC) and polar motion series. BIH circular D 5 day values used.

- Planetary ephemeris (JPL DE200/LE200). The values given at 0.0 hours TDB each day are interpolated using Everetts algorithm.

- Start day and year to begin the computations.

- Integer second difference between UT1 and UTC at the start of computation. This was 23 seconds before 1/1/88 and 24 seconds after 1/1/88 for the GPS data analysed.

Output

The output is contained in a random access which has the forty days of daily Chebyshev polynomial coefficients for,

- Nutation matrix.

- Precession matrix.

- Planetary ephemeris.

Linear interpolation coefficients are provided for,

- (UT1 - UTC).

- Polar motion.

4.3 GPS Software Package

In the last seven years, nine postgraduate students have been involved with GPS research projects at Nottingham. The programs currently in use have been written, modified and updated by several of the students and it is difficult to attribute programs to particular authors. The reader is referred to [de la Fuente, 1988] for the description of the GPS software up to 1988. The programs described in this section refer only to those required for the GPS orbit determination, using data collected from the TI 4100 receiver. Data preprocessing programs have also been written for the WM 101 and the Trimble satellite receivers.

4.3.1 TIDECODE

TIDECODE was developed specifically for decoding the data collected on the TI 4100 receiver. The program forms the pseudorange and carrier observables, the time tags at which they were recorded and the satellite ephemeris from the binary data strings recorded by the receiver. Further data can be decoded as required, such the broadcast ionospheric corrections. The measurements are extracted and placed into two types of file,

1. Measurement file containing pseudoranges, carrier phase, time tags and satellite identification numbers.

2. Ephemeris files for each satellite.

The program also calculates third differences with time during the decoding process, to check for the occurrence of cycle slips.

4.3.2 EAFILTER

EAFILTER is a data filtering program, which serves three main purposes,

1. Re-orders the data into a specified satellite order and rejects any unwanted satellites.

2. Rejects epochs containing less than a specified number of satellites.

3. Rejects satellites which lie below a specified elevation angle. This is normally selected as 15° to minimise the effects of atmospheric refraction.

4.3.3 NORMAL

NORMAL is a data reduction program, which produces normal points for specified spans of data. A low order polynomial is fit to the span of data using a least squares technique and a normal point is produced at the nearest data point to the middle of the span. Specified input parameters are,

- Epoch separation of the input data.

- Epoch separation required for the output data.

- Order of polynomial to use.

For TI 4100 data recorded at three second intervals, a second order polynomial has normally been used for producing one minute normal points. For one minute normal points, the program will select a one minute span of data from which to fit the polynomial and no data points are used more than once. The program also selects the spans of data so that the normal points are produced simultaneously for all the satellites and receivers, which is necessary for the phase differencing techniques (section 2.6.1).

The output from NORMAL can be given in two forms,

1. Normal pointed pseudoranges and carrier phases at specified time tags. (Similar format to the input data.)

2. Normal pointed pseudoranges and the polynomial coefficients a, b, c representing the carrier phase readings for each span of data. These coefficients describe the phase Φ as $\Phi = a + bt + ct^2$ at a given time t. (section 2.6.2).

4.3.4 PSEUDO

PSEUDO computes the three dimensional coordinates of the receiver and the receiver clock offset using the pseudorange observable. The program uses the data from a whole observation period (several minutes to several hours) and carries out a least squares adjustment, solving for the receiver coordinates and the receiver clock offset. A choice of receiver clock models can be made,

1. Solve for one clock offset per epoch,

2. Solve for a clock offset, drift and ageing terms (2nd order polynomial).

The main use of the program in orbit determination is in the estimation of the receiver clock parameters, which can then be used for the time correction of the phase data in **TIMECOR**.

4.3.5 TIMECOR

TIMECOR corrects the phase measurements for the receiver clock error. The clock model obtained from **PSEUDO** is used to alter the carrier phase measurements to allow for the receiver clock offset at the measurement epoch. This is achieved in two ways,

1. Using the actual carrier phase readings output from **NORMAL** and linearly interpolating the phase shift due to the receiver clock offset.

2. Using the polynomial coefficients output from **NORMAL** to determine the phase rate $\partial\Phi/\partial t$ $(= b + 2ct)$ and produce a more accurate time correction method (section 2.6.2).

The output file obtained will then contain the time corrected carrier phase readings, necessary for the input to the orbit adjustment program **DDORB**.

4.3.6 DDORB

DDORB was developed by the author from **PANIC**, the GPS network adjustment program [de la Fuente, 1988]. **DDORB** performs a simultaneous least squares adjustment of the receiver coordinates, initial phase ambiguities,

satellite state vector and the solar radiation pressure coefficients for all the required satellites and receivers. It can be used for multiple day solutions, solving for a new set of integer ambiguities each day. The number of unknown parameters estimated can grow quite large, particularly with the multiple day solution. The number of unknowns is equivalent to,

$$nostns \times 3 + nosats \times norb + (nosats - 1) \times (nostns - 1) \times nday \quad (4.1)$$

Where nostns = total number of stations in the network.

nosats = total number of satellites observed.

norb = number of orbital parameters estimated per satellite.

nday = number of days of data.

Input requirements

The jobdeck contains several options for the input and various flags for different controlling options.

1. Flag selecting reference system. i.e. WGS 84 or WGS 72. This defines the semi-major axis and the flattening of the reference ellipsoid.

2. Flag selecting frequency. L1, L2 or L1/L2 (ionospherically corrected).

3. Flag selecting tropospheric correction

    (a) No model.

    (b) Simplified Hopfield.

    (c) Saastamoinen/Marini.

    (d) Hopfield.

    (e) Saastamoinen (section 2.5.2).

    (f) Standard Atmosphere (section 2.5.2).

4. Flag selecting the use of a geometrical correlation matrix.

5. Input day number at start of data.

6. Flag selecting output of double difference phase residuals.

7. Input maximum number of satellites in data set.

8. Input PRN numbers of satellites.

9. Input PRN number of base satellite.

10. Flag selecting PRN number of any satellite required to be held fixed in the adjustment.

11. Input maximum number of receivers (sites).

12. Input any site whose coordinates are to be held fixed in the adjustment.

13. Input the approximate coordinates of the receivers and the antenna heights above the site markers.

14. Input the independent baseline definitions. For a network of n receivers there will be (n-1) independent baselines to define.

15. Flag to select integer fixing option.

16. Input the time interval in seconds of the ephemeris. This will be equivalent to the predictor-corrector integration step length used in ORBIT.

17. Input the time at the start of the ephemeris in seconds of the GPS week.

18. Input the year and day number at the start of the ephemeris.

19. Input the number of orbital parameters to be estimated for each satellite.

3 - initial position vectors only.

6 - initial position and velocity vectors.

7 - initial position and velocity vectors and direct solar radiation pressure coefficients.

8 - initial position and velocity vectors, direct solar radiation pressure coefficients and y bias accelerations.

20. Input number of days of data.

21. Flag selecting the time correction option (Chapter 7).

A number of files are also required by the program. These are,

- Chebyshev polynomial coefficient file (**CHEBPOL**).

- Earth fixed ephemeris file (**ORBIT**).

- Partial derivative file (**ORBIT**).

- Measurement data file for each receiver, for each day (**TIMECOR**).

- Satellite state vector file.

- Meteorological data file (For options 3 - b,c,d and e).

General Outline

A brief program description is given below, describing the main steps in the computation.

1. Input parameters (in jobdeck).

2. Convert time of satellite state vector into modified julian day.

3. Read in first epoch of GPS data from each receiver.

4. Compute correlation matrix.

5. Compute earth-fixed satellite coordinates at the time of signal transmission. This is done by interpolating the ephemeris from **ORBIT** using an 8th order Everett interpolation algorithm for each satellite.

6. Compute the rotation matrix for transforming the earth-fixed satellite coordinates into inertial J2000.0 coordinates. The matrix is computed at the time of satellite transmission using the Chebyshev polynomial coefficients [Agrotis, 1984].

7. Compute the satellite coordinates in inertial J2000.0 coordinates using this matrix.

8. Compute the rotation matrix for transforming the earth-fixed receiver coordinates into inertial J2000.0 coordinates at the time of signal reception at each receiver.

9. Compute the coordinates of each receiver in inertial J2000.0 coordinates using this matrix, ready for forming the partial derivatives for the orbital unknowns.

10. Compute tropospheric corrections.

11. Compute *observed* double difference phase.

12. Compute *computed* double difference phase.

13. Form partial derivatives for,

   - Satellite state vectors.

   - Solar radiation pressure coefficients (one or two parameters per satellite).

   - Receiver coordinates.

   - Initial phase ambiguities.

   The partial derivatives of the satellite to receiver range with respect to the orbital unknowns (section 3.7) are obtained from **ORBIT** and interpolated to the required epoch using Everetts interpolation algorithm.

14. Form double difference observation equations.

15. Apply correlation matrix and form the normal equations.

16. Return to step (3) for successive epochs.

17. Form observation equations for fixing any required receiver coordinates or any other parameter and add to the normal equations.

18. Solve normal equations using Choleski's method of triangular decomposition.

19. Compute double difference phase residuals.

20. Solve for the covariance matrix.

21. Output (see below).

Output

The amount of output is specified by the program user in the jobdeck. The estimated parameters output are,

1. Cartesian coordinates of each receiver.

2. Baseline lengths between all the receivers.

3. Geodetic coordinate differences $(\Delta\Phi, \Delta\lambda, \Delta h)$ between receivers.

4. Satellite state vectors for each satellite.

5. Solar radiation pressure coefficient for each satellite (if specified).

6. Y bias acceleration for each satellite (if specified).

7. Initial phase ambiguities for each satellite, each day.

The double difference phase residuals may also be output for each satellite-receiver pair. A statistical analysis is carried out to compute the covariance matrix, rms error of an observation of unit weight (unit variance) and the standard errors of all the estimated quantities. These are output along with the relevant parameters.

General comments

Once the new estimates of the orbital parameters have been obtained, they can be used to recompute a more accurate orbit for the satellites, using ORBIT. These new ephemeris and partial derivative files can then be used in DDORB to recompute the solution. This iterative process continues until no further change in the solution occurs. In practice, no change in the solution has been seen after the first iteration, the only iteration being necessary is to recompute the orbits using ORBIT for comparison purposes. An example of a jobdeck used for this program is given in Appendix A.

103

4.3.7 PLOTARC

PLOTARC is a plotting program, which compares the cartesian coordinates of two separate orbits and plots a graph of the radial, along track and cross track component differences between them (figure 4.2).

Radial component

Along track component

Cross track component
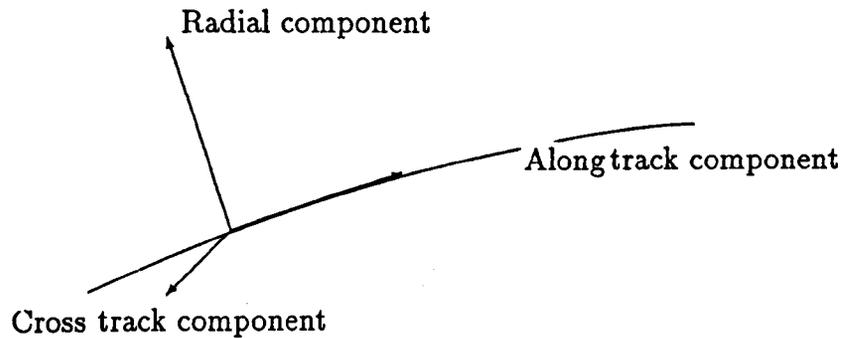
Figure 4.2: Orbit component directions

The program requires the x, y and z coordinates of both orbits and the $\dot{x}, \dot{y}, \dot{z}$ velocities of one of the satellites, at the times when the orbits are to be compared. These can be obtained from **ORBIT** or from the precise ephemeris.

For small orbit differences, the unit vector $\vec{e_r}$ in the radial direction can be approximated by,

$$\vec{e_r} \approx \left(\frac{x}{R}, \frac{y}{R}, \frac{z}{R} \right) \qquad (4.2)$$

Where $R = (x^2 + y^2 + z^2)^{\frac{1}{2}}$ for either satellite.

The unit vector $\vec{e_a}$ in the along track direction can be estimated from the

velocity vector,

$$\vec{e}_a \approx \left(\frac{\dot{x}}{\dot{R}}, \frac{\dot{y}}{\dot{R}}, \frac{\dot{z}}{\dot{R}} \right) \qquad (4.3)$$

Where $\dot{R} = (\dot{x}^2 + \dot{y}^2 + \dot{z}^2)^{\frac{1}{2}}$ for either satellite.

The unit vector $\vec{e}_c$ in the cross track direction is given by the vector cross product,

$$\vec{e}_c = \vec{e}_r \wedge \vec{e}_a \qquad (4.4)$$

The errors in each of these components can be approximated by the vector dot products,

$$
\begin{aligned}
error_{radial} &= \vec{e}_r.\Delta R \\
error_{along\ track} &= \vec{e}_a.\Delta R \\
error_{cross\ track} &= \vec{e}_c.\Delta R \qquad (4.5)
\end{aligned}
$$

Where $\Delta R = (\Delta x, \Delta y, \Delta z)$, the differences between the cartesian coordinates of the two orbits.

Chapter 5.
The GINFEST Campaign

The GINFEST Campaign

In 1982, a proposal was made to carry out VLBI, SLR, GPS and CERI[1] observation campaigns at sites in Europe. This Geodetic Intercomparison Network For Evaluating Space Techniques (GINFEST) would be used to compare the relative accuracies and to determine any systematic biases between the techniques. The network lies over a tectonically stable region of Europe, and could be used as a reference network for testing other geodetic techniques.

The GINFEST VLBI observation campaign was comprised of two twelve hour sessions. These were observed in June and October in 1987, at the radio telescope sites of,

- Effelsberg

- Jodrell Bank

- Medicina

- Onsala

- Westerbork.

The GINFEST SLR data sets were selected from two existing observation campaigns. The first set is made up from five discrete, seven day orbital arcs, taken from the 1984 MERIT Intensive Campaign. The second set consisted of a one month continuous arc, taken from the Monte Generoso Campaign. The complete data set contains data from the following sites,

---

[1]Connected Element Radio Interferometry

- Monte Generoso

- Zimmerwald

- Kootwijk

- Wettzell

- Grasse

- Graz

- Royal Greenwich Observatory (RGO)

- Matera.

The GINFEST GPS campaign was part of a feasibility study for a European tracking network [Boucher et al, 1986], which had the aims to,

1. determine satellite orbits over the region,

2. produce an ionospheric model for the region,

3. test the use of differential positioning between the tracking sites and the mobile receivers.

The data set is described in detail in the following section.

5.1 GINFEST GPS Campaign

5.1.1 Data Description

The GINFEST GPS observation campaign took place on the 18th, 19th and 20th of November 1986. These are referred to by the day numbers 322, 323 and 324 in the following text. Ten TI 4100 NAVSTAR Navigator receivers were deployed, near the SLR and VLBI sites shown in figure (5.1). The TI 4100 receivers can acquire both the C/A and the P code, enabling measurements of both the L1 and L2 frequencies. The data was recorded on magnetic cassettes, capable of storing a maximum of half an hour of data each. The dual tape drive was used to enable a quick change-over of cassettes.

△ VLBI STATION

● SLR STATION

ONSALA △

JODRELL BANK △

RGO ●

△ WESTERBORK
● KOOTWIJK

△ EFFELSBERG

△ WETTZELL

ZIMMERWALD
●   ● GRAZ

● GRASSE
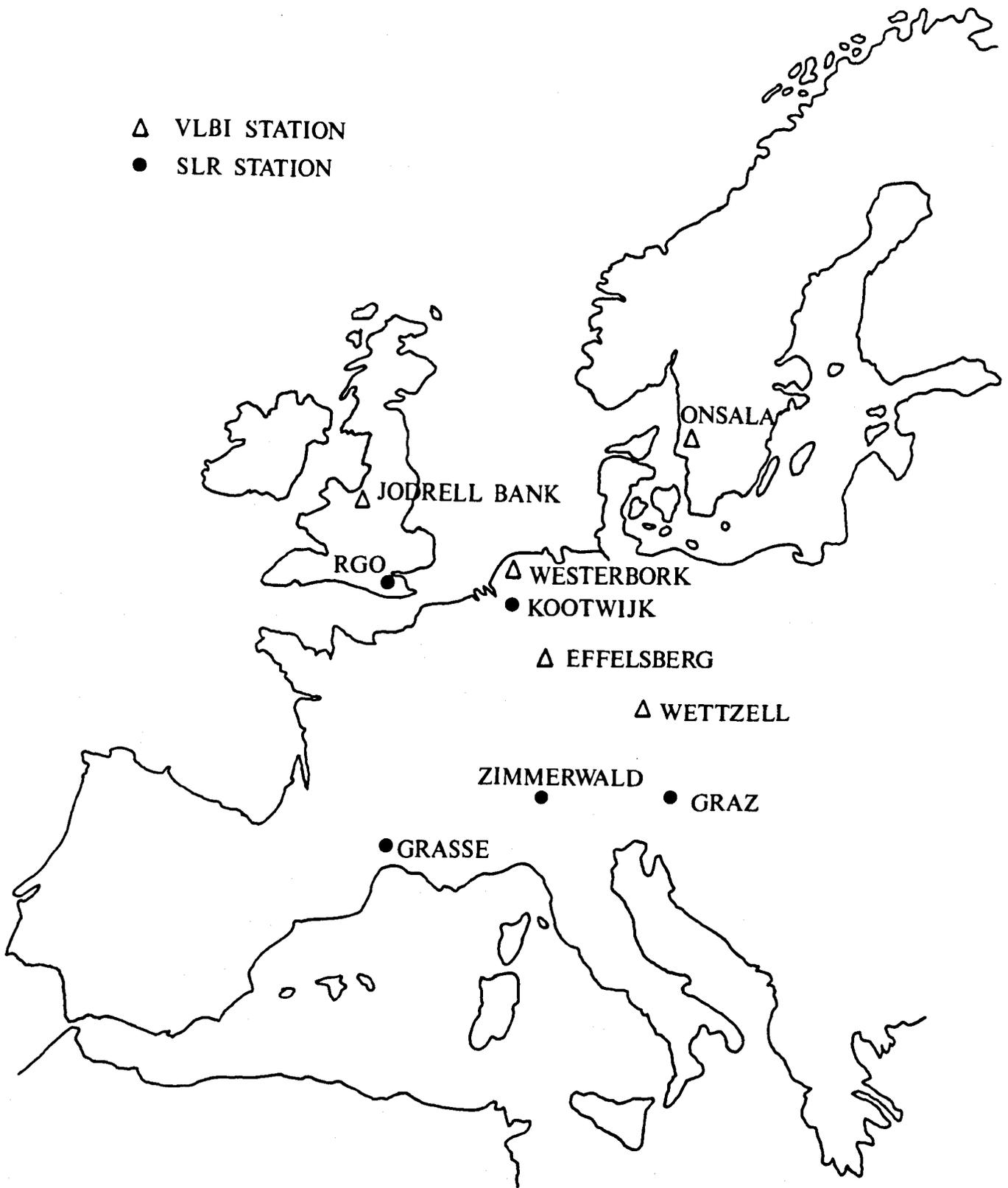
Figure 5.1: Sites for the GINFEST GPS campaign

One limitation of the TI 4100 is its ability to only track four satellites simultaneously. With the satellite constellation at the time of the campaign, two separate constellations were observed. These were,

- Satellites 6, 9, 11, 12 from 0:50 to 2:20 UTC (Session A)

- Satellites 9, 11, 12, 13 from 2:20 to 3:50 UTC (Session B)

The satellite numbers refer to the PRN numbers of the satellites. The times are the approximate observation times, which precess by four minutes each day. A maximum of three hours of data was recorded at each of the sites.

A sky-plot showing the azimuth and elevation angles of the satellites during the campaign is given in figure (5.2).

Meteorological data (pressure, wet and dry temperatures) were recorded at each site, to allow tropospheric corrections to be made. However, no meteorological data was recorded at Graz for the whole campaign. This data was estimated using the meteorological data from the two nearest sites, Wettzell and Zimmerwald. The temperature and pressure were assumed to decrease uniformly with increasing height, from these two sites and this was used to predict values corresponding to the height of Graz.

5.1.2 Data Format

The data was written on three, nine track magnetic tapes, at 1600 bits per inch. A total of 146 files were contained on the tapes, each containing half an hour of data. (Figure 5.3).

At the time of the processing, no data was available for the site at Zimmerwald. Also, no data was recorded at Wettzell on day 322, due to an equipment failure.

5.1.3 Data Preprocessing

A preprocessing of the data was carried out to compress the data, to correct any cycle slips and to time correct the data for the receiver clock biases. The following stages were carried out, using the computer programs described in chapter 4.
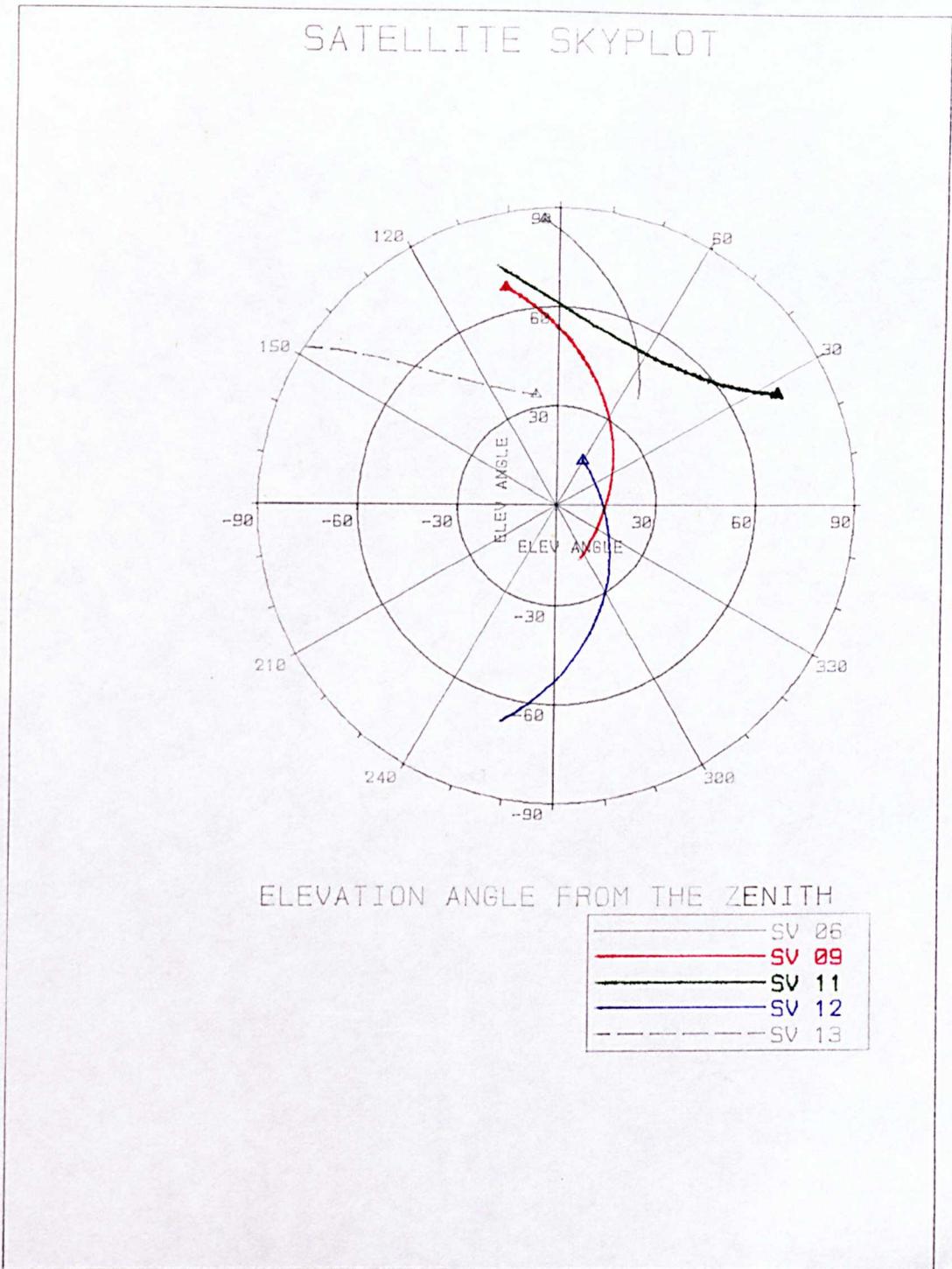
Figure 5.2: Satellite sky-plot for the GINFEST GPS campaign

Tape 1	Kootwijk	A	B	C
	Onsala	A	B	C
(53 files)	Westerbork	A	B	C

Tape 2	Grasse	A	B	C
	RGO	A	B	C
(37 files)	Jodrell Bank			C

Tape 3	Effelsberg	A	B	C
	Wettzell		B	C
(56 files)	Graz	A	B	C
	Jodrell Bank	A	B	

A = Day 322

B = Day 323

C = Day 324

Figure 5.3: GINFEST : Raw data availability

1. Each file was decoded using **TIDECODE**, to convert the binary data into the respective measurement and ephemeris files. The third differences were also output from the program. Any significant jumps in the third differences were attributed to cycle slips. These were corrected by estimating the value of the cycle slip from the third differences and correcting each observation after the occurrence of the slip.

2. Each file was filtered using **EAFILTER**. The flags in the program were set to ignore any satellites below 15° elevation angle and any epoch containing less than four satellites.

3. The 146 files were then concatenated to form files, containing the data from one site, for each session, for each day. This produced 52 files.

4. Each of these files were then normal pointed using **NORMAL**, to produce the data at intervals of sixty seconds.

5. The files from sessions A and B were then joined together, to give one file per site , per day.

6. A point positioning solution was carried out using **PSEUDO**. This was to determine the approximate coordinates for each site and to obtain the values of the receiver clock offsets for each receiver. With up to three hours of data at each site , a polynomial clock model would have been unsuitable, so a receiver clock offset term was determined at every epoch.

7. The phase data was then corrected for the receiver clock offsets using **TIMECOR**.

8. A final stage of the preprocessing was to correct the cycle slips which occurred during the change of session, from observing satellites 6,9,11,12 to observing satellites 9,11,12,13. When the receivers were attempting to acquire satellite 13, a loss of lock often occurred on the other satellites. The approximate value of these cycle slips were estimated using the pseudorange difference between successive epochs, to compute the

112

phase difference. The accuracy of this method was estimated to be in the order of twenty five cycles. Further cycle slips were detected at the half hour intervals, when the magnetic cassettes were changed in the receiver. These slips were corrected using the above technique.

The data remaining after this preprocessing stage is shown in figure (5.4). The filtering of the data, and the removal of the some epochs where a lot of cycle slips occurred, has left some large gaps in the data. Furthermore, the data from Westerbork on day 323 was rejected as only a few epochs remained.

5.2 Determination of the GINFEST Site Coordinates

Precise coordinates for the GINFEST SLR and VLBI sites have been determined in many different solutions. The coordinate set chosen for comparison with the GPS solutions, were calculated by Dr. C.J.Hill [Hill, 1989], using the *SODAPOP* suite of programs (Chapter 4). This solution was calculated using a short-arc method, with the GINFEST SLR data set. The short-arc method of analysis was considered the best way of producing precise coordinates of the SLR sites, using the available data. However, a short arc solution will not provide a good orientation and scale for the network. This was achieved by transforming the short-arc solution onto a ten month long-arc solution, using a seven parameter Helmert transformation (table C.1). This coordinate set, designated IESSG-T, will have the same origin, orientation and scale as the long-arc solution, but will have the precise geometry associated with the short-arc solution. The long-arc solution was computed from 1986 data, using the GEM-T1 geopotential model.

Two of the GPS solutions were based on the broadcast and precise ephemerides, which were given in the WGS 72 terrestrial system, at the time of the GINFEST GPS campaign. Hence, it is necessary to determine whether there are any systematic biases between the coordinates derived in the WGS 72 terrestrial system and the IESSG-T solution.

The IESSG-T solution was compared with the WGS 84 coordinate set given in *Boucher et al* [1988], through a seven parameter Helmert transfor-

Grasse
Graz
Effelsberg
RGO
Kootwijk
Westerbork
Onsala
Jodrell Bank

Day 322

Grasse
Graz
Effelsberg
RGO
Kootwijk
Wettzell
Onsala
Jodrell Bank

Day 323

Grasse
Graz
Effelsberg
RGO
Kootwijk
Westerbork
Onsala
Jodrell Bank
Wettzell

Day 324
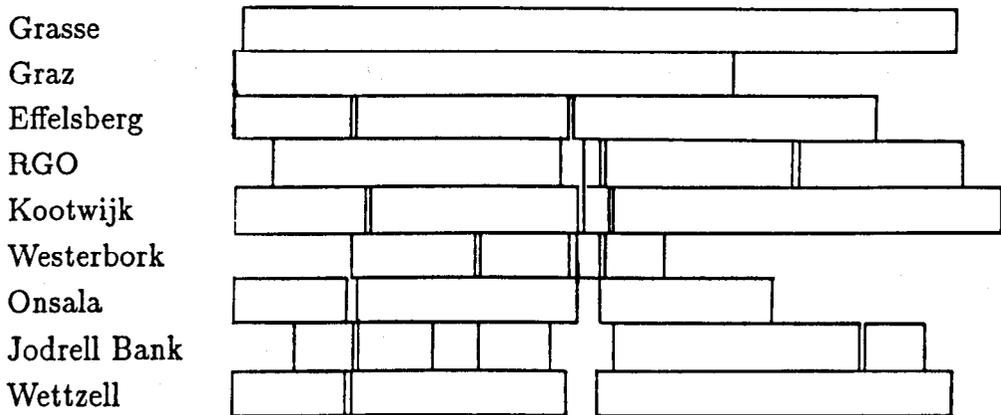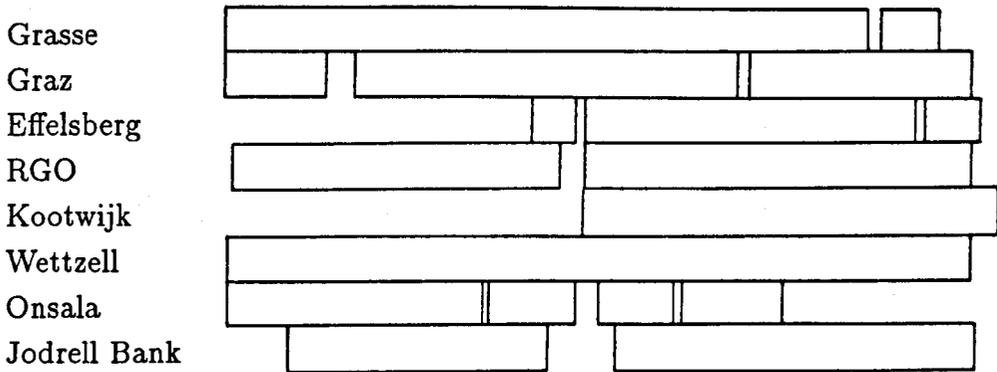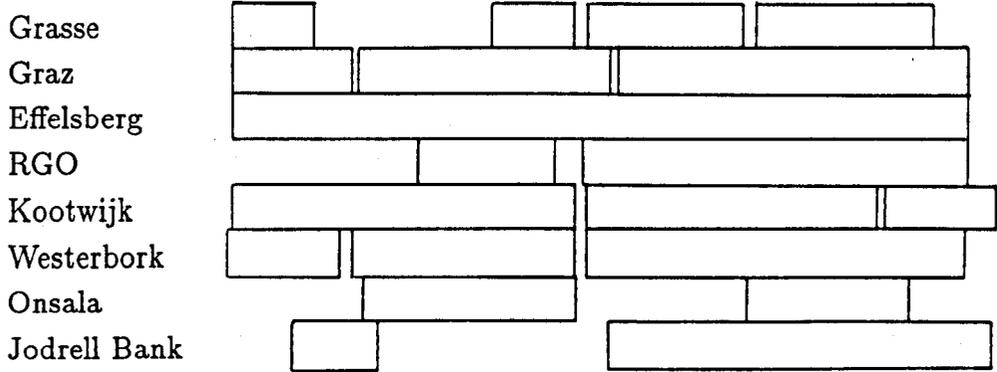
Figure 5.4: Processed data availability

mation. The resulting transformed coordinates, designated IESSG-T84 and their derivation are given in table (C.2). These coordinates were then transformed into the WGS-72 terrestrial system by applying the transformation parameters given in table (C.3). The resulting coordinate set IESSG-T72 would then have the same scale, origin and orientation as the WGS-72 terrestrial system, but the precise inter-site geometry associated with the IESSG SLR short-arc solution.

The eccentricities, between the SLR facilities and the L1 phase centres of the GPS antennas, were obtained from terrestrial observations. These eccentricities were applied to the IESSG-T72 coordinate set, to provide consistent WGS-72 coordinates for the GPS L1 phase centres (table 5.1).

	x(m)	y(m)	z(m)
Graz	4194426.429	1162690.069	4647240.002
R.G.O.	4033361.889	24036.622	4924371.434
Kootwijk	3899219.837	396756.676	5015067.465
Grasse	4581712.927	556126.883	4389330.653
Wettzell	4075554.175	931813.664	4801583.792

Table 5.1: GINFEST GPS L1 phase centre coordinates : WGS 72

5.3 Analysis of Data

To test the relative accuracies of processing the GPS observables with different ephemerides, three different solution types have been computed. These are

- Broadcast Ephemeris Solution.

- Precise Ephemeris Solution.

- Orbit Determination Solution

All the solutions have been computed using the Saastamoinen model to account for the tropospheric delays. The combined L1/L2 frequency has been used as a first order correction for the ionospheric delays.

5.3.1 Broadcast Ephemeris Solutions

A different solution was computed for each of the three days, using the broadcast ephemeris. On each day, the coordinates of Kootwijk were held fixed to the WGS-72 coordinates.

The double difference phase residuals were inspected each day for any remaining cycle slips and these were then corrected. On day 323, the data from Effelsberg was rejected, due to a large number of cycle slips.

In order to test the repeatability of the broadcast ephemeris solutions, the baseline lengths determined from days 322 and 323 were compared with the baselines determined on day 324. The results of this comparison are given in tables (C.5) and (C.6) of the appendices. A summarised version of the results are shown in table (5.2), showing the root-mean-square (rms) baseline differences between the two days.

	number of baselines	rms baseline differences (cm)
Day 324 minus Day 322	28	13.6
Day 324 minus Day 323	21	9.3

Table 5.2: Daily baseline repeatability : Broadcast ephemeris

The baseline lengths vary from 98 km to 1553 km, and typically the differences between the solutions were less than 0.5 ppm.

A comparison has been made between the WGS-72 coordinates derived from the SLR solution and the baselines determined from the GPS solution from day 324. The differences between the baseline lengths and the relative baseline errors are presented in table (5.3).

The baseline differences are less than 0.6 ppm, which is typical of the accuracy of the broadcast ephemeris. However, there appears to be a systematic effect, with the GPS determined baselines generally larger than the SLR determined baselines. The GPS solution was computed using the WGS-72 coordinates for the satellites and the fixed station of Kootwijk. The SLR coordinates were transformed onto the WGS-72 terrestrial frame, so no scale

		Baseline length (km)	Difference (cm)	ppm
Kootwijk	- Graz	899	-40.0	0.445
	- Grasse	939	-46.6	0.496
	- RGO	406	0.5	0.013
	- Wettzell	602	-12.2	0.202
Graz	- Grasse	764	-13.1	0.171
	- RGO	1182	-38.1	0.322
	- Wettzell	302	-18.6	0.617
Grasse	- RGO	932	-49.8	0.533
	- Wettzell	753	-13.2	0.175
RGO	- Wettzell	917	-6.8	0.074
			rms = 29.3	

Table 5.3: Comparison of day 324 broadcast ephemeris solution with the SLR solution

difference should have been apparent between the two coordinate sets. The baseline error has been plotted against baseline length in figure (5.5), to investigate this scale difference. It can be seen from the figure, that the baseline error generally increases with the baseline length, although there is no significant linear relation between the two values.

The height differences between the SLR solution and the GPS solutions are compared in table (5.4), for day 324. The height differences are shown for baselines from Kootwijk, which is in the centre of the network. It is apparent that there is a discrepancy between the height differences to Graz. This is unlikely to be caused by a rotation of the network, because the height differences to the nearest station, Wettzell are of the opposite sign. The most likely cause is the use of the incorrect eccentricity vector, or by an error in the antenna height.

5.3.2 Precise Ephemeris Solutions

The precise ephemeris for the GINFEST GPS campaign was provided by the Naval Surface Warfare Center, in the WGS 72 coordinate system. This
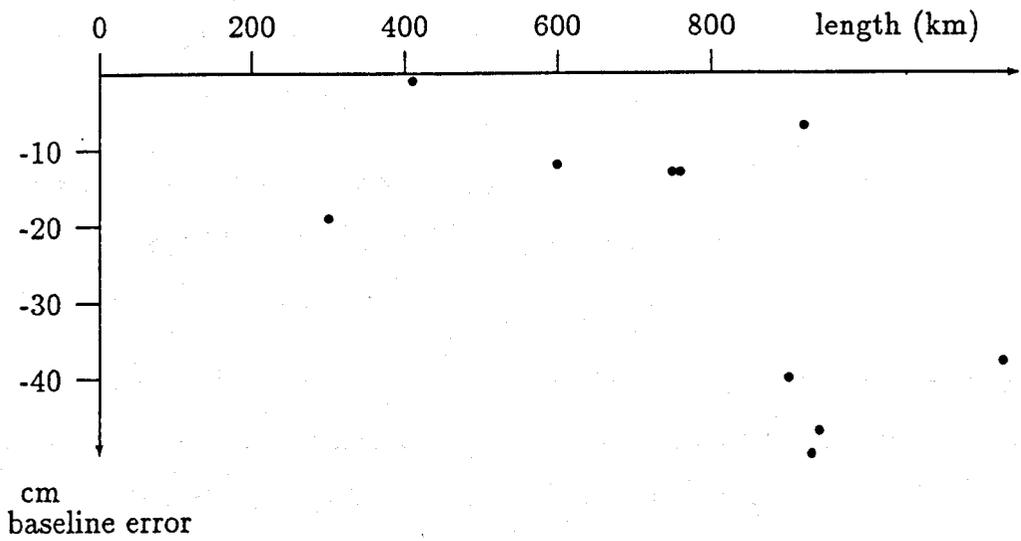
Figure 5.5: Baseline error plotted as a function of baseline length : Day 324 for the broadcast ephemeris

Height differences in metres		WGS72 (SLR)	Day 324 (GPS)	Difference
Kootwijk	- Graz	-447.247	-448.694	1.447
	- Grasse	-1228.809	-1228.620	-0.189
	- RGO	22.557	22.634	-0.077
	- Wettzell	-568.698	-568.436	-0.268

Table 5.4: Height differences for the broadcast ephemeris solution

ephemeris was given at fifteen minute epochs and it was interpolated to the required epoch using an 8th order Everetts interpolation algorithm.

Two different types of solution were computed,

- Single day solutions were computed in a similar way to the broadcast ephemeris solutions.

- A three day solution was computed using all the data from the GIN-FEST campaign. For this solution, a new set of integer ambiguities were estimated for each day.

The day to day repeatability of the single day solutions were investigated by comparing the baselines determined from each day with the three day solution. The differences between the solutions are given in tables (C.7),(C.8) and (C.9) of the appendices, with a summary given in table (5.5) showing the rms baseline differences.

Day	number of baselines	rms baseline differences (cm)
Day 322	28	18.9
Day 323	21	5.7
Day 324	36	9.7

Table 5.5: Daily baseline repeatability : Precise ephemeris

The baseline agreement between the second two days of the campaign and the three day solution shows a slight improvement over the broadcast ephemeris solution. On day 322 the main discrepancy appears to be with the baselines connected to Jodrell Bank. Excluding this station from the comparison gives a rms baseline difference of 8.3 cm, between day 322 and the three day solution. No obvious reason could be found for the poor determination of the coordinates of Jodrell Bank, especially when considering that no such differences were seen in the broadcast ephemeris solution.

The three day solution has been compared with the SLR determined baselines, and the comparisons are shown in table (5.6).

		Length (km)	Difference (cm)	ppm
Grasse	- Kootwijk	939	-29.3	0.312
	- Graz	764	-10.6	0.139
	- Wettzell	753	-8.1	0.107
	- RGO	932	-26.6	0.285
Kootwijk	- Graz	899	-27.5	0.306
	- Wettzell	602	-4.7	0.076
	- RGO	406	-14.2	0.348
Graz	- Wettzell	302	-13.1	0.432
	- RGO	1182	-34.8	0.294
Wettzell	- RGO	917	-10.1	0.110
			rms = 20.5	

Table 5.6: Comparison of the three day precise ephemeris solution with the SLR solution

The rms baseline differences for table (5.6) of 20.5 cm, gives a better agreement with the SLR solution, than the broadcast ephemeris solution. The differences in the baseline lengths are less than 0.4 ppm, which is within the expected accuracy of the precise ephemeris. An improvement in the solution would also be expected when using the three days of data, when compared to the single day of data used for the broadcast ephemeris solution. However, as in the case of the broadcast ephemeris solution, the GPS determined baselines are all larger than the SLR determined baselines. The baseline errors have been plotted against the baseline length in figure (5.6), showing a similar trend to figure (5.5).

An examination of the height components of the baselines in table (5.7), shows the same discrepancy in the height of Graz, that was seen in the broadcast ephemeris solution. Although the baseline agreement is better for the precise ephemeris, the agreement between the height components is somewhat worse than for the broadcast ephemeris solution.
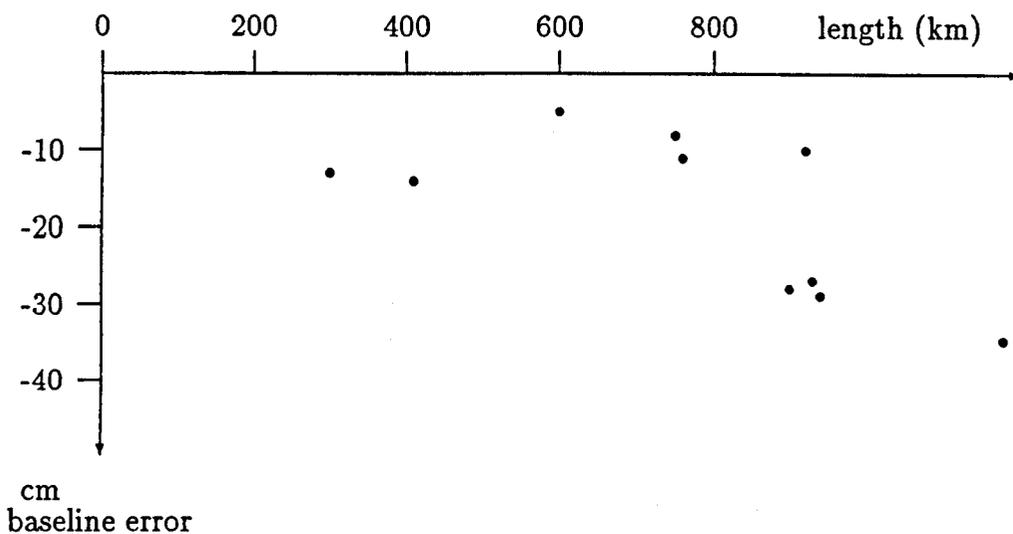
Figure 5.6: Baseline error plotted as a function of baseline length : Three day solution for the precise ephemeris

Height differences in metres		WGS 72 (SLR)	3 day precise ephemeris (GPS)	Difference
Kootwijk	- Grasse	-1228.809	-1228.103	-0.706
	- Wettzell	-568.694	-568.754	0.060
	- RGO	22.557	22.928	-0.371
	- Graz	-447.247	-449.272	2.025

Table 5.7: Height differences for the precise ephemeris solution

5.3.3 Orbit Determination Solutions

A solution has been computed to test the fiducial network concept for orbit determination over Europe. The first stage is the selection of the fiducial sites, which will be held fixed in the solution. To test the repeatability of the daily solutions, it was preferable to use the same three fiducial sites on each day. No data was available for Wettzell on the first day, and the uncertainty in the height of Graz made this site unsuitable. This left the three SLR sites at RGO, Grasse and Kootwijk.

The geometry of these sites is not ideal for a tracking network, because they are not well distributed with respect to the rest of the network, instead the remaining GINFEST GPS sites lie outside these three sites (figure 5.1). For this reason it was decided to strengthen the network by including the GPS receiver located near the VLBI site at Onsala.

The coordinates of the VLBI site at Onsala in the same reference frame as the SLR sites were obtained from *Boucher et al* [1988]. These coordinates are given in the WGS 84 terrestrial system. A seven parameter Helmert transformation was used to determine the systematic biases between the WGS 84 coordinates and the IESSG-T coordinates, using the SLR sites of Kootwijk, Wettzell, Grasse, Graz and Grasse. These biases were then applied to the WGS 84 coordinates of Onsala to obtain coordinates consistent with the IESSG-T SLR coordinates. The addition of the eccentricity vector to the VLBI mark give the coordinates of the L1 phase centre of the GPS antenna at Onsala The full set of coordinates of the GPS L1 phase centres in the IESSG-T reference frame is given in table (5.8).

The long arc solution on which this solution was based was computed using the GEM-T1 gravity field. In order to keep a level of consistency in the processing, it was decided to use the IESSG-T coordinate set as the fiducial coordinates and use the GEM-T1 gravity field up to degree and order eight in the orbit integration. The value of the product GM was taken to be $3986004.36 \times 10^8 m^3 s^{-2}$.

Two distinct types of solution were computed,

1. Three solutions were computed for each day of the campaign, with the

Site	x (m)	y (m)	z (m)
Grasse	4581711.574	556145.934	4389335.920
Graz	4194423.493	1162708.617	4647244.487
RGO	4033361.731	24054.932	4924377.521
Kootwijk	3899218.720	396774.851	5015073.052
Wettzell	4075551.760	931832.094	4801588.598
Onsala	3370658.685	711884.374	5349787.625

Table 5.8: GINFEST GPS L1 phase centre coordinates : IESSG-T

coordinates of Grasse, RGO and Onsala held fixed. The parameters estimated included the remaining receiver coordinates, the initial phase ambiguities and the six parameter state vector for each satellite. No a priori constraints were placed on any of the estimated parameters.

2. A three day solution was computed for the whole campaign. The co-ordinates of Grasse, RGO and Onsala were held fixed as in the single day solution. The remaining receiver coordinates were computed for the whole three days, with a new set of integer ambiguities computed for each day. To assess the effect of the solar radiation pressure, two different solution were computed. The first solution solving for the six parameter state vector and the direct solar radiation scaling coefficient for each satellite. Secondly a solution was computed solving for these seven parameters and a constant y-bias acceleration for each satellite.

The results of the two, three day solutions are given in tables (5.9) and (5.10), and these show the baseline differences between the SLR determined baselines and the GPS determined baselines.

On examination of both solutions, the worse baseline agreements are on the long baselines connected to Graz and Wettzell. These two sites are also the furthest away from the three fiducial sites. The rms double difference phase residual for the first solution is 0.10744 cycles, with the second solution, solving for the additional satellite y bias accelerations, having a lower value of 0.08831. The rms baseline differences for the two solutions are 14.0 cm

		Length (km)	Difference (cm)	ppm
Grasse	- Kootwijk	939	8.7	0.093
	- Graz	764	1.1	0.014
	- Wettzell	753	16.6	0.220
RGO	- Kootwijk	406	-6.5	0.160
	- Graz	1182	-18.5	0.157
	- Wettzell	917	-1.1	0.012
Onsala	- Kootwijk	700	-9.6	0.137
	- Graz	1172	-32.7	0.279
	- Wettzell	919	-20.0	0.218
Kootwijk	- Graz	899	-6.3	0.070
	- Wettzell	602	4.8	0.080
Graz	- Wettzell	302	-0.4	0.013
		rms = 14.0		

Table 5.9: Comparison of orbit determination solution with the SLR solution : Solving for the satellite state vector and the direct solar radiation pressure

and 11.7 cm respectively.

The second solution which solves for the y-bias acceleration appears to have a slight improvement on the first solution, although the worst agreement with the SLR solution in either case is about three parts in 10^7. In these solutions there are no obvious systematic effects giving the scale differences that were apparent in the broadcast and precise ephemeris solutions.

A comparison of the height components of the baselines is given in table (5.10) for the second solution. It can be seen again that the height difference to Graz is very high, in this case giving a height error of around two meters.

Three single day solutions were computed, solving for the receiver co-ordinates, initial phase ambiguities and the six parameter state vector for each satellite. No significant estimates for the direct solar radiation pressure coefficient could be obtained. For these single day solutions, it was apparent

		length (km)	Difference (cm)	ppm
Grasse	- Kootwijk	939	5.4	0.058
	- Graz	764	-8.2	0.107
	- Wettzell	753	8.4	0.112
RGO	- Kootwijk	406	-11.3	0.278
	- Graz	1182	-20.8	0.176
	- Wettzell	917	-3.6	0.039
Onsala	- Kootwijk	700	1.7	0.024
	- Graz	1172	-25.8	0.220
	- Wettzell	919	-13.1	0.142
Kootwijk	- Graz	899	-4.8	0.053
	- Wettzell	602	6.4	0.106
Graz	- Wettzell	302	-0.4	0.013
			rms = 11.7	

Table 5.10: Comparison of GPS orbit determination solution with the SLR solution : Solving for the satellite state vector, direct solar radiation pressure and the constant y-bias acceleration

Height differences in metres	IESSG-T (SLR)	3 day GPS orbit determination solution	Difference (m)
Kootwijk - Grasse	-1228.280	-1228.130	-0.150
- Wettzell	-568.627	-568.726	0.099
- RGO	22.717	22.868	-0.151
- Graz	-447.084	-449.232	2.148

Table 5.11: Height differences for the GPS three day orbit solution : Solving for satellite state vector, solar radiation pressure coefficient and the y-bias acceleration

that the satellite state vector was sufficient to account for any deficiencies in the satellite force model. The coordinates of Grasse, RGO and Onsala were held fixed in the adjustment, as in the three day solution.

The repeatability of the three single day solutions have been tested by comparing the results from each day with the three day solution (solving for the y bias force). The full comparisons are shown in tables (C.10), (C.11) and (C.12) of the appendices. Figure (5.7) shows the rms differences between the baseline components for each day and the rms differences between the north, east and height components of the baselines.

Generally the north components of the baselines were less well determined than the east components. The rms baseline differences are comparable with the three day precise ephemeris solution

An inspection of the results for day 322 shows that the sites that gave the worst baseline agreements were Jodrell Bank and Graz, which both lie on the extreme edges of the network. The results of day 323 and 324 showed similar trends. In general, the sites that were in the middle of the network give the closest agreement, whereas the sites that lie well outside the three fixed fiducial sites show the largest differences.

5.4 Discussion of Results

One of the main problems encountered with the GINFEST GPS data set was the correction of cycle slips. The slips were easily corrected to within one
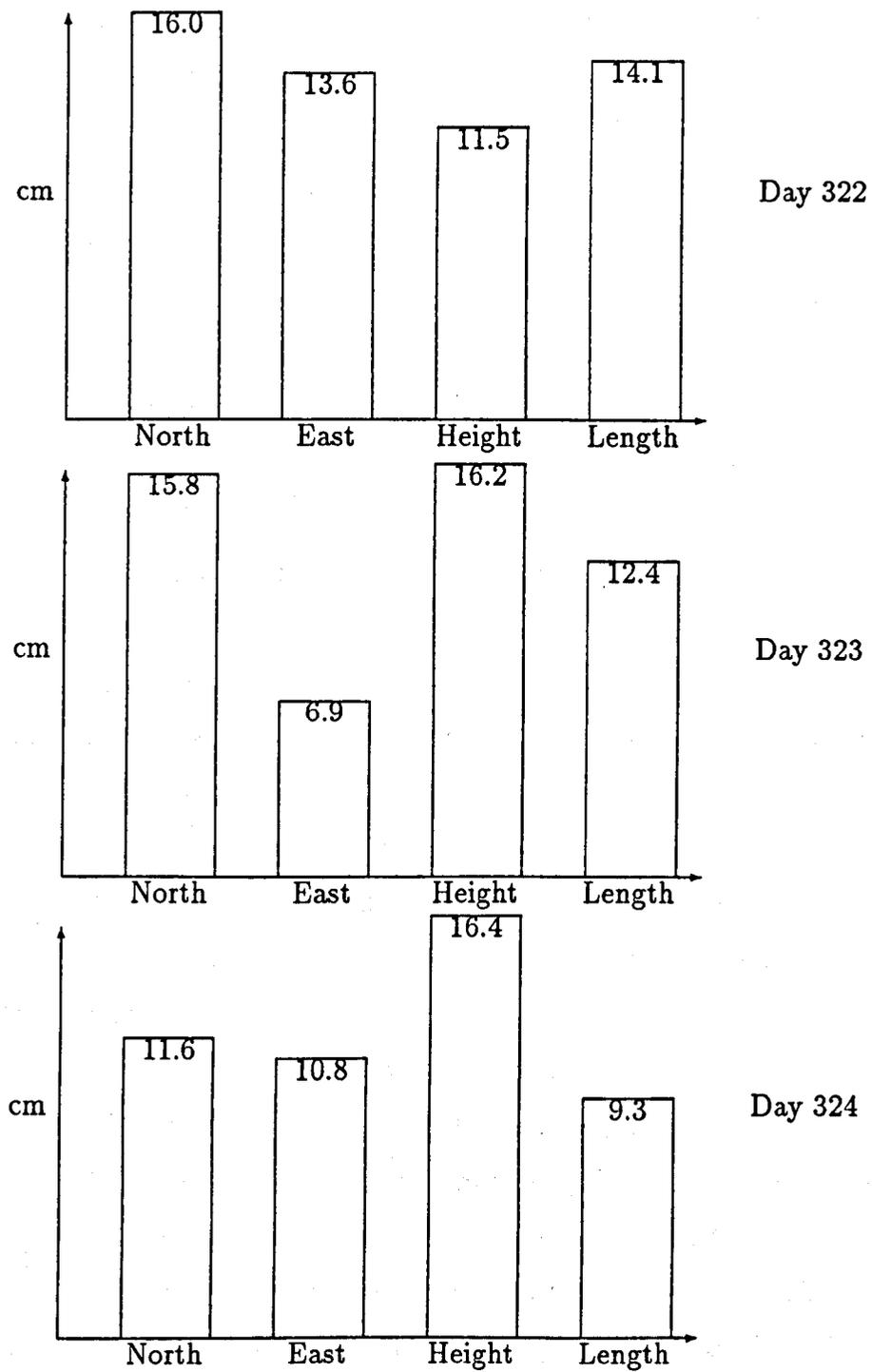
Figure 5.7: RMS baseline component differences : Single day orbit determination solution compared with the three day solution

127

or two cycles, but further refinement proved difficult when the slip occurred after a gap in the data. This final stage of cycle slip repair was done by visual inspection of the double difference phase residuals. The L1 and L2 frequency solutions were computed separately, to check for the cycle slips on each frequency. Unfortunately, the unmodelled ionospheric delay on the single frequency solutions produced large residuals over the long baselines. This made the task of determining the value of the cycle slip troublesome and sometimes uncertain.

The occurrence of cycle slips should affect the broadcast and precise ephemeris solutions similarly. However, in the orbit determination solution, any remaining cycle slips in the data from the fixed fiducial sites will affect the accuracy of the orbit and these errors will propagate into the coordinates of the non fiducial sites.

One limitation of the current generation of GPS software at Nottingham University, is the necessity to use the data from the same number of satellites, at every receiver site. Hence, if one of the sites in the network is only observing three satellites, when the other sites are observing four, then all the data from that site will be rejected at that epoch. This causes particular problems between sessions A and B, when the receivers drop satellite 6 in order to acquire satellite 13. This had the effect of lengthening the gap between the two observing session, making the cycle slip reparation task even more difficult.

The single day broadcast ephemeris solutions gave a surprisingly good repeatability. Most of the baseline lengths were well within the one part per million accuracy expected from this ephemeris. The use of the precise ephemeris gave a different solution to the broadcast ephemeris, although there was no significant improvement in the solution. Both the precise and broadcast ephemeris baseline solutions were larger than the SLR determined WGS 72 baseline lengths. A seven parameter Helmert transformation was used to determine whether there were any significant scale biases between the two coordinate sets. The scale biases and their standard errors are given in table (5.12).

	scale bias ppm	standard error
Broadcast ephemeris	-0.320	0.3582
Precise ephemeris	-0.234	0.4015

Table 5.12: Scale biases between the WGS 72 coordinate set and the broadcast and precise ephemeris solutions

It can be seen from table (5.12) that there were scale biases between the two coordinate sets, although they both had large standard errors. If these scale biases are applied to the broadcast ephemeris day 324 solution and the precise ephemeris three day solution, the rms baseline differences compared to the WGS 72 coordinate set are reduced to 13.7 cm and 7.7 cm respectively. This compares to 29.3 cm and 20.5 cm before applying the biases.

The orbit determination solution, with the three fixed fiducial stations, did not exhibit these particular scale biases, suggesting that the coordinates of the fiducial sites constrained the scale of the network. On day 322 there were only 51 epochs (or minutes) of data observed simultaneously by the three fiducial sites. This day also produced the largest baseline differences with the three day solution. Days 323 and 324 both had over 100 epochs of simultaneous data from the fiducial sites, and these both produced better baseline agreements with the three day solution. The reason for this could be twofold; the last two days of the GPS campaign both shared more common data with the three day solution than day 322 or it may indicate that more observations were necessary to satisfactorily determine both the orbit and the unknown receiver coordinates for the single day solutions.

The fiducial network approach for orbit determination is particularly susceptible to errors in the fixed fiducial coordinates. In this solution, the coordinates of Onsala (determined from VLBI) may not have been consistent with the SLR determined coordinates of Grasse and RGO. Ideally, the fiducial sites would have been situated close to either SLR or VLBI facilities, but not a combination of the two. In Europe, the only site with both SLR and VLBI facilities is Wettzell, from which it is not possible to determine

the systematic biases between the two coordinate reference frames.

The solar radiation pressure models adopted for the three day solutions demonstrated that modelling for the constant y-bias acceleration gave only a slight improvement in the solution. The y-bias force is relatively small, and only for longer arcs are the effects expected to be particularly significant.

The satellite geometry, which affects all the solutions, was not optimal for the duration of the GINFEST GPS campaign. The sky plot shown in figure (5.2), shows that for the first half of the observation period, the satellites are all in a line running from the West to the East. The geometry improves slightly, during the second half of the observation period when satellite 13 is included. It is worth comparing this West-East satellite geometry, with the baseline components determined in figure (5.7), where the east components of the baselines were generally better determined than the north components.

The accuracy of all the solutions computed were in the order of a few parts in 10^7. At this level of accuracy, other error sources may become significant. The meteorological model used was the Saastamoinen model, which is based upon surface weather readings. This is expected to satisfactorily model the dry component of the troposphere, but the wet component, which can produce scale errors of the order of one part in 10^7, is more difficult to model. Furthermore, no surface weather data was recorded at Graz, and this station produced the largest baseline differences in all the solutions.

Chapter 6.
The Tide Gauge Project

CHAPTER 6

The Tide Gauge Project

6.1   Introduction

The tide gauge project was established to investigate the disrepancies be-
tween the oceanographic and the geodetic levelling techniques, which have
been used around the coast of Great Britain. The 3rd UK Scientific Levelling
Network of the Ordnance Survey, which connects the tide gauges of Great
Britain, indicates that there is a *sea slope* of $6.7\,cm\,/\,100\,km$, along the north-
south coastline. However, the oceanographic evidence suggests that there is a
sea slope of about $1.4\,cm\,/\,100\,km$. The investigations would involve comput-
ing the ellipsoidal height differences between several of the tide gauges along
the east coast of Great Britain, using GPS observations. The orthometric
height differences between these tide gauges could then be obtained from the
GPS solutions, using a geoidal model. This would allow a direct comparison
to be made between the two levelling techniques and the GPS derived height
differences. The majority of the work is being undertaken in a separate re-
search project [Basker, 1989] and this chapter is primarily concerned with
the determination of a precise ephemeris for the GPS computations.

6.2   GPS Campaign

The GPS campaign was designed to occupy 26 sites along the east coast of
Great Britain, from Leith in Scotland down to Lowestoft in Suffolk. Five of
these GPS sites were located adjacent to the tide gauge stations of Leith,
North Shields, Whitby, Immingham and Lowestoft. The campaign lasted a
total of eight days, starting from the 25th May 1988. Five roving receivers
were used on each day, initially occupying the five most northerly sites. On
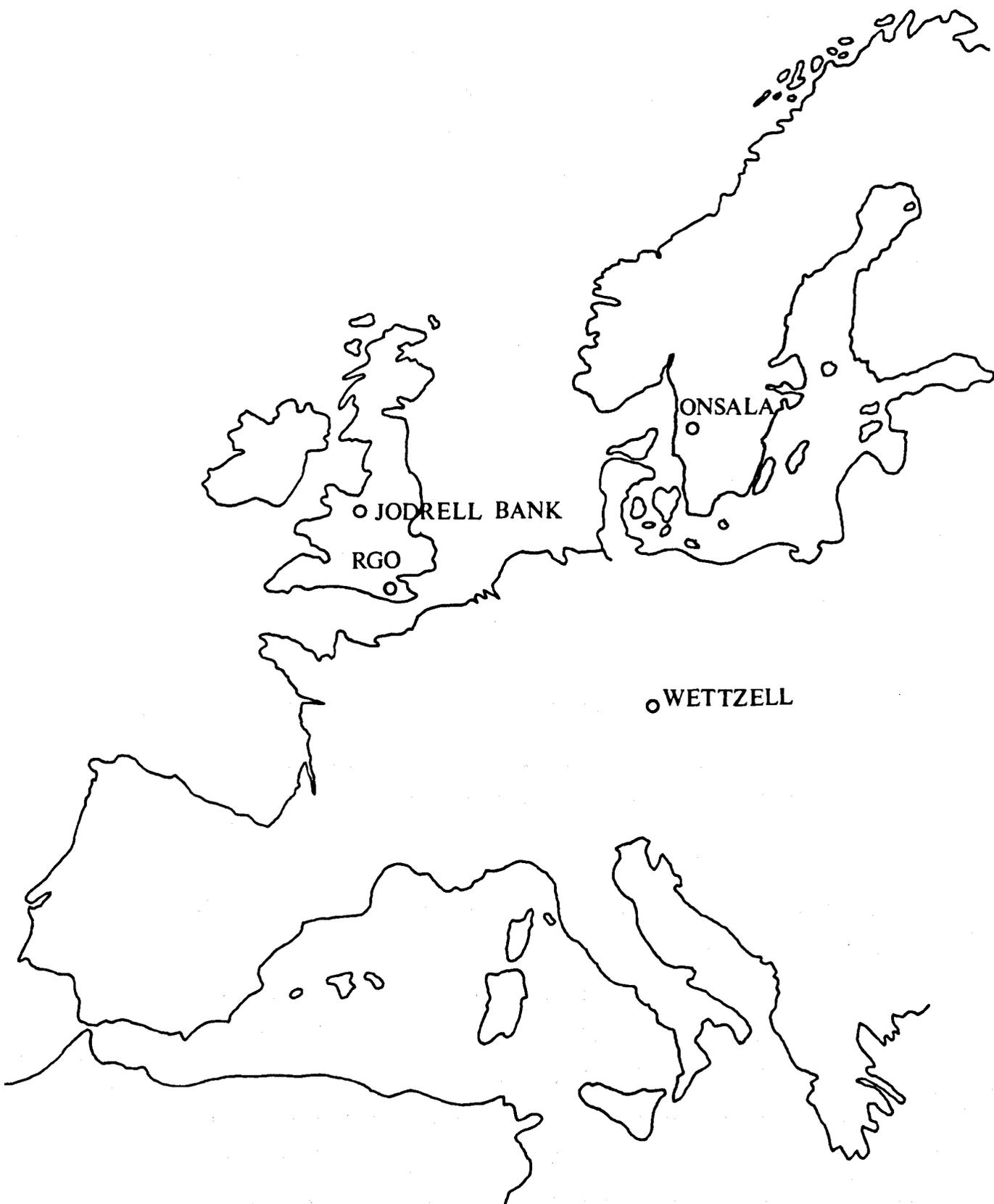
Figure 6.1: Location map for the tide gauge project

each successive day, the five receivers were moved south by three sites, such that two common sites were occupied on adjacent days. This system produced a common baseline on the adjacent days, which could be used to check the repeatability of the GPS solution and to provide a safeguard against missing data. The effects of the ionosphere were minimised by limiting the lengths of the baselines between adjacent sites to about 30 km.

At the same time, GPS receivers located at Onsala, Wettzell, Jodrell Bank and the Royal Greenwich Observatory (RGO) were recording simultaneous data (figure 6.1). These four receivers were located adjacent to VLBI or SLR facilities and would be used as fiducial sites in the computation of the satellite ephemerides.

The observing sessions for the roving receivers were designed to give maximum coverage of two particular satellite constellations and to give compatible data with the receivers located at the fiducial sites. These times are shown in table (6.1) for Wednesday 25th May (day number 146).

	Satellite (PRN)				Times (local times)
Session A	6 9	11	12		12:20 - 13:30
Session B	9	11	12	13	13:50 - 15:00
Session C	3	11	12	13	15:00 - 16:10

Table 6.1: Observing sessions for the roving receivers

The observing sessions for the static receivers at the two fiducial sites of RGO and Jodrell Bank were selected to be compatible with the observing periods of the permanent CIGNET tracking sites at Wettzell and Onsala. The times are given in table (6.2) for day number 146.

The times of the observing sessions precessed by four minutes each day after the times given in tables (6.1) and (6.2). TI 4100 GPS receivers were used at each site, with the data recorded on IBM personal computers. Meteorological data was recorded at each site at fifteen minute intervals.

The satellite configuration for the tide gauge campaign is shown in figure (6.2) with the majority of the satellites located in the western part of the sky. This is not an ideal geometrical configuration, but no improvement could be
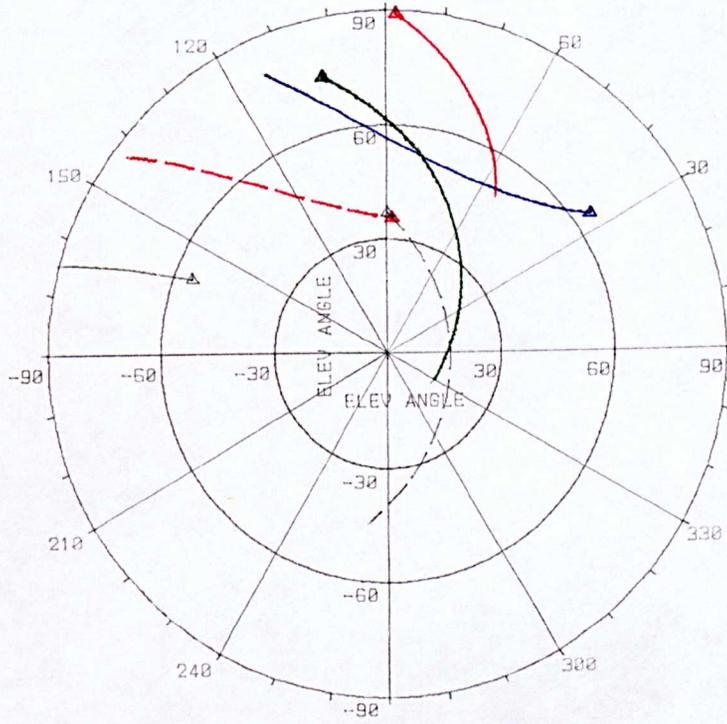
Figure 6.2: Satellite sky-plot for the tide gauge project

	Satellite (PRN)					Times (local times)
Session A	6	9	11	12		12:28 - 13:48
Session B		9	11	12	13	13:48 - 14:52
Session C	3	9	11		13	14:52 - 15:56
Session D	3			12	13	15:56 - 17:08

Table 6.2: Observing sessions for the static receivers

made with the current satellite constellation.

6.3   Derivation of the Fiducial Site Coordinates

WGS 84 coordinates for the L1 phase centre of the TI 4100 antennas at the
fiducial sites of Onsala and Wettzell were obtained from [Boucher et al, 1988].
Consistent WGS 84 coordinates of the intersection of the axes for the SLR
facility at RGO were obtained from the same source. These coordinates were,

$$x = 4033463.921$$
$$y = 23661.435$$
$$z = 4924304.741$$

The *solar pillar* was used for the duration of the tide gauge campaign at
the RGO, with the eccentricity vectors to the SLR intersection of axes given
as,

$$\Delta x = -4.651$$
$$\Delta y = -36.078$$
$$\Delta z = -1.946$$

The height of the L1 phase centre above the solar pillar bench mark was
measured as 1.168 m. The final WGS coordinates of the L1 phase centres for
the GPS antennas at RGO, Onsala and Wettzell are given in table (6.3).

6.4   Data Preprocessing

The data from the roving receivers, Jodrell Bank and RGO was recorded on
three and a half inch floppy discs at three second intervals. The data was then
loaded onto the hard disc of a Zenith personal computer and transferred onto

Site	x (m)	y (m)	z (m)
RGO	4033460.008	23625.361	4924303.700
Onsala	3370659.739	711876.241	5349787.910
Wettzell	4075546.159	931824.800	4801598.990

Table 6.3: L1 phase centre coordinates for the tide gauge fiducial sites : WGS 84

the ICL 3900 mainframe computer at Nottingham University using *Kermit*, a file transfer protocol. The data from the CIGNET sites at Onsala and Wettzell was obtained from the U.S. National Geodetic Survey (NGS) on a magnetic tape, which contained the satellite ephemeris, meteorological data and the measurement data at thirty second intervals.

The data from the roving receivers was processed by another postgraduate student, as part of his research project [Basker, 1989]. The preprocessing work work done by the author was confined to the fiducial sites only. At the time of the data processing, no accurate eccentricity vectors were available for Jodrell Bank and this site was left out of the preliminary computations. Figure (6.3) shows the availability of data from the three remaining fiducial sites.

	Day number							
	146	147	148	149	150	151	152	153
RGO	X	X	X	X	X	X	X	X
Wettzell	X	X	X	X	X		X	X
Onsala	X	X	X	X	X	X		

Figure 6.3: Fiducial site data availability

Unfortunately, no data was recorded at the site Wettzell on day 151 and no data was recorded at Onsala on days 152 and 153.

The data from Onsala and Wettzell is provided by the US National Geodetic Survey in a standard format, already decoded into measurement data at thirty second intervals. The data from RGO was decoded using **TIDE-CODE** to obtain the measurements at three second intervals. The data

from all these sites was then filtered to remove all the satellites below a 15° elevation angle using **EAFILTER**.

In order to produce simultaneous measurement data for the three sites, the RGO data was normal pointed to the same epochs as the thirty second data from Onsala and Wettzell. This was done by fitting a series of second order polynomials to each thirty second span of the RGO data using **NORMAL**. The receiver clock offsets were determined in the pseudorange solution (**PSEUDO**) and these were used to time correct the carrier phase data using **TIMECOR**.

The last stage of the preprocessing was to detect and correct for any cycle slips. The data from the three fiducial sites was used in a single frequency L1 double difference solution for each day. The residuals of each solution were then examined to detect the size and location of any cycle slips. These were then corrected for the L1 frequency and the process repeated for the L2 frequency. A combined L1/L2 (ionospherically corrected) solution was then computed to check the quality of the *cycle slip free* data.

6.5   Analysis of Data

The main objective of the GPS data analysis was to produce precise ellipsoidal height differences between the roving receiver sites. The height differences between the tide gauges could then be obtained by precise levelling between the tide gauges and the adjacent roving receiver sites. Two methods were considered possible to produce these GPS height differences,

1. Process the data from the roving receivers and the three fiducial sites simultaneously for each day. The fiducial site coordinates would be held fixed in the adjustment and estimates made for the roving receiver coordinates, satellite state vectors and the initial phase ambiguities.

2. Process the data from the fiducial sites separately to produce a *precise* ephemeris. This precise ephemeris could be used in a separate solution to determine the coordinates of the roving receivers for each day.

The first method would be similar to the processing technique used for the single day GINFEST solutions (chapter 5). An examination of the observing sessions for the roving and static receivers shows there is some incompatibility between the observation times of the different satellite sessions and also the session C constellations are different. The data for the first five days of the campaign, from the static receivers at the fiducial sites was of a reasonable quality, with no large breaks in the data. However, on the last three days of the campaign, only two of the fiducial sites recorded data.

Single day solutions were computed for the first five days of the campaign, using both the fiducial and roving receiver data, solving for the roving receiver coordinates and the satellite state vectors. However, the standard errors of the estimated receiver coordinates were of the order of one metre and of the order of several hundred metres for the satellite state vectors. A check on the repeatabilities of the solutions were made by comparing the common baseline lengths on the adjacent days. The differences between the common baseline lengths were up to 20 cm for baselines of between 12 km and 29 km, giving typical repeatabilities of between five and ten parts per million. This poor estimation of the coordinates may have been influenced by the satellite and receiver geometry. An examination of the sky-plot in figure (6.2) shows the position of the satellites, which are mainly at low elevation angles in one quadrant of the sky. In addition, on the first few days of the campaign the roving receivers were poorly located with respect to the fiducial sites (figure 6.1), with all the sites lying outside the fiducial network. This combination of receiver and satellite geometry would appear to have contributed to the poor repeatability of the GPS solutions. This problem is exacerbated by the loss of data which occurs when combining the data from the different observing sessions of the fiducial and roving receivers. One method of fully utilising the fiducial site data is to process it independently of the roving receiver data. This is the approach adopted for the second option.

The fiducial data was divided into two sets to allow the computation of two sets of four day orbits, covering day numbers 146 to 149 and day numbers 150 to 153. The length of the arcs were limited to four days to reduce the

amount of data to be processed in each batch and to reduce the effect of any unmodelled force model components. The second set of four day orbits (150 → 153), would also test the effect of determining the orbit with only two fiducial sites for part of the solution.

For each set of four day orbits, the following parameters were estimated,

- Initial phase ambiguities for each day.

- Satellite state vector for each satellite.

- Direct solar radiation pressure coefficient for each satellite.

- Y bias acceleration for each satellite.

For all the solutions, the ionosphere was corrected using the combined L1/L2 frequency and the troposphere was corrected with Saastamoinen's model, using the surface meteorological data recorded at each site.

Two main points were noted in the processing,

1. No estimates could be made for satellite 3 for both sets of orbits, mainly due to a lack of observations to this satellite. The satellite was then rejected from all the computations.

2. The lack of the fiducial data in the second set of orbits was apparent with the number of double difference observations in the first set of orbits as 4672 and the number in the second set as 2390.

For each four day solution, the estimated orbital parameters were used in **ORBIT** to integrate the orbits again. This iterative process was repeated until no further change in the estimated parameters were noted.

Single day solutions were then computed using only the data from the roving receivers, but with the satellite coordinates obtained from the orbits computed in the previous two solution. The estimated parameters included only the receiver coordinates and the initial phase ambiguities. The baseline lengths between the roving receiver sites varied between ten and thirty kilometres. It is over this length of baseline that the double difference solution may become sensitive to the effects of the ionosphere. Three types of

solution were computed with the aims to test the effect of modelling for the ionospheric delay and to test the effect of constraining the phase ambiguities to integer values.

1. Combined L1/L2 solutions were computed with the standard first order ionospheric correction (section 2.5.2).

2. Single frequency L1 solutions were computed, which do not include an ionospheric correction.

3. An integer *fixed* solution was computed for the single frequency L1. In this solution the estimated *integers* from solution (2) were constrained to integer values.

Each solution was computed with the position of one of the sites constrained to the coordinates determined in the pseudorange solution. The meteorological data recorded at each site was not used to correct for the troposphere, instead the standard atmosphere model (section 2.5.2) was used. This would prevent the solutions being biased by possible uncalibrated meteorological equipment, which is more noticeable on shorter baselines.

The receiver sites used in the computations and the identification letters used are,

Quixwood Moor	QUI
Shoreswood	SHO
Shilbottle	SHI
Helm	HEL
High Moorsley	HIG
Billingham	BIL
Whitby	WHI
Cloughton	CLO
Atwick Sands	ATW
Tunstall	TUN
Binbrook	BIN
Castcliffe Hill	CAS
Thornham	THO
Great Massingham	GRE

Table (6.4) shows the baseline lengths and heights for the ionospherically corrected L1/L2 solution. The single frequency L1 solution results are given in table (6.5). Table (6.6) shows the results of the single frequency L1 solution with the phase ambiguities constrained to integer values. These integers were obtained from the previous L1 solution.

No data was available from the roving site QUI on day 147, preventing a determination of the QUI - SHO baseline on day 147.

There is no external source by which to compare these results. The only method of assessing the accuracy is to check the repeatability of the common baseline lengths and height differences for the adjacent day solutions. These repeatabilities are shown in table (6.7) for the seven baselines available, for each of the three different solutions.

The most consistent solution for both the baseline length and height differences is the L1 fixed ambiguity solution. The process of constraining the *integer* ambiguities to integers gives a better solution than the L1 frequency with no integer constraint.

Day	Baseline	length (km)	Height Difference (m)
146	QUI - SHO	25152.084	151.172
147	QUI - SHO	no data	
	SHI - HEL	12070.097	3.444
148	SHI - HEL	12070.171	3.422
	HIG - BIL	28933.506	150.679
149	HIG - BIL	28933.539	150.564
	WHI - CLO	17377.650	-188.573
150	WHI - CLO	17377.632	-188.543
	ATW - TUN	21310.098	-3.340
151	ATW - TUN	21310.122	-3.359
	BIN - CAS	18714.862	-8.288
152	BIN - CAS	18714.850	-8.237
	THO - GRE	23085.674	-42.504
153	THO - GRE	23085.552	-42.456

Table 6.4: Tide gauge project : L1/L2 solution

Day	Baseline	length (km)	Height Difference (m)
146	QUI - SHO	25152.091	151.090
147	QUI - SHO	no data	
	SHI - HEL	12070.095	3.440
148	SHI - HEL	12070.122	3.437
	HIG - BIL	28933.490	150.559
149	HIG - BIL	28933.512	150.644
	WHI - CLO	17377.634	-188.549
150	WHI - CLO	17377.611	-188.492
	ATW - TUN	21310.081	-3.340
151	ATW - TUN	21310.070	-3.320
	BIN - CAS	18714.826	-8.263
152	BIN - CAS	18714.846	-8.216
	THO - GRE	23085.649	-42.443
153	THO - GRE	23085.583	-42.468

Table 6.5: Tide gauge project : L1 ambiguity free

Day	Baseline	length (km)	Height Difference (m)
146	QUI - SHO	25152.098	151.075
147	QUI - SHO	no data	
	SHI - HEL	12070.090	3.440
148	SHI - HEL	12070.085	3.487
	HIG - BIL	28933.478	150.616
149	HIG - BIL	28933.508	150.660
	WHI - CLO	17377.638	-188.555
150	WHI - CLO	17377.600	-188.514
	ATW - TUN	21310.078	-3.338
151	ATW - TUN	21310.075	-3.338
	BIN - CAS	18714.834	-8.279
152	BIN - CAS	18714.830	-8.235
	THO - GRE	23085.627	-42.467
153	THO - GRE	23085.618	-42.489

Table 6.6: Tide gauge project : L1 ambiguity fixed solution

144

Repeatabilities in centimetres							
Baseline	(km)	Baseline length			Height differences		
		L1	L1 fixed	L1/L2	L1	L1 fixed	L1/L2
SHI-HEL	12	2.7	0.5	7.4	0.3	4.7	2.2
HIG-BIL	29	2.2	3.0	3.3	8.5	4.4	11.5
WHO-CLO	17	2.3	3.8	1.8	5.7	4.1	3.0
ATW-TUN	21	1.1	0.3	3.3	2.6	0.0	1.9
BIN-CAS	19	2.0	0.4	1.2	4.7	4.4	5.1
THO-GRE	23	6.6	0.9	12.2	2.5	2.2	4.8

Table 6.7: Repeatability of the common baselines

The effect of neglecting the ionospheric delay is considered to be a contraction in the scale of a network (section 2.5.2). A comparison of the baseline lengths given in tables (6.4) and (6.5) would generally support this theory. However, the combined L1/L2 frequency (ionospherically corrected) solution has produced the largest anomalies for both the baseline length and the height differences. The two largest discrepancies in the L1/L2 solution also correspond with the largest differences in the L1 ambiguity free solution. The ionospheric delay would be of a similar magnitude on the eight consecutive days of the GPS campaign, because the same satellite constellations were observed at the same time of day. The ionospheric delay would then be expected to cause a similar scale effect on each of the networks determined over these eight days. Hence, this may explain why the L1 solutions give a better repeatability than the ionospherically corrected, but noisier L1/L2 solutions.

The repeatability of the WHI-CLO baseline is worth consideration as it is determined at the break between the two sets of four day orbits. Therefore, this represents a better test of the repeatability of the solutions, because the coordinates of WHI and CLO on the adjacent days were determined from two independent sets of orbits. However, the repeatability of this baseline can be seen to be comparable with the baselines determined on the other days.

No obvious differences can be seen between the repeatabilities of the base-lines determined from the two sets of orbits, with the possible exception of the THO-GRE baseline, which was determined at the end of the second set of orbits. This may well have been caused by the lack of data from the fiducial sites during the latter part of the observation campaign. A comparison has been made between the height differences obtained in these solutions and the height differences obtained in a broadcast ephemeris solution [Ashkenazi et al, 1989]. Whilst the average agreement between the height differences during the first set of four day orbits was of the order of three millimetres, this increased to over three centimetres during the second set of four day orbits. These differences suggest that the loss of the data from the fiducial sites, in particular the use of only two fiducial sites on the last three days, has degraded the accuracy of the orbits. The inclusion of the data from Jodrell Bank may strengthen the orbit determination solution, but the location of the site is not ideal, when considering the missing fiducial site data is from Onsala and Wettzell.

Whilst the loss of the fiducial site data has led to larger differences in the heights during the second four days, the effect of using the different solution types (L1, L1 fixed ambiguities and the L1/L2) would appear to be more significant. This may indicate that the GPS derived height differences are less susceptible to errors in the orbit than from other error sources, such as atmospheric effects, for this length of baseline.

These results do show the advantage of using longer arcs in the orbit determination process, where there is a loss of tracking data from the fiducial sites. The longer arcs have improved the solution when comparing the repeatabilities with those obtained from the single day solutions. One disadvantage of the TI 4100 GPS receiver is that a maximum of four satellites can be observed at any one time. The use of a receiver capable of tracking all the available satellites would produce more data for each satellite. This would prevent the problems encountered with this project, where the fiducial and roving receivers observed slightly different satellite sessions. Currently some of the TI 4100 receivers at the CIGNET sites (section 2.4.2) are being

replaced by Mini Mac receivers, which are currently capable of tracking all the available satellites.

The repeatabilities of the GPS height components are of the order of a few centimetres for baselines up to 30 km. However, the discrepancy between the oceanographic and geodetic levelling techniques is of the order of 5 cm per 100 km. Clearly, this level of accuracy has not yet been reached if the repeatability of the solution is of a similar magnitude to the accuracy. A very common source of error when using GPS, is the measurement of the antenna heights. For this campaign, where the heights were critical, each antenna height was measured with a Wild level and with a tape measure, in order to reduce the possible errors. Therefore, it is unlikely that the high repeatabilities were caused by errors in the antenna heights.

A limiting factor in the determination of the satellite orbits was the geometry between the fiducial sites and the satellites. Whilst this does not change throughout the eight day campaign, the use of the continuous four day orbits would appear to have provided more constraint to the solution, giving the much better repeatabilities on the baselines of the adjacent days. Further improvement may have been possible by including data from additional fiducial sites, preferably located in a better distributed network.

It is not possible to determine the height difference between the tide gauges at Leith and Lowestoft with the data collected in the GPS campaign in 1988, due to the loss of data at several of the sites. There have been two GPS tide gauge campaigns since this date, but they were not recorded with data from any fiducial sites and they have not been investigated here. The results of these campaigns and the estimated GPS height difference between the Leith and Lowestoft tide gauges can be found in *Basker* [1989].

Chapter 7.
The GPS Standard Data Set

CHAPTER 7

The GPS Standard Data Set

7.1 Introduction

A five year GPS campaign was started in December 1986, to measure tectonic motions in central and southern California. The initial observations were comprised of three, five day observation periods. The last five days of the observation campaign were recorded between the 3rd and 7th of January 1987 and this is the data set analysed in this chapter. All the observations were recorded using the dual frequency TI-4100 NAVSTAR Navigator receivers

In this campaign, nine receivers were deployed at sites around the Californian coastline and islands. These local sites were situated near places of tectonic interest. Five more receivers were located at regional sites within California, four of which, Owens Valley, Mojave, Palos Verdes and Vandenburg have been surveyed using VLBI observations.

A further five receivers were placed outside California, at sites around North America. These continental sites were located at Austin, Churchill, Algonquin, Platteville and Westford. The last three of these sites have been surveyed using VLBI observations

A description of all the sites may be found in *Dong and Bock* [1988]. The regional and continental sites are shown in figure (7.1).

7.2 Description of Data Set

The GPS data set collected between the 3rd and 7th of January 1987, has been archived by the Massachusets Institute of Technology (MIT). The
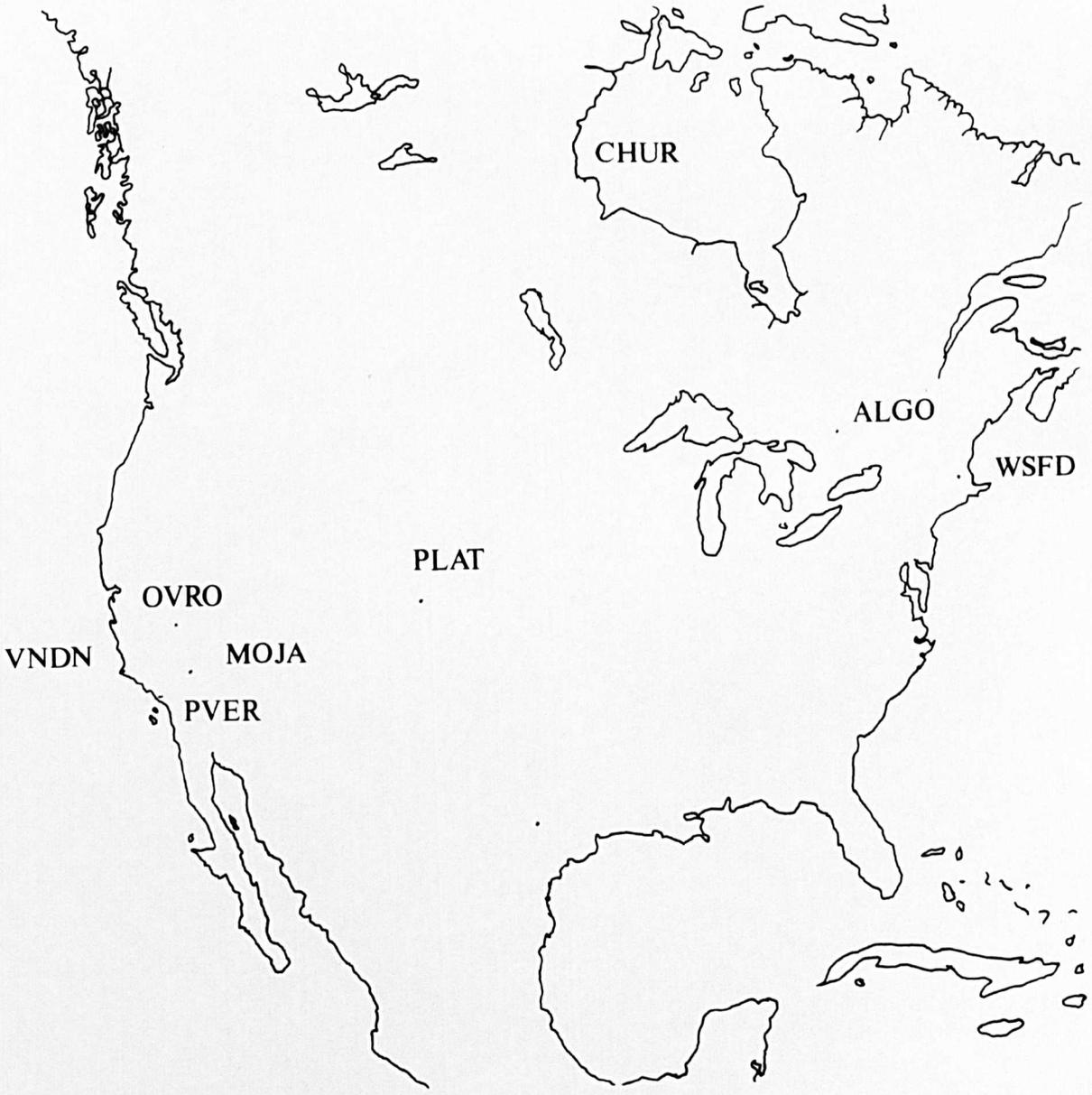
Figure 7.1: Regional and continental sites in North America

CSTG[1] GPS subcommission are distributing this *standard data set* to enable comparisons to be made of different GPS data processing techniques. The standard data set is available from the US National Geodetic Survey , on a nine track magnetic tape. The data is stored in two forms; the raw data sampled at 30 second intervals and a cycle slip free data set, at 120 second intervals. Also stored on the tape are the site coordinates, broadcast ephemerides and precise ephemerides.

The site coordinates are given in spherical geocentric form, in the SV 4 reference frame developed at the MIT (Appendix D). The antenna heights above the ground stations are given in a separate document.

The five day campaign spans over the GPS week 364 (January 3) and week 365 (January 4, 5, 6 and 7), which coincides with the change of reference systems used by the Defense Mapping Agency for the satellite ephemeris. The precise ephemeris for week 364 was given in WGS 72 coordinates and the precise ephemeris for week 365 was given in WGS 84 coordinates.

No surface weather data was available for the data processing, and a standard atmosphere model was used to account for the tropospheric delays. The observations were recorded at night to minimise the effects of the ionosphere.

The satellite constellation was selected to maximise the observation periods of satellites (PRNs) 3, 6, 9, 11 and 13. Satellite 12 was also tracked, but for a much shorter period. The satellite geometry was predominantly in a line running North-South (figure 7.2), with all the satellites exceeding an elevation angle of 60° at some point during the pass.

For the results presented in this chapter, only the GPS receivers located at the regional and continental sites were considered. The distribution of the data is shown in table (7.1).

---

[1]Commission on International Coordination of Space Techniques for Geodesy and Geodynamics (CSTG) was established in 1979 as Commission VIII of the International Association of Geodesy.
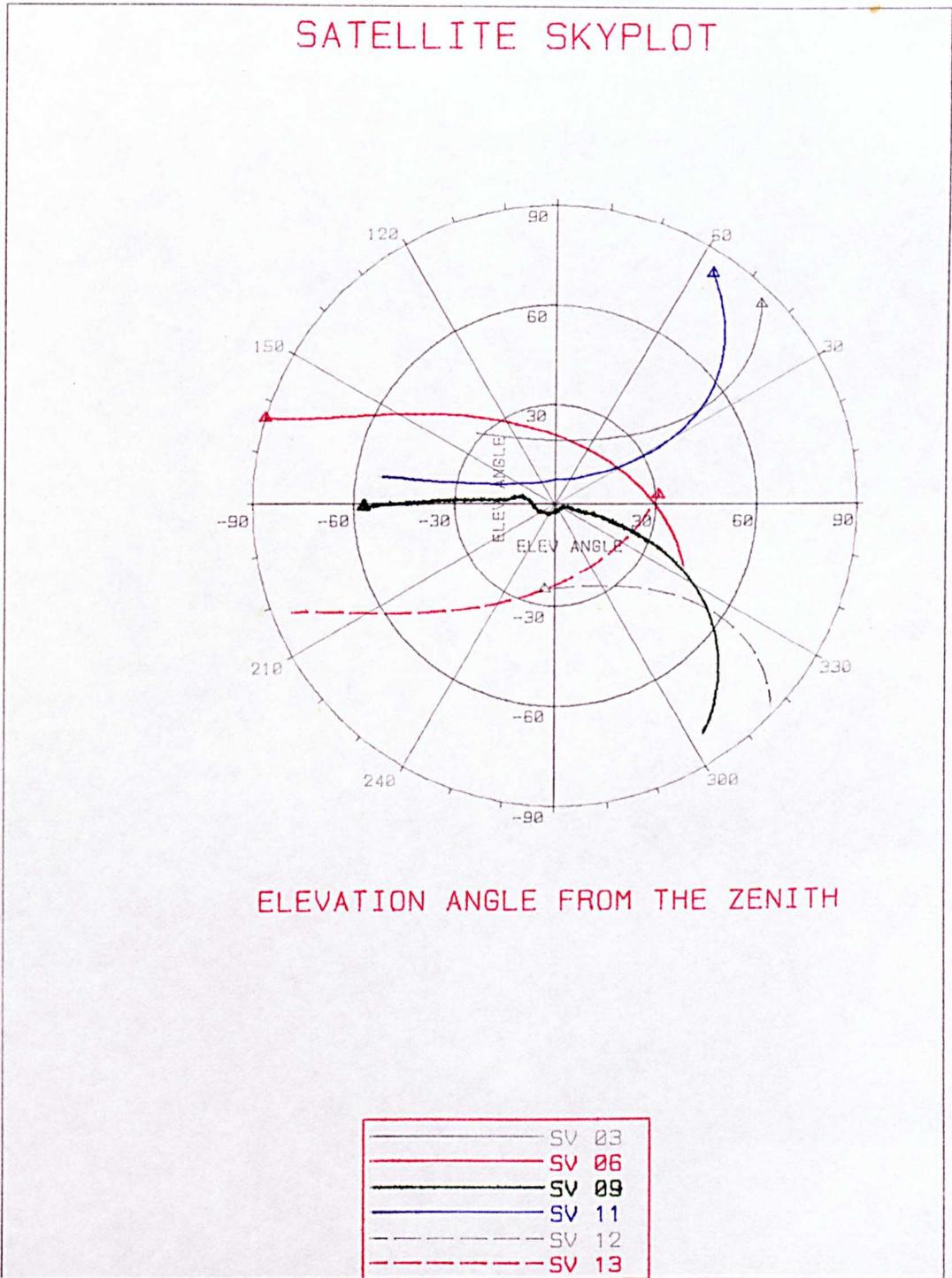
Figure 7.2: Satellite sky-plot for the North American data

	Day number	3	4	5	6	7	
	Continental						
Algonquin	(ALGO)	X	X	X	X	X	VLBI site
Platteville	(PLAT)	X	X	X	X	X	VLBI site
Westford	(WSFD)	X	X	X	X		VLBI site
Churchill	(CHUR)	X	X	X	X	X	
Austin	(AUST)				X	X	
	Regional						
Owens Valley	(OVRO)	X	X	X	X	X	VLBI site
Ford Ord	(FTOR)	X	X	X	X	X	
Mojave	(MOJA)				X	X	VLBI site
Palos Verdes	(PVER)	X	X	X	X	X	VLBI site
Vandenburg	(VNDN)	X	X	X	X	X	VLBI site

Table 7.1: Data distribution for the regional and continental sites

7.3 Analysis of Data

The standard data set was provided in two formats; the 30 second raw data and the 120 second cycle slip free data. The 120 second data was selected for the analysis to simplify the data preprocessing stage, especially with the data already having been *cleaned* of cycle slips.

With the 120 second data, it was not possible to time correct the phase data for the receiver clock bias, using the phase rate expression derived in equation (2.62), because of the 120 second interval between the phase measurements. Instead, it was decided to correct the carrier phase time tags using the pseudoranges.

If the satellite clock bias, broadcast in the satellite navigation message, is removed from the pseudorange, then the corrected pseudorange is comprised of the true range (in seconds) and the receiver clock bias. If this corrected pseudorange is subtracted from the carrier phase time tag, then the time of signal transmission at the satellite in GPS System Time remains. This was then used as the time tag in the analysis.

The orbit integration was started from a satellite state vector, obtained from the NSWC precise ephemeris. An initial value for the direct solar radiation pressure coefficient was estimated to be 1.5. This was equivalent to an acceleration of about 0.848×10^{-7} ms^{-2}, which was estimated from previous computations. The WGS 84 geopotential model was used for the numerical integration up to degree and order 8, with the recommended value of the product GM taken to be 3986005.0×10^8 m^3s^{-2}. This was used to allow a comparison to be made with the NSWC precise ephemeris.

Four different lengths of solution were considered:

- Single day solutions were computed for each day, solving for the six parameter initial state vector for each satellite, receiver coordinates and the initial phase ambiguities. Comparable single day solutions were also computed by Mr. M. Aquino, using the orbit relaxation techniques (section 3.8).

- Two continuous, two day solutions were computed for the days 4 and 5,

and the days 6 and 7. For these, solutions were produced to investigate the effect of solving for the direct solar radiation pressure coefficient for each satellite.

- A continuous three day solution was computed, for the days 4, 5 and 6. The effects of solving for the constant y bias acceleration for each satellite were investigated.

- A continuous four day solution was computed, for the days 4, 5, 6 and 7. The effects of solving for the constant y bias acceleration were investigated, as in the three day solution.

All the multiple day solutions estimated a new set of initial phase ambiguities for each day.

In all the solutions, the L1/L2 combined frequency was used to correct for the ionospheric effects. The tropospheric delay was accounted for, using the standard atmosphere model given in section (2.5.2).

The coordinates of Owens Valley (OVRO), Platteville (PLAT) and Algonquin (ALGO) were held fixed to their SV4 coordinates in all the solutions. These sites were selected to provide the best geometrical configuration with the most reliable data.

7.3.1 Single Day Solutions

The single day solutions were computed for the days 3, 4, 5 and 6, using the data from the VLBI fiducial sites. A comparable solution was also computed using the orbit relaxation technique. No comparisons are given for day 7, because of problems encountered with the orbit relaxation technique when using the broadcast ephemeris on that day.

The solutions for day 3 are presented in table (7.2). The differences shown are the VLBI determined baselines minus the GPS determined baselines for both types of solution. PVER had no simultaneous data observed with the other sites and consequently the data couldn't be used.

It can be seen that the differences between the GPS and VLBI computed baseline lengths, are of a similar magnitude for both the orbit determination

154

		Orbit Determination		Orbit Relaxation	
	Length (km)	Difference (cm)	ppm	Difference (cm)	ppm
ALGO - VNDN	3727	-7.5	0.020	11.1	0.030
- WSFD	642	7.4	0.115	-4.6	0.072
PLAT - VNDN	1533	-6.7	0.044	9.9	0.065
- WSFD	2752	7.1	0.026	-8.3	0.030
OVRO - VNDN	363	-7.0	0.193	7.8	0.213
- WSFD	3929	7.1	0.018	-6.0	0.015
VNDN - WSFD	4228	-0.3	0.001	5.5	0.013
		rms = 6.6		rms = 7.9	

Table 7.2: Single day solution baseline differences with VLBI : Day 3

		Orbit Determination		Orbit Relaxation	
	Length (km)	Difference (cm)	ppm	Difference (cm)	ppm
ALGO - VNDN	3727	9.1	0.024	5.8	0.015
- WSFD	642	-1.5	0.023	18.7	0.291
PLAT - VNDN	1533	11.0	0.072	4.0	0.026
- WSFD	2752	-2.8	0.010	-3.1	0.011
OVRO - VNDN	363	6.5	0.179	8.3	0.228
- WSFD	3929	-3.1	0.008	0.7	0.002
VNDN - WSFD	4228	6.4	0.015	4.2	0.010
		rms = 6.6		rms = 8.4	

Table 7.3: Single day solution baseline differences with VLBI : Day 4

and the orbit relaxation solutions. Baseline errors of up to 2 parts in 10^7 occur on the shorter 363 km OVRO-VNDN baseline, for both the solutions. The errors on the other baseline lengths are generally less than one part in 10^7.

Similar results were obtained for day 4, given in table (7.3). Again, the OVRO-VNDN baseline produces the largest discrepancy from the VLBI solution. The orbit relaxation solution has also given a poor estimate for the ALGO-WSFD baseline, producing an error of 3 parts in 10^7.

		Orbit Determination		Orbit Relaxation	
	Length (km)	Difference (cm)	ppm	Difference (cm)	ppm
ALGO - VNDN	3727	-11.0	0.030	8.7	0.023
PLAT - VNDN	1533	-9.7	0.063	7.1	0.047
OVRO - VNDN	363	-8.7	0.239	7.4	0.202
		rms = 9.8		rms = 7.8	

Table 7.4: Single day solution baseline differences with VLBI : Day 5

The solutions for day 5 are presented in table (7.4). Unfortunately the data from WSFD had two satellites missing and could not be used in the analysis. PVER had no compatible data with the other sites and also had to be rejected. Therefore, the solutions had only one station to make a any baseline comparisons with. The orbit determination and relaxation solutions both gave similar answers, with maximum baseline differences of up to 2 parts in 10^7. It is interesting to note that the differences between the two solutions are of opposite sign. This was also noted on day 3.

The solutions for day 6 are presented in table (7.5). This day produced the largest differences for both the orbit determination and the orbit relaxation solutions. The Californian sites at MOJA and PVER produced the largest differences for the orbit determination solutions. All the baseline differences were less than 2 parts in 10^7 except for the OVRO-MOJA baseline, which gave an error of 4 parts in 10^7. However, for the orbit relaxation technique,

			Orbit Determination		Orbit Relaxation	
		Length (km)	Difference (cm)	ppm	Difference (cm)	ppm
ALGO	- MOJA	3407	18.3	0.054	7.8	0.023
	- PVER	3611	20.9	0.058	5.3	0.015
	- WSFD	642	-1.9	0.030	37.6	0.585
PLAT	- MOJA	1196	18.5	0.155	5.6	0.046
	- PVER	1407	20.4	0.145	1.4	0.010
	- WSFD	2752	1.8	0.007	26.3	0.095
OVRO	- MOJA	245	-10.0	0.407	4.2	0.172
	- PVER	387	3.8	0.098	10.7	0.277
	- WSFD	3929	-1.9	0.005	29.9	0.076
MOJA	- PVER	224	2.6	0.116	-1.9	0.086
	- WSFD	3903	17.4	0.045	35.5	0.091
PVER	- WSFD	4096	20.0	0.049	32.0	0.078
			rms = 14.0		rms = 21.5	

Table 7.5: Single day solution baseline differences with VLBI : Day 6

the largest differences were for the baselines connected to WSFD. This gave an error of 6 parts in 10^7 on one of the baselines, with the other differences less than 3 parts in 10^7.

In general, the orbit determination technique gave better results than the orbit relaxation technique, when comparing the baseline lengths with the VLBI coordinates. Both of the solutions were computed using the same number of observations and the same tropospheric models. This would suggest that the differences are caused by the different methods of modelling the orbit. The orbit relaxation technique solves for the corrections to the broadcast elements which describe the mean orbital ellipse. Hence, any errors in the other nine broadcast elements, which describe the perturbations from this mean ellipse will not be accounted for. Therefore, this method relies upon the quality of the broadcast ephemeris. However, in the orbit determination technique, the force model should account for any orbital perturbations.

The root-mean-square (rms) differences between the baseline components of the single day orbit determination solution and the VLBI solution are shown in figure (7.3). It can be seen that the north components of the baselines are generally better determined than the east components. This is particularly noticeable on day 6, where the rms differences for the two components are 2.1 cm and 17.1 cm respectively. This has produced the large discrepancies in the determination of the baselines from ALGO and PLAT to PVER and MOJA. An examination of the sky-plot in figure (7.2) shows the predominant north-south satellite geometry, which appears to produce a better determination of the north-south baseline components.

The height components of the baselines are also determined better than the east components. This is in contrast to the GINFEST data, where the height components produced the largest errors.

For the orbit determination solution, no estimates were made for the direct solar radiation pressure coefficient. Attempts were made to solve for this parameter, but no significant estimates could be made. It was assumed that the six parameter satellite state vector was sufficient to absorb any unmodelled accelerations on the satellite, for the arc lengths of only a few

158
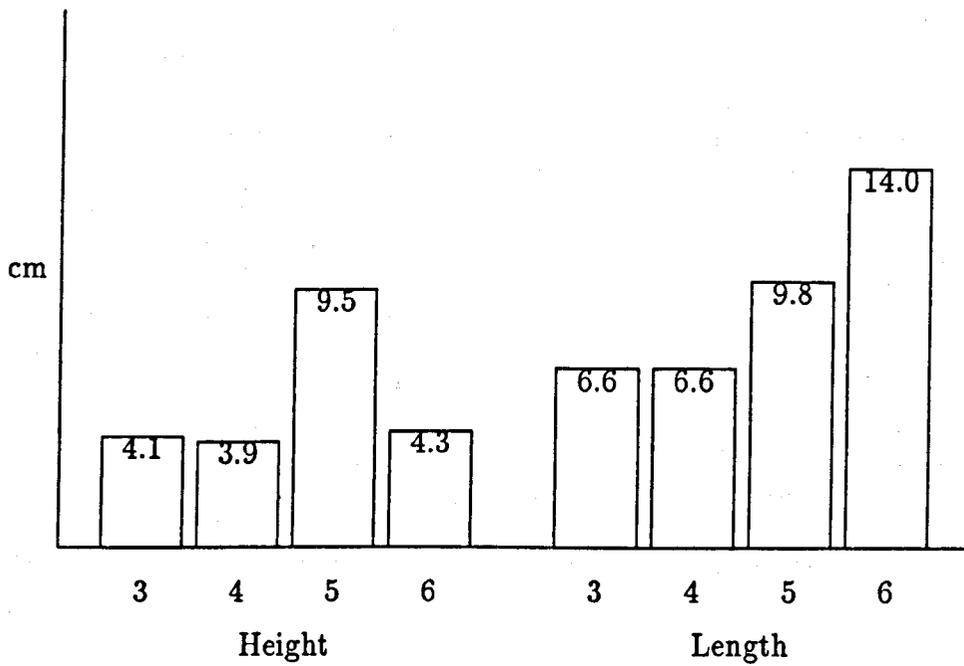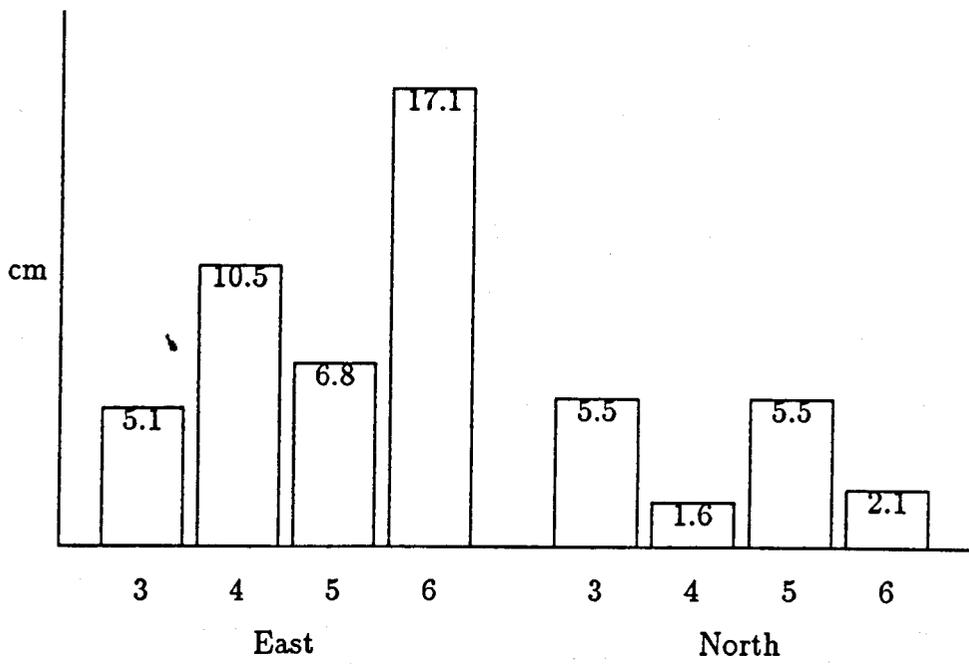
Figure 7.3: RMS baseline vector differences from VLBI : Single day orbit determination solutions

hours.

Average of the single day solutions

A coordinate set has been computed from the unweighted mean of the four single day solutions, for both the orbit relaxation and orbit determination methods. These coordinates have been compared with the VLBI coordinate set and the baseline differences are given in table (7.6) for both solutions.

For the orbit determination solution, a significant improvement is seen, in comparison with the individual single day solutions. The maximum baseline error, is reduced to 8 parts in 10^8, with all the other baselines less than 2 parts in 10^8.

For the orbit relaxation solutions, no significant improvement can be seen from the individual single day solutions, with the baseline errors up to 2 parts in 10^7. This error occurs on the short baseline, as with the case of the single day solutions.

			Orbit determination		Orbit relaxation	
		Length (km)	Difference (cm)	ppm	Difference (cm)	ppm
ALGO	- VNDN	3727	-3.1	0.008	8.5	0.023
	- WSFD	642	1.4	0.020	17.2	0.268
PLAT	- VNDN	1533	-1.8	0.012	7.0	0.046
	- WSFD	2752	0.8	0.007	5.0	0.018
OVRO	- VNDN	363	-3.0	0.084	7.8	0.216
	- WSFD	3929	0.7	0.002	8.2	0.021
VNDN	- WSFD	4228	3.1	0.007	4.9	0.011
			rms = 2.2		rms = 9.2	

Table 7.6: Average of the single day solutions : differences from the VLBI baselines

The rms differences between the VLBI and the averaged orbit determination solution are shown in figure (7.4). It can be seen that the largest rms difference is in the height component and this is mainly caused by the

160

OVRO-VNDN height component, which is in error by 1.6 parts in 10^7. All the other baseline components agree with the VLBI solution better than 1 part in 10^7.
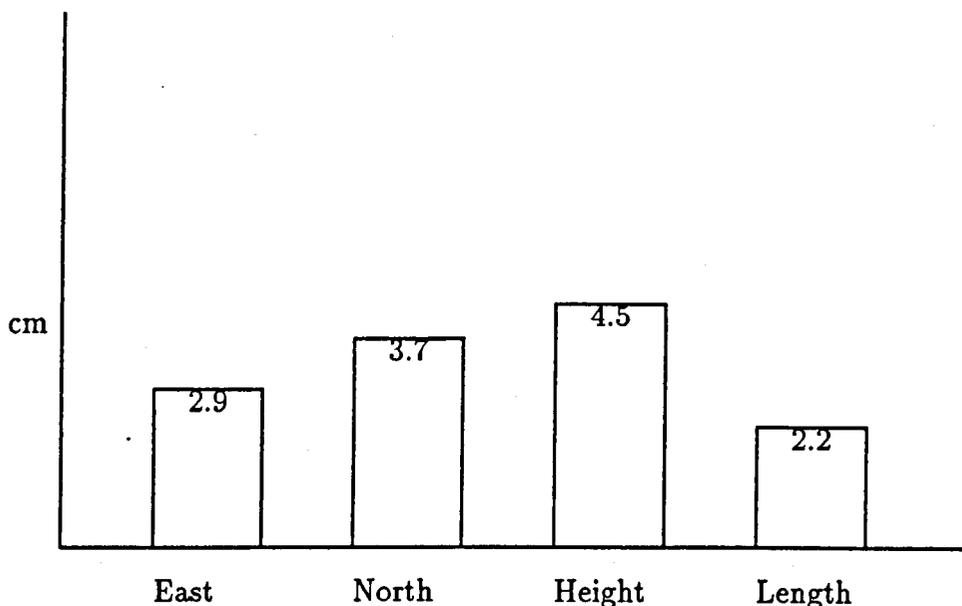
Figure 7.4: Average single day baseline vector differences from VLBI

The results of these few comparisons, suggests that there is some form of systematic error present in the orbit relaxation solution, possibly caused by using the broadcast ephemeris. This effect was not seen in the orbit determination solution, where the average solution gave a much better agreement with the VLBI coordinate set.

7.3.2   Two Day Solutions

The two continuous, two day solutions were computed for the days 4 and 5, and the days 6 and 7. For each solution, the receiver coordinates and the initial state vector for each satellite were estimated for the whole two days. A new set of initial integer ambiguities were estimated for each day of the solution. For each two day data set, a further solution was computed to solve for the direct solar radiation coefficient for each satellite, in addition to the other parameters. These two solutions are referred to in the text as the six

161

and seven parameter (per satellite) solutions respectively. No comparable solutions could be computed using the orbit relaxation technique and all the comparisons given here are with VLBI determined coordinates.

The differences between the VLBI determined baselines and the two day (4 and 5) solution, are given in table (7.7). In the six parameter solution, no estimates were made for the direct solar radiation pressure coefficient C_R. Instead, the value of 1.5 was used for C_R in the orbit integration. In the seven parameter solution, the coefficient C_R was estimated for each satellite.

			Six parameter solution		Seven parameter solution	
		Length	Difference (cm)	ppm	Difference (cm)	ppm
ALGO	- VNDN	3727	13.3	0.036	8.5	0.023
	- WSFD	642	21.1	0.328	13.1	0.204
PLAT	- VNDN	1533	14.4	0.094	8.9	0.058
	- WSFD	2752	12.2	0.044	5.0	0.019
OVRO	- VNDN	363	11.3	0.311	6.4	0.176
	- WSFD	3929	16.0	0.041	6.4	0.016
VNDN	- WSFD	4228	29.0	0.069	14.5	0.034
			rms = 17.7		rms = 9.6	

Table 7.7: Two day solution baseline differences with VLBI : Days 4 and 5

It can be seen from comparing the two solutions, that solving for the coefficient C_R, reduces the baseline differences by a factor of two. The two largest differences are on baselines connected to WSFD, where there is data on day 4 only. However, for the seven parameter solution, the baseline errors are all less than 2 parts in 10^7. The rms double difference phase residual for the six and seven parameter solutions are 0.11103 and 0.05055 cycles respectively.

The rms differences between the baseline components of the VLBI and the GPS orbit determination solutions are shown in figure (7.5). The improvement in the solution after solving for C_R for each satellite is obvious

from the figure. In this case the east components of the baselines are better determined than the north components. The errors in the height components of the baselines were also significantly reduced with the second solution.

The baseline differences between the VLBI and the GPS orbit determination solutions for days 6 and 7 are given in table (7.8). In this case it can be seen that both solutions give remarkably low rms baseline differences of 3.3 cm and 3.4 cm. All the baseline errors are reduced to less than 1.5 parts in 10^7. The rms double difference phase residual for the six and seven parameter solutions are 0.10187 and 0.05064 cycles respectively.

			Six parameter solution		Seven parameter solution	
		Length	Difference (cm)	ppm	Difference (cm)	ppm
ALGO	- MOJA	3407	-2.2	0.006	4.4	0.012
	- PVER	3611	-3.6	0.010	6.2	0.017
	- VNDN	3727	-3.9	0.010	2.4	0.006
PLAT	- MOJA	1196	-2.4	0.020	3.3	0.028
	- PVER	1407	-4.3	0.031	4.6	0.033
	- VNDN	1533	-4.9	0.032	1.3	0.008
OVRO	- MOJA	245	1.6	0.065	0.7	0.029
	- PVER	387	1.8	0.047	5.1	0.132
	- VNDN	363	-4.6	0.127	-0.6	0.017
MOJA	- PVER	224	-1.0	0.045	1.7	0.076
	- VNDN	351	-2.5	0.071	-1.4	0.040
PVER	- VNDN	223	3.6	0.161	3.5	0.157
			rms = 3.3		rms = 3.4	

Table 7.8: Two day solution baseline differences with VLBI : Days 6 and 7

The rms baseline component differences between the GPS and the VLBI solutions are shown in figure (7.6). It can be seen that there is no significant improvement in the seven parameter solution, which solves for the coefficient C_R for each satellite. Instead, the baseline component differences are
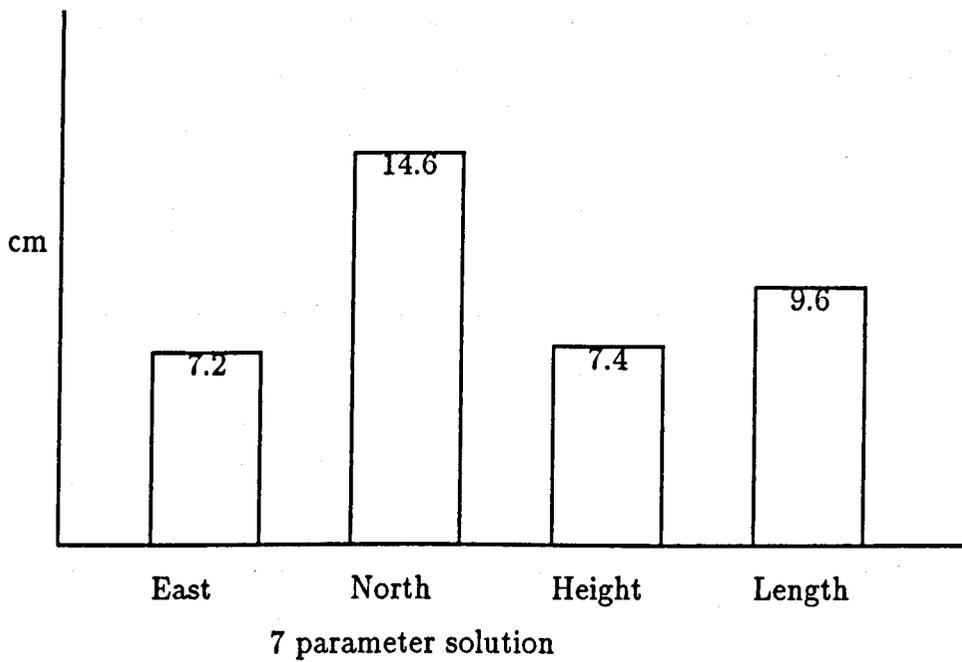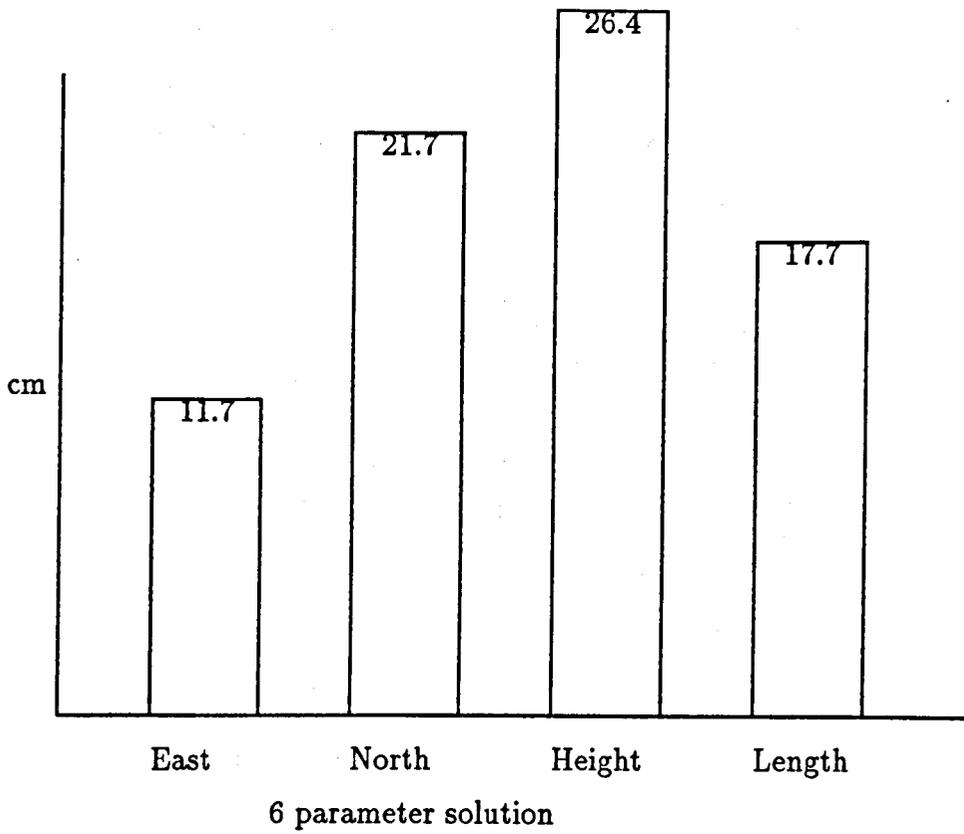
Figure 7.5: RMS baseline vector differences from VLBI : 2 day solution for days 4 and 5

generally slightly larger than the six parameter solution.

A comparison of the values of C_R, estimated in the two solutions are given in table (7.9). It can be seen that the initial estimate of 1.5 for C_R was generally too low for all the satellites. This was particularly noticeable for satellites 6 and 9, which lie in a different orbital plane to satellites 3, 11 and 13.

Satellite	Days 4 and 5	Days 6 and 7
PRN number	C_R	C_R
3	1.5071	1.4812
6	1.7202	1.6601
9	1.6749	1.5970
11	1.5186	1.5199
13	1.5507	1.5503

Table 7.9: Two day solution : Solar radiation pressure coefficients

Orbit repeatability for the two day solutions

Two independent orbits have been computed for each satellite, using the same data set as in the previous solutions. The same parameters were estimated as in the previous solution,

- Initial phase ambiguities for each day

- Selected receiver coordinates for the whole solution

- Satellite state vectors for the whole solution

- Solar radiation pressure coefficients for the whole solution

The estimated values of the satellite state vectors and solar radiation pressure coefficients were then used to initialise the orbit integration again. This iteration proceeded until there was no further change in the estimated orbital parameters.

The first orbit (arc 1) was determined from the data of days 4 and 5, and spanned the observing periods of days 4, 5 and 6. The second orbit (arc 2)
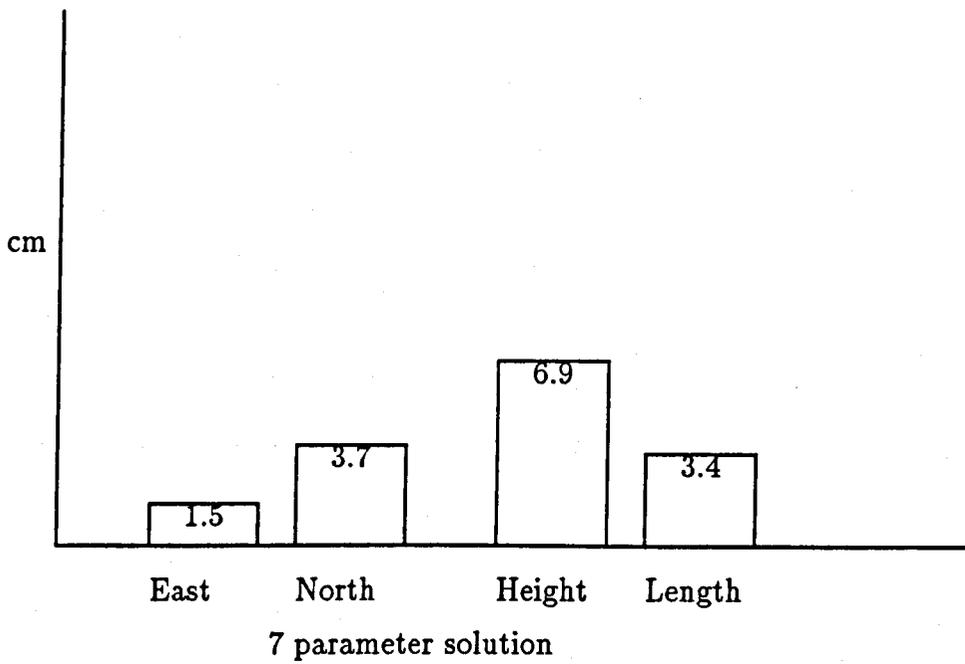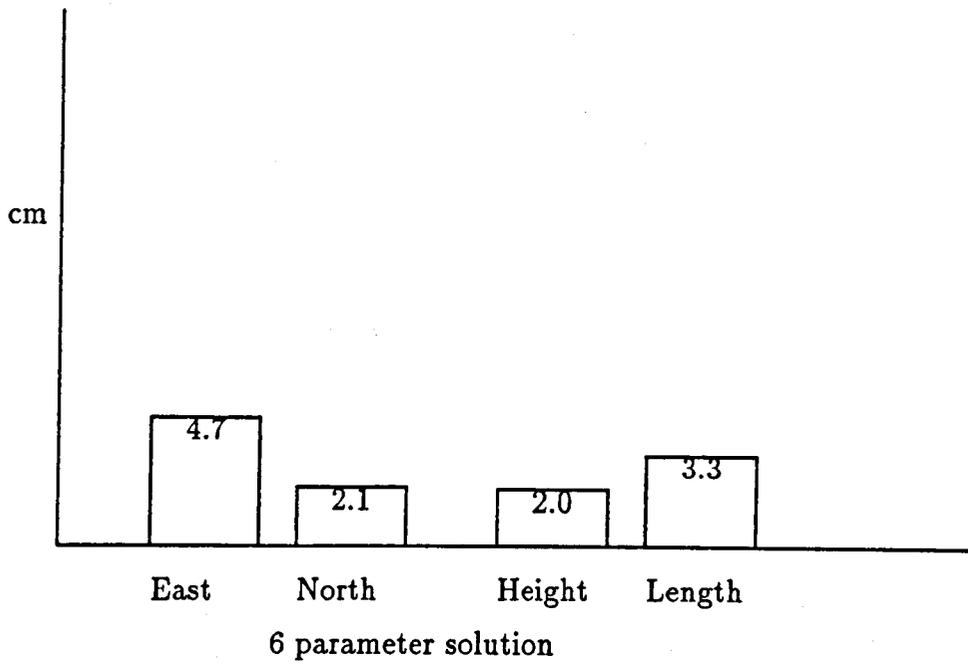
Figure 7.6: RMS baseline vector differences from VLBI : 2 day solution for days 6 and 7

was determined from the data of days 6 and 7, and spanned the observing period of days 6 and 7 only (figure 7.7).
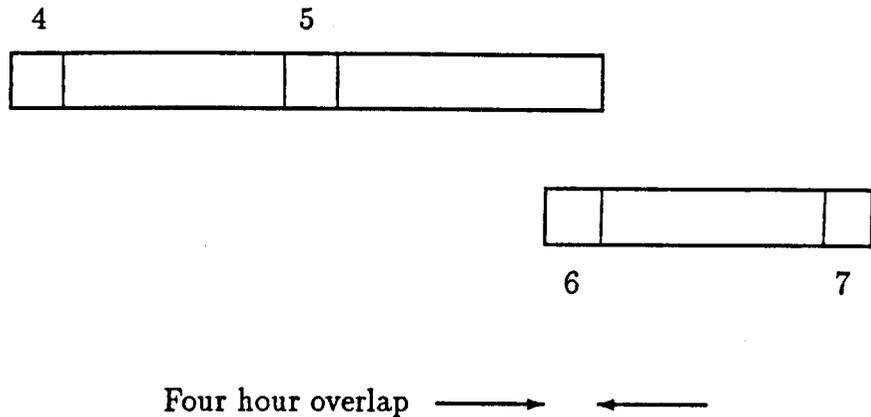
Figure 7.7: Orbit repeatability test definition

For each satellite, the differences between the two orbits have been computed, during the observing period on day 6. These differences have been separated into the along track, across track and radial components of the orbit. The rms differences of these components are given in figure (7.8), for satellite PRNs 3,6,9 and 11 for the four hour overlap period on day 6.

The radial component shows the best agreement between the two orbits, with an average repeatability of 1.7 metres. The along track and across track components gave a higher average repeatability of 5.9 and 6.4 metres respectively.

Satellite 11 was chosen as the base satellite for processing, and has the highest number of observations measured from it. Predictably, this gives the best repeatability of all the satellites. Satellites 12 and 13 were not included in the repeatability tests, as very few observations from these satellites were used in the processing.

Figure (7.9) shows the differences between arc 1 and arc 2, for satellite 11, which was the best tracked satellite. In this example arc 1 was extrapolated over the whole length of arc 2. All three components of the orbit show periodic differences, equivalent to the orbital period of the satellite. Again,
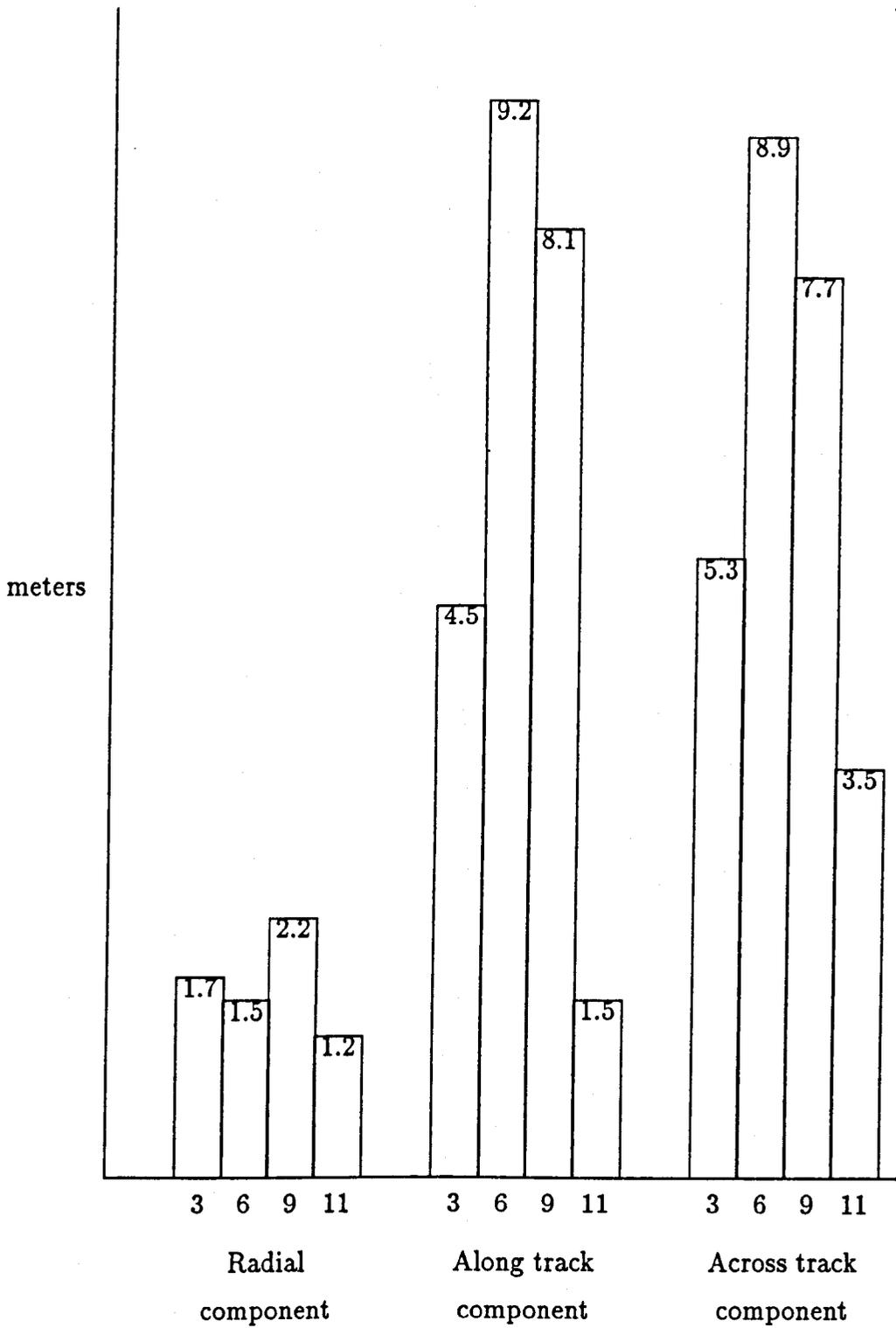
Figure 7.8: Orbit repeatability : rms orbit component differences

IESSG 2 day solution comparison. Satellite 11
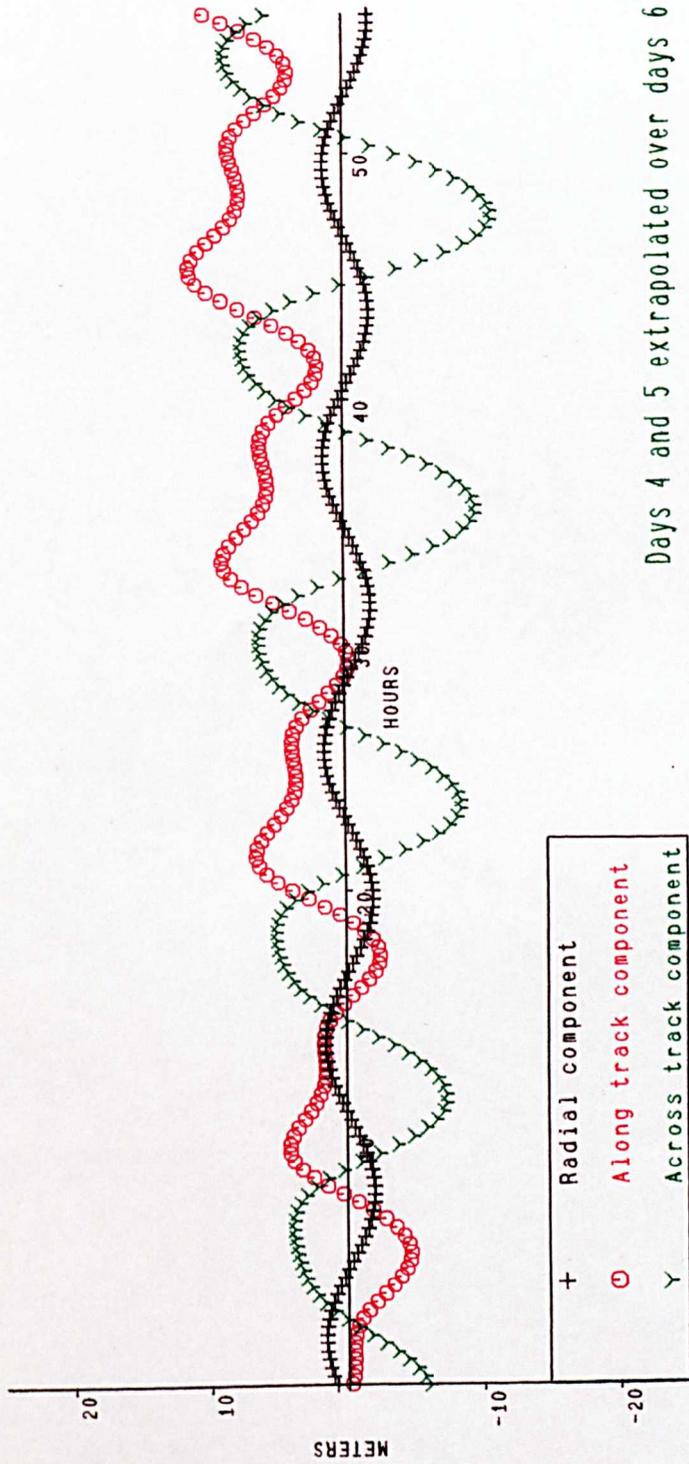
WGS 84 E.G.M.
2 Day arcs
Solving for :
State vector
Cr

	Radial component
+	
⊙	Along track component
Y	Across track component

METERS

HOURS

Days 4 and 5 extrapolated over days 6 and 7

Figure 7.9: Orbit repeatability for satellite 11

169

the radial component gives the best agreement, with the maximum difference less than two meters, even up to 48 hours after the last measurement that was used to determine arc 1. The periodic differences seen in the across track component are less stable and gradually increase with time. The along track component shows both periodic and secular variations. The differences between the other satellites revealed similar trends, but those satellites having fewer observations tended to produce larger differences, especially in the along track component.

Two day orbit comparison with the precise ephemeris

A comparison has been made between the orbits determined from the data collected during days 6 and 7, and the NSWC precise ephemeris. The NSWC precise ephemeris was computed using the WGS 84 geopotential model to produce satellite coordinates in the WGS 84 reference frame. The IESSG[2] orbit computed for the comparison also used the WGS 84 geopotential model , but the coordinates for the fixed fiducial sites were in the SV 4 reference frame. The transformation parameters between these two reference frames were not known at the time of writing.

The comparisons for two of the satellites, 9 and 11 are given in figures (7.10) and (7.11). Satellite 11 was chosen because it was the most tracked satellite and satellite 9 was more representative of the other satellites. The orbits were identical to the *arc* 2 orbits used in the repeatability tests.

The radial components again produce the smallest difference between the orbits. The along track component in both cases produces differences up to 15 metres. If the orbits are compared only when the observations were made (i.e. the satellite passing over the tracking sites), a much better agreement is seen. This is particularly noticeable in the along track component, where differences are reduced to less than five meters.

Clearly, it is not easy to detect whether the differences are due to errors in the NSWC precise ephemeris or the IESSG computed orbit. Futhermore, the differences between the two coordinate reference frames, which were used to

---

[2]Refers to all the GPS orbits computed using the Institute of Engineering Surveying and Space Geodesy orbit determination software
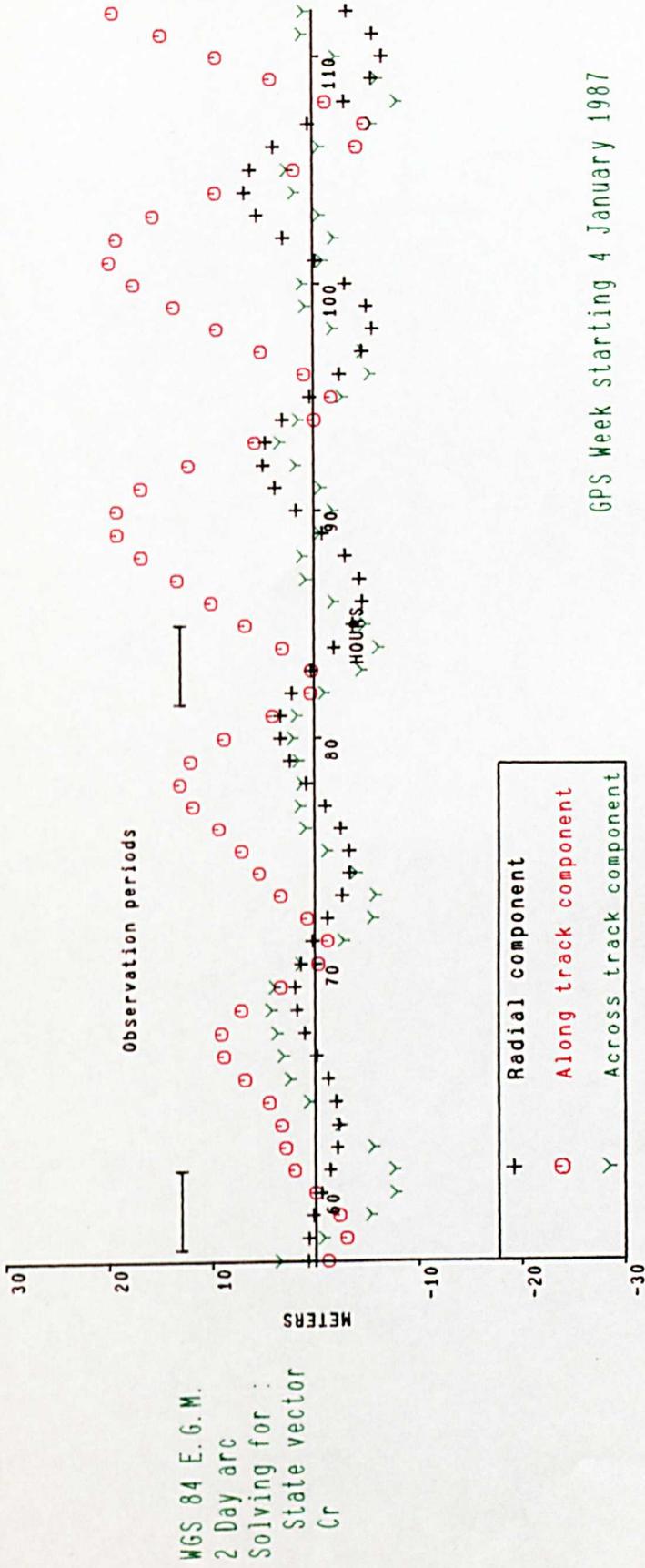
Figure 7.10: NSWC precise ephemeris comparison for satellite 9 : Two day solution.

171
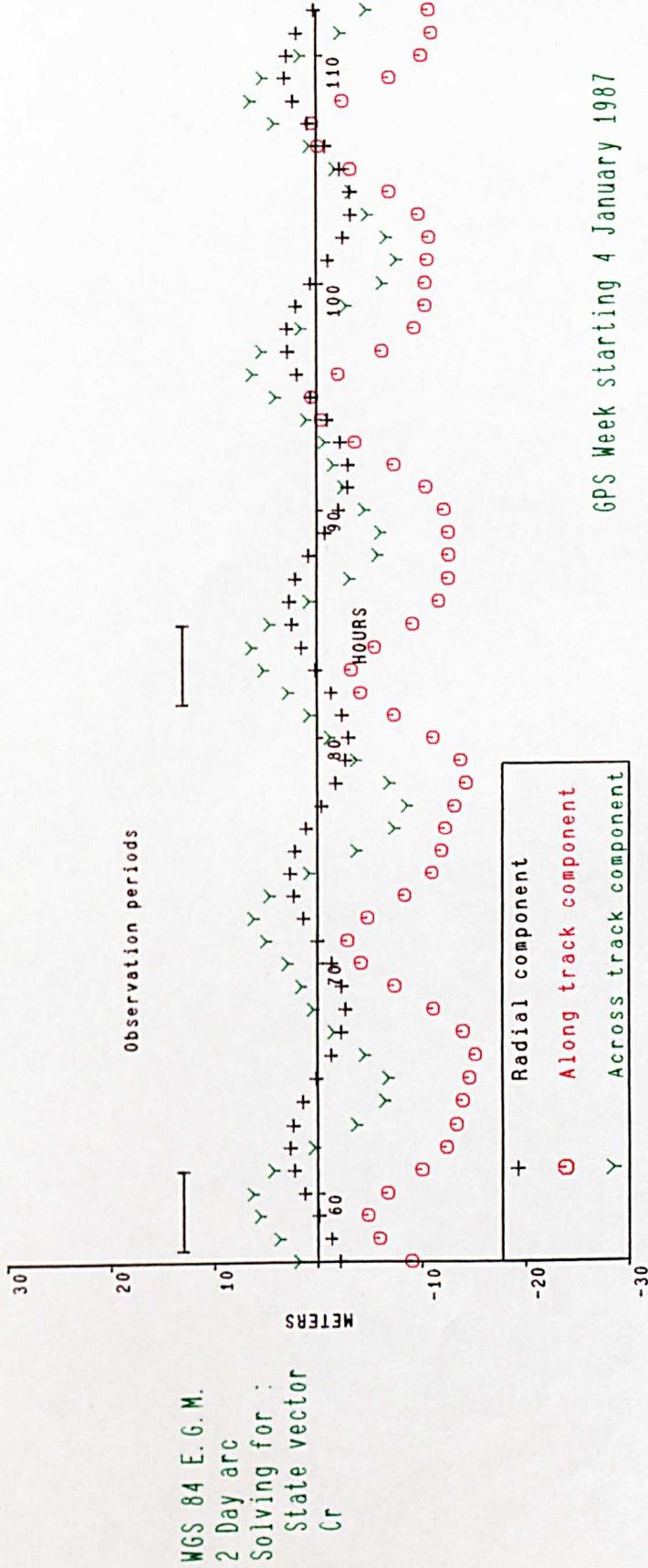
Figure 7.11: NSWC precise ephemeris comparison for satellite 11 : Two day solution.

172

compute the orbits, could produce systematic differences between the orbits. However, the large differences seen between the two orbits when the satellites are away from the North American tracking sites, are likely to be caused by only using a continental network for the IESSG orbit. The NSWC precise ephemeris is produced from a global tracking network, and would be expected to produce a more consistent orbit for the whole satellite revolution.

The main point which this comparison shows is that the IESSG orbit determined from the continental network will give good agreement with the precise ephemeris over the continental tracking network, but the accuracy of the IESSG orbit will degrade when the satellite passes away from the tracking sites.

7.3.3 Three day solutions

The continuous three day solution was computed using the data collected during the days 4, 5 and 6. Two different solutions were computed. The first solution (seven parameters per satellite) solved for the following parameters.

- One set of initial phase ambiguities for each day.

- One set of receiver coordinates for the whole solution.

- One set of satellite state vectors for each satellite, for the whole solution.

- One set of direct solar radiation pressure coefficients for each satellite, for the whole solution.

A second solution (eight parameters per satellite) was computed, which estimated the constant y-bias acceleration for each satellite, in addition to the above parameters.

The baseline differences from the VLBI solutions are given in table (7.10). In this case, a significant improvement with the solution solving for the y-bias acceleration can be seen. The largest baseline error, which is on the shorter OVRO-VNDN baseline is reduced from three parts in 10^7 to one part in 10^7, with all the other errors less than four parts in 10^8.

173

			Seven parameter		Eight parameter	
		length (km)	Difference (cm)	ppm	Difference (cm)	ppm
ALGO	- VNDN	3727	14.5	0.039	5.2	0.014
	- WSFD	642	-13.3	0.207	-2.8	0.044
PLAT	- VNDN	1533	15.9	0.103	5.8	0.038
	- WSFD	2752	-20.2	0.074	-7.9	0.029
OVRO	- VNDN	363	12.2	0.334	3.7	0.103
	- WSFD	3929	-20.3	0.052	-6.6	0.017
VNDN	- WSFD	4228	-6.0	0.014	-1.4	0.003
			rms = 15.3		rms = 5.2	

Table 7.10: Three day solution : Baseline comparison with VLBI

In figure (7.12), it can be seen that the main error in the baseline is in the east component, with the estimation of the satellite y-bias acceleration reducing the differences by a factor of two.

The estimated values of the solar radiation pressure coefficients are given in table (7.11), with their standard errors. Although the direct solar radiation pressure coefficients are of a similar magnitude for each satellite, there is a much larger variation in the y-bias accelerations, from 0.346×10^{-9} to $1.120 \times 10^{-9} ms^{-2}$. The basic shape and orientation of the satellites, which will affect the C_R parameter, are similar, but the structural misalignment of the solar panels, which are believed to cause the y bias acceleration, would be more likely to vary from satellite to satellite.

In this solution, the inclusion of the constant y-bias acceleration reduces the rms double difference phase residual from 0.08889 to 0.05199 cycles.

Three day orbit comparison with the precise ephemeris

The IESSG three day orbit used for the comparison was obtained from the eight parameter solution described in the previous section, computed from the data collected during days 4, 5 and 6.

The differences between the IESSG orbits and the NSWC precise ephe-
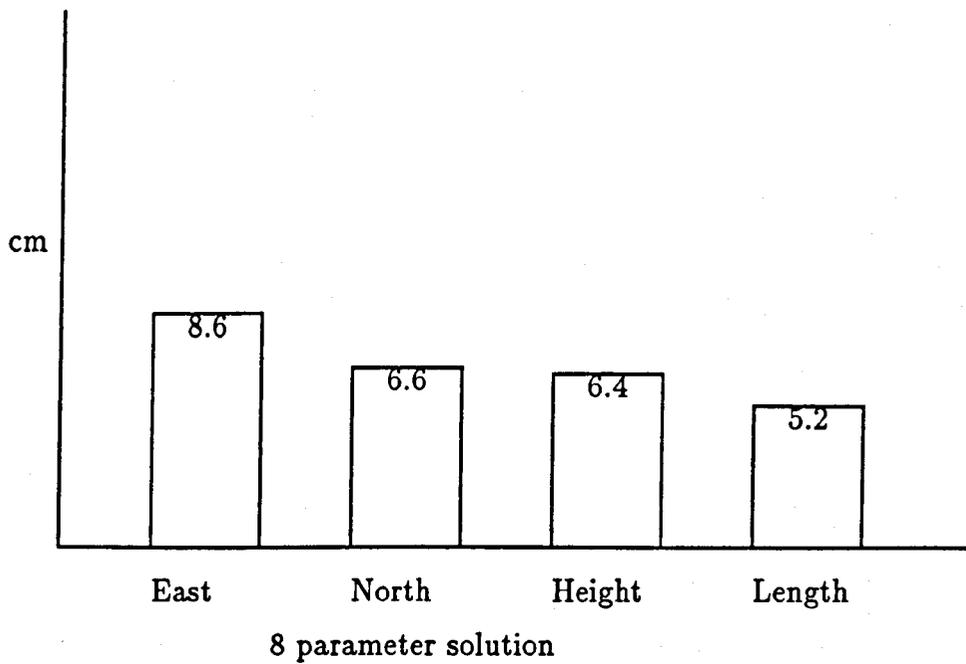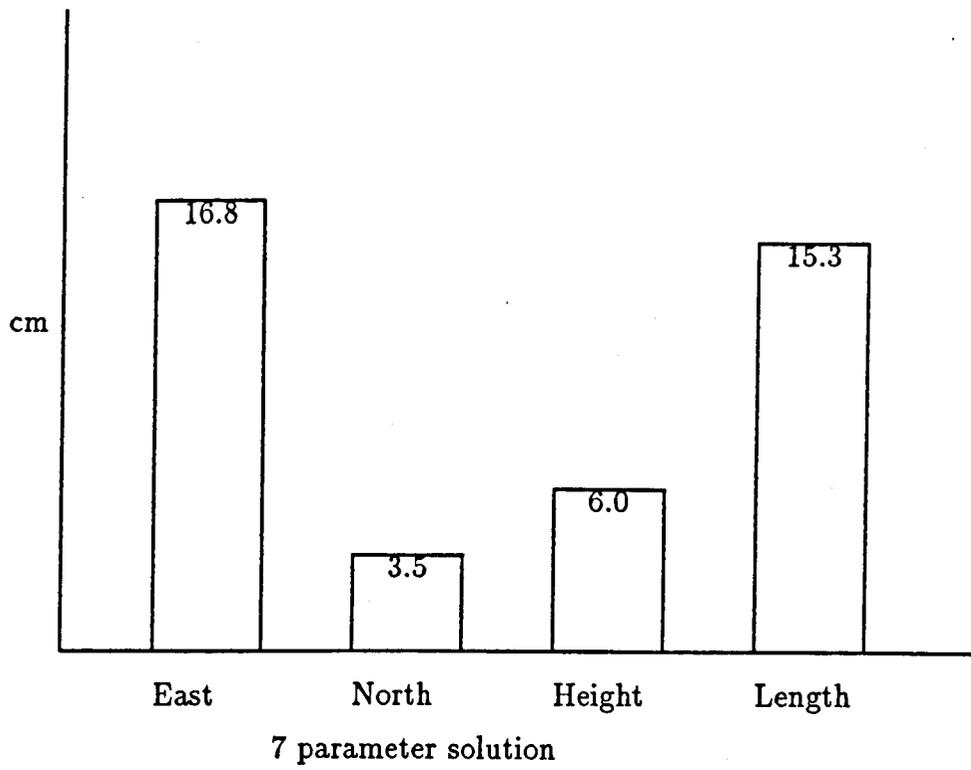
Figure 7.12: RMS baseline vector differences from VLBI : 3 day solution for days 4, 5 and 6

	Seven parameter		Eight parameter			
Satellite PRN	C_R	σ	C_R	σ	C_y $10^{-9}ms^{-2}$	σ $10^{-9}ms^{-2}$
3	1.5038	0.0026	1.4835	0.0030	1.120	0.180
6	1.7184	0.0025	1.7211	0.0015	0.642	0.020
9	1.6568	0.0042	1.6821	0.0025	0.724	0.014
11	1.5234	0.0007	1.5132	0.0005	0.346	0.020
13	1.5593	0.0094	1.5511	0.0056	0.347	0.035

Table 7.11: Three day solution : Solar radiation pressure coefficients

meris for satellites 9 and 11 are shown in figure (7.13) and (7.14). The figures show the same trends as the two day orbits described previously. It is particularly noticeable that the differences in the along track component are at a minimum during the periods of observation. This is also seen to a lesser extent in the radial component.

Similar conclusions must be drawn from the three day solution as those in the two day solution, with the differences between the IESSG orbits and the precise ephemeris less than five meters when the satellite passes overhead, but increasing up to fifteen meters when the satellite passes away from the tracking sites.

7.3.4 Four day solution

The continuous four day solution was computed from the data collected from days 4, 5, 6 and 7. A similar approach to the three day solution was adopted and two separate solutions were computed. The first solution estimated the parameters,

- One set of initial phase ambiguities each day.

- One set of receiver coordinates for the whole solution.

- One set of satellite state vectors for each satellite for the whole solution.

- One direct solar radiation pressure coefficient for each satellite for the whole solution.

176
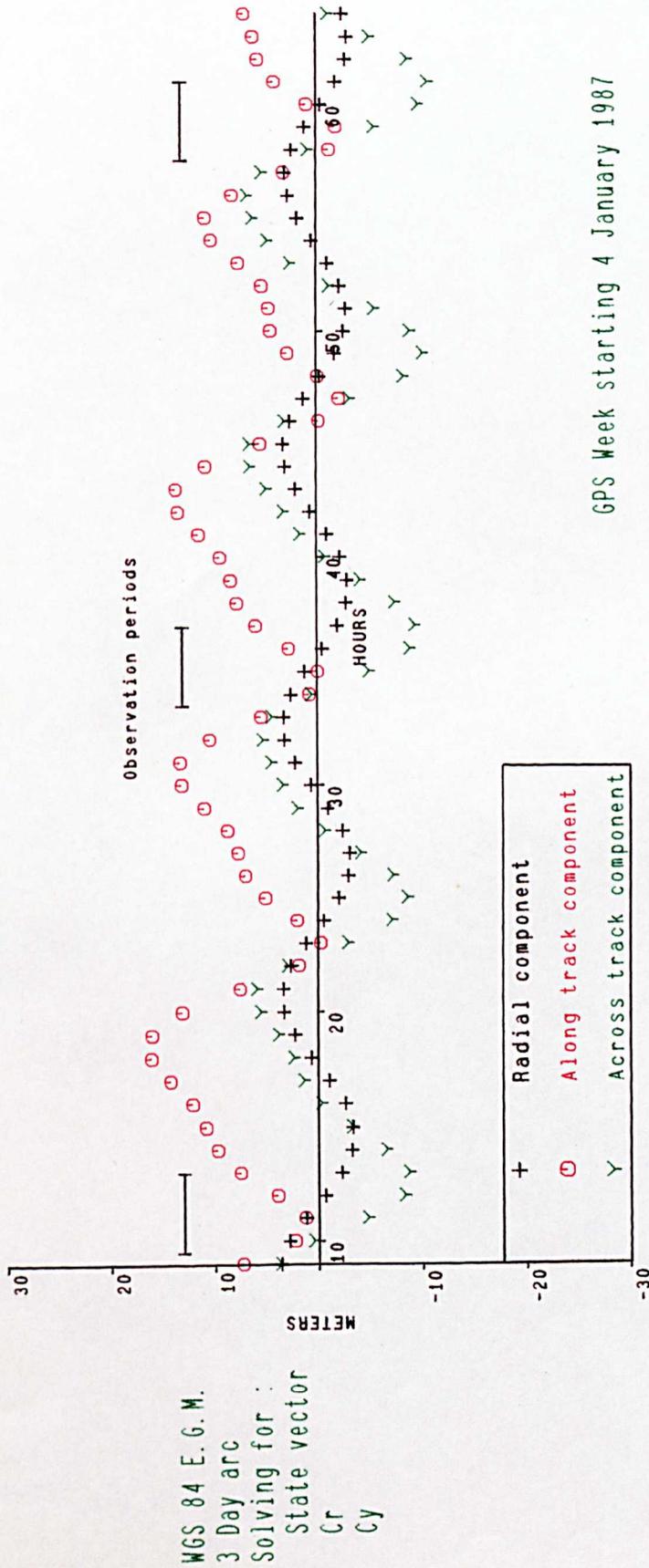
Figure 7.13: NSWC precise ephemeris comparison for satellite 9 : Three day solution.
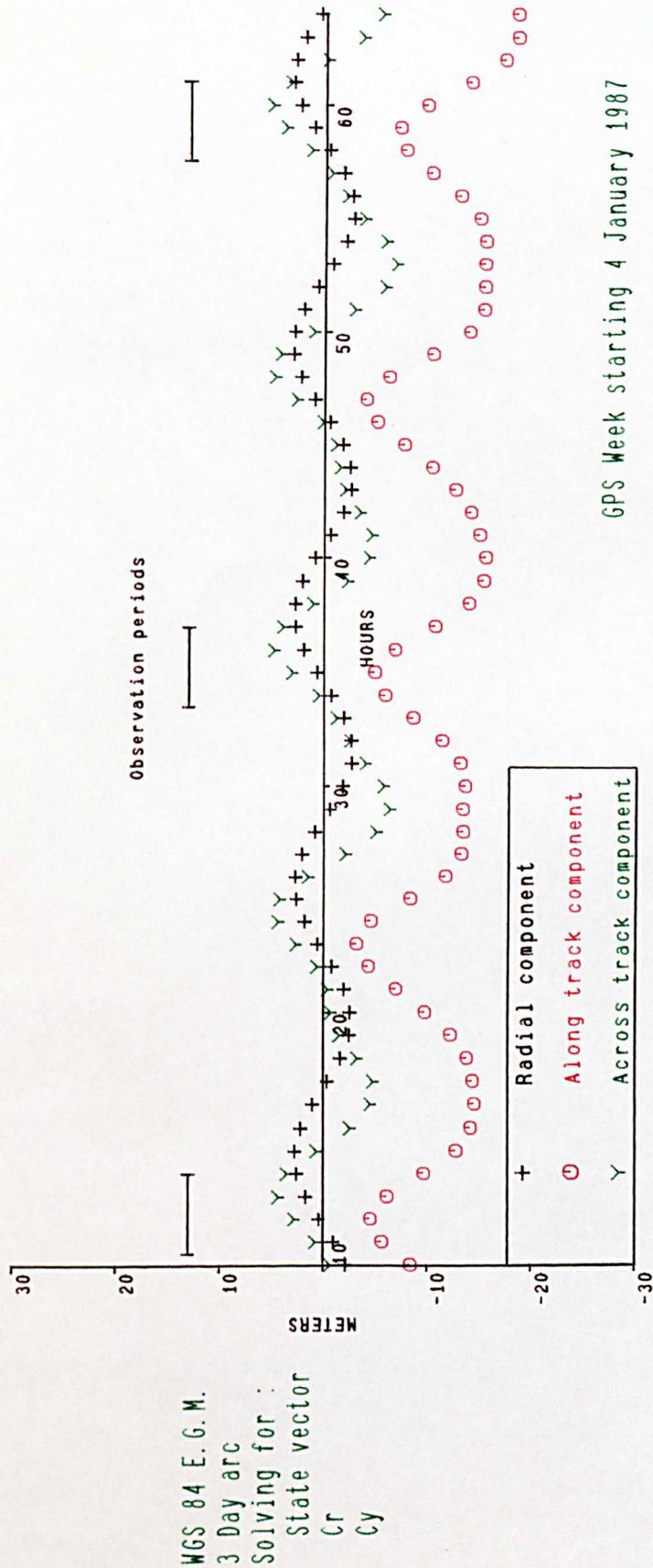
Figure 7.14: NSWC precise ephemeris comparison for satellite 11 : Three day solution.

The second solution estimated an additional y-bias acceleration for each satellite.

The baseline differences between the VLBI and the first solution (seven parameters per satellite) are given in table (7.12). The most obvious errors are in the long east-west baselines, which stretch from ALGO and PLAT to the Californian sites of VNDN, MOJA and PVER. These have caused particularly large baseline errors of up to 5 parts in 10^7 on certain baselines, and a large rms baseline difference of 21.3 cm.

		length (km)	Seven parameter Difference (cm)	ppm	Eight parameter Difference (cm)	ppm
ALGO	- VNDN	3727	21.4	0.057	12.0	0.032
	- MOJA	3407	24.1	0.071	13.1	0.038
	- PVER	3611	38.0	0.105	20.2	0.056
PLAT	- VNDN	1533	22.6	0.147	11.9	0.077
	- MOJA	1196	23.6	0.197	12.5	0.105
	- PVER	1407	36.1	0.256	18.5	0.131
OVRO	- VNDN	363	15.5	0.426	8.4	0.230
	- MOJA	245	-7.0	0.285	-0.7	0.027
	- PVER	387	12.0	0.309	11.1	0.286
VNDN	- MOJA	351	0.7	0.020	0.7	0.019
	- PVER	223	-4.5	0.200	2.6	0.116
MOJA	- PVER	224	11.1	0.494	5.9	0.264
			rms = 21.3		rms = 11.5	

Table 7.12: Four day solution : baseline differences with VLBI

The second solution (eight parameters per satellite) baseline differences are shown in the same table. There is a significant reduction in the rms baseline difference down to 11.5 cm. This brings the maximum baseline error down to 3 parts in 10^7. However, the largest baseline differences are still on the longer east-west lines.

The rms baseline component differences are shown in figure (7.15). The largest component error of 26.6 cm in the east direction is reduced to 10.6 cm with the addition of the y-bias acceleration per satellite. The determination of the east component of PVER appears to be producing these large differences. This was also noted in the single day solution of day 6 (table 7.5). The differences between the single day 6 solution and the four day solution for the ALGO-PVER and the PLAT-PVER baselines are only 7 mm and 19 mm respectively.

The values for the solar radiation pressure coefficients are given in table (7.13). The direct solar radiation pressure coefficient C_R produces values similar to the three day solution as expected, but the y-bias acceleration shows much larger changes, especially for satellite 3 which has the least observations. The standard errors of these accelerations have been reduced by a factor of two by the additional day of data.

	Seven parameter		Eight parameter			
Satellite PRN	C_R	σ	C_R	σ	C_y $10^{-9}ms^{-2}$	σ $10^{-9}ms^{-2}$
3	1.4944	0.0023	1.4839	0.0016	0.757	0.091
6	1.6946	0.0024	1.7073	0.0010	0.710	0.009
9	1.6754	0.0050	1.6666	0.0021	0.653	0.006
11	1.5206	0.0006	1.5134	0.0003	0.312	0.011
13	1.5090	0.0101	1.5585	0.0043	0.455	0.017

Table 7.13: Four day solution : Solar radiation pressure coefficients

A comparison has been made between the double difference phase residuals obtained from the two four day solutions for the satellites 9 and 11, and the sites of PLAT and OVRO. Figure (7.16) shows the residuals from the solution using seven parameters per satellite and figure (7.17) shows the residuals from the eight parameter per satellite solution.

The noticeable drift seen in the residuals in figure (7.16) for the first three days has been very much reduced, by the addition of the y-bias acceleration estimation, to give a much more random distribution of the residuals in figure
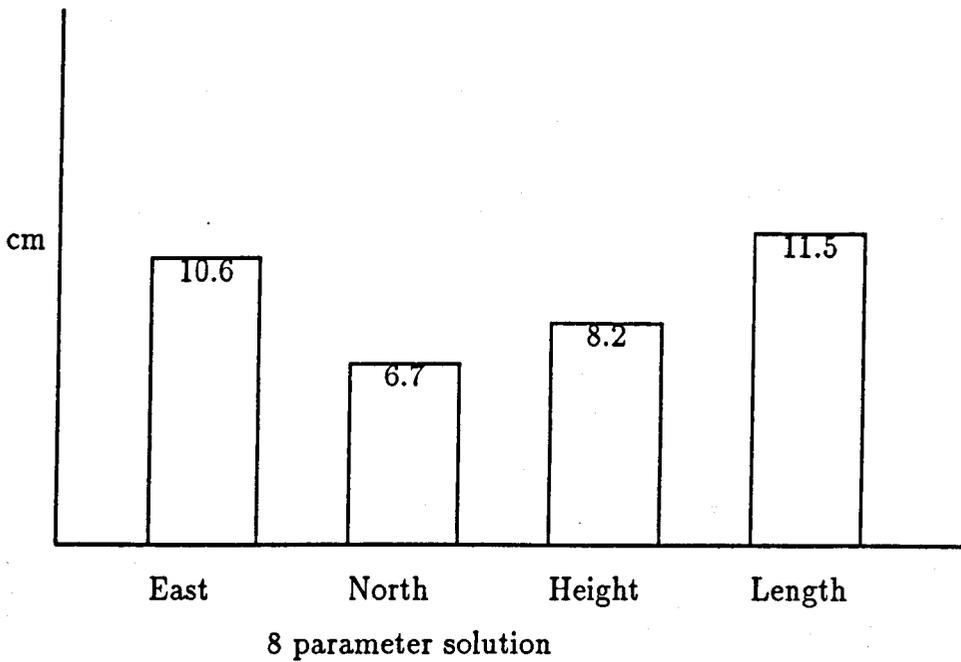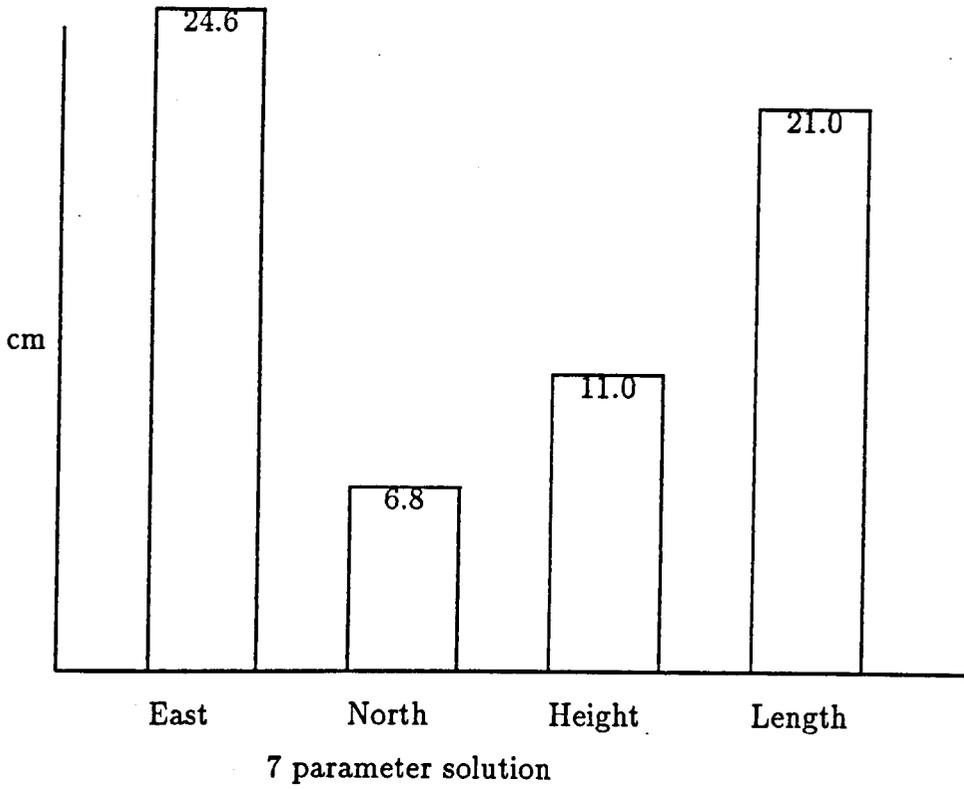
Figure 7.15: RMS baseline vector differences from VLBI : 4 day solution for days 4, 5, 6 and 7
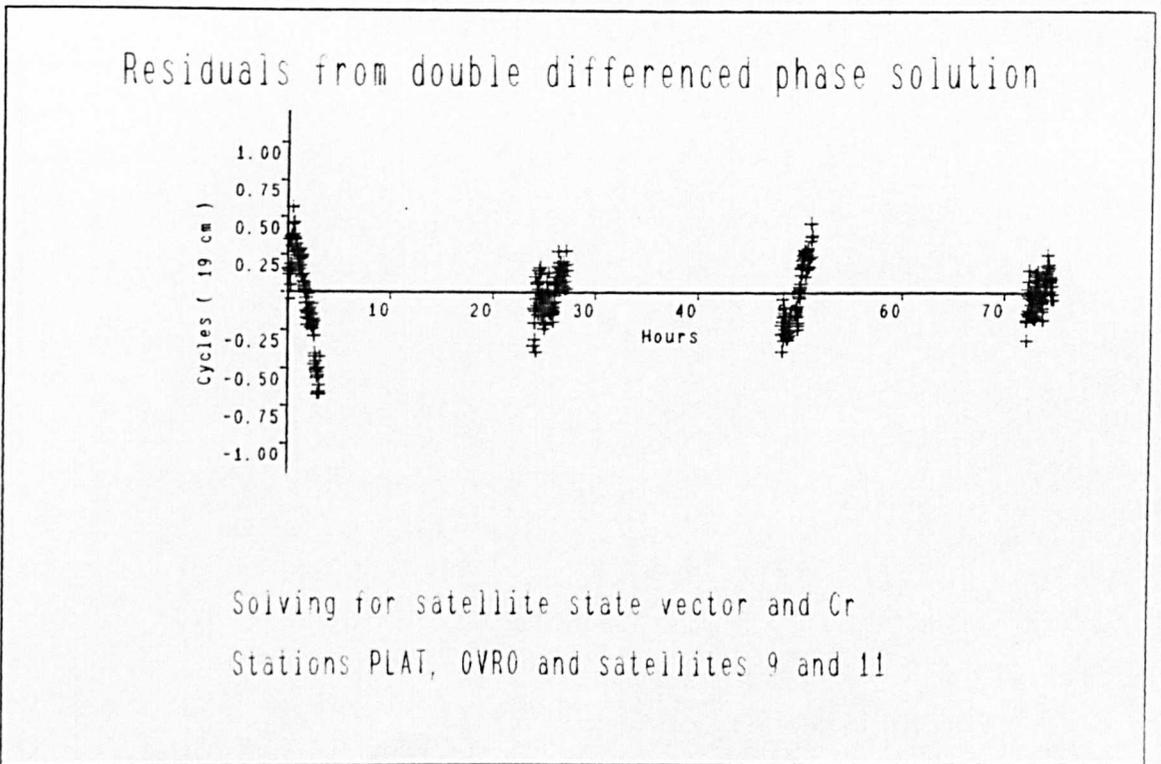
Figure 7.16: Double difference phase residuals from the four day solution (PLAT and OVRO) : seven parameters estimated per satellite
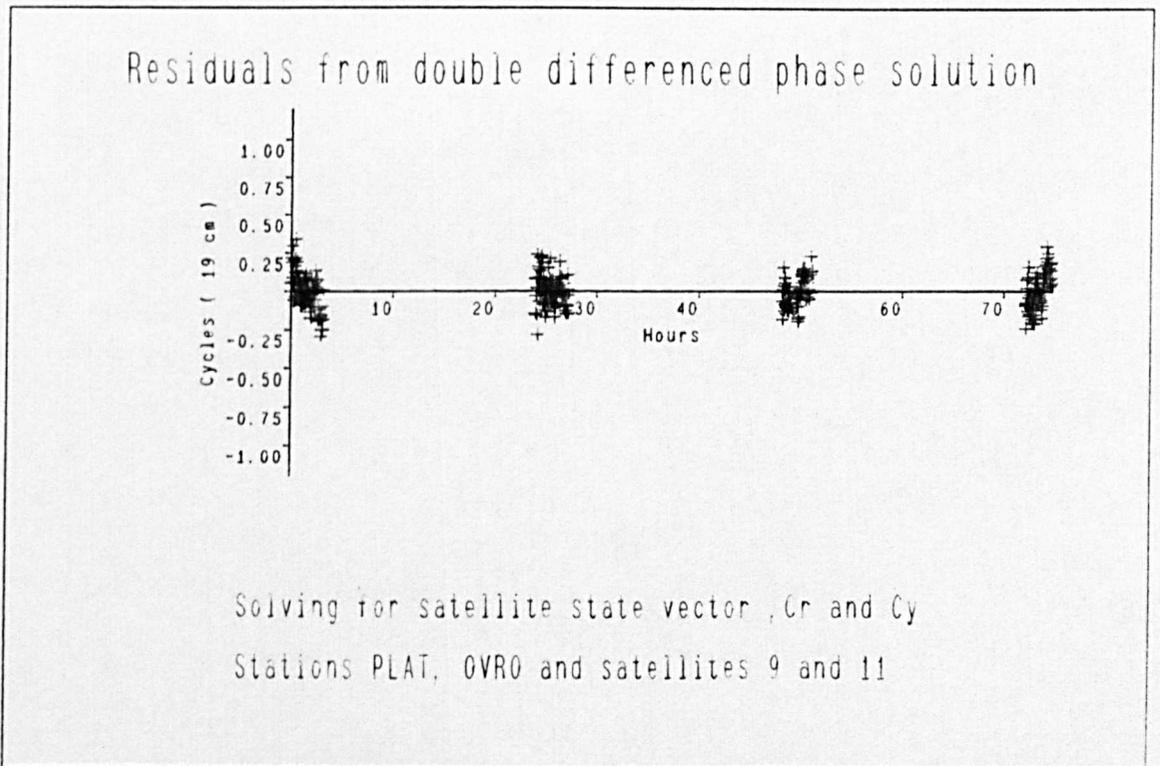
Figure 7.17: Double difference phase residuals from the four day solution (PLAT and OVRO) : eight parameters estimated per satellite

(7.17). The largest residual is now approximately 0.3 cycles or 5.7 cm.

A similar pattern is seen in figures (7.18) and (7.19) for the sites of PLAT and VNDN, although there is still a slight drift in the first and last days of the solution. The improvement in the solution is reflected in the rms double difference phase residual, which reduces from 0.14596 to 0.06055 with the estimation of the satellite y-bias acceleration.

7.3.5 The Effect of Using Different Geopotential Models

The three day solution was computed using two different geopotential models to predict the orbit. Both of the solutions were computed using the same data sets and the same parameters were estimated.

The orbit integrations for the first solution used the WGS 84 geopotential model up to degree and order eight. For this the value of the product GM was $3986005.00 \times 10^8 m^3 s^{-2}$.

The orbit integrations for the second solution used the GEM T1 geopotential model up to degree and order eight. The value of GM was taken to be $3986004.36 \times 10^8 m^3 s^{-2}$.

The differences between the baseline lengths of the two solutions are given in table (7.14). It can be seen that the differences between the baselines for the two solutions are of the order of a few millimetres, corresponding to a maximum baseline error of the order of three parts in 10^9.

Beutler et al [1987] derives a theoretical equation to determine the effect of using different values of GM in the computations. The formula,

$$\frac{\Delta l}{l} = 0.07 \times \frac{\Delta GM}{GM} \tag{7.1}$$

relates the change in baseline length Δl expected when the value of GM is changed by ΔGM. When using the differences of the value of GM between the WGS 84 and the GEM T1 geopotential models, a baseline difference of 0.008 ppm would be expected. This is comparable with the baseline differences seen in table (7.14). The differences between the two solutions would indicate that the effect of using a different geopotential model is very small and for the determination of ground coordinates, it is relatively insignificant.

183
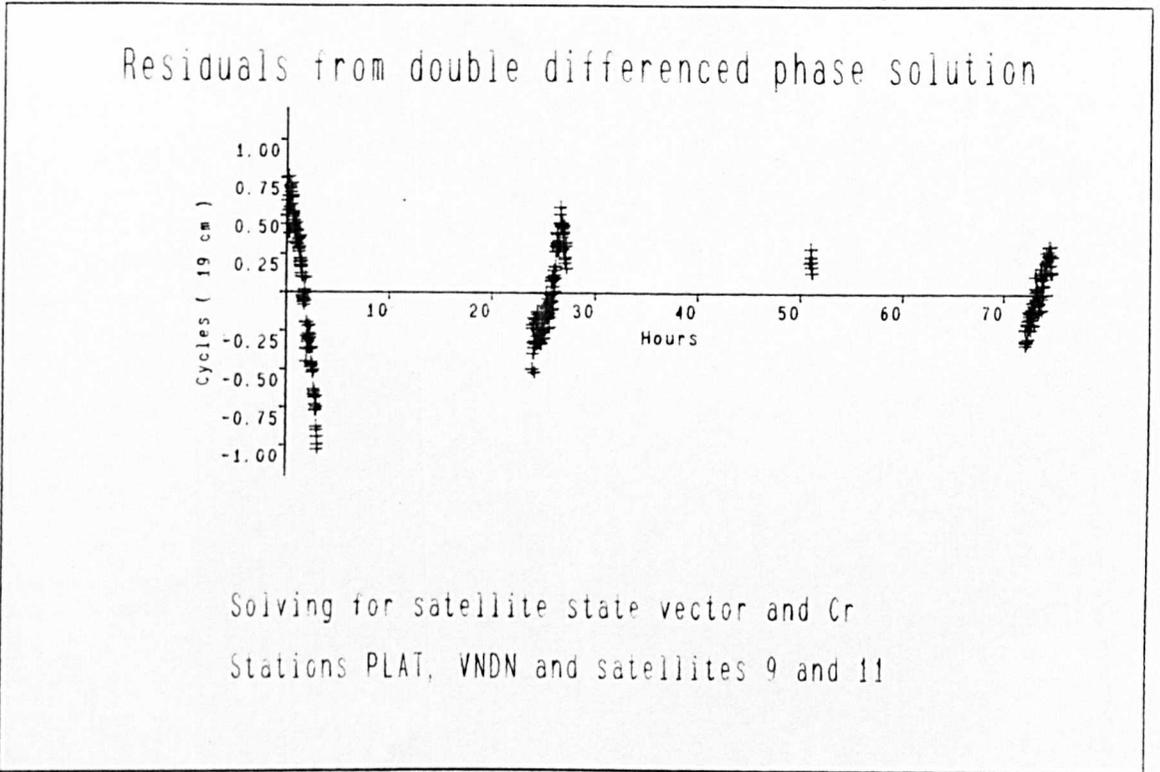
Figure 7.18: Double difference phase residuals from the four day solution (PLAT and VNDN) : seven parameters estimated per satellite
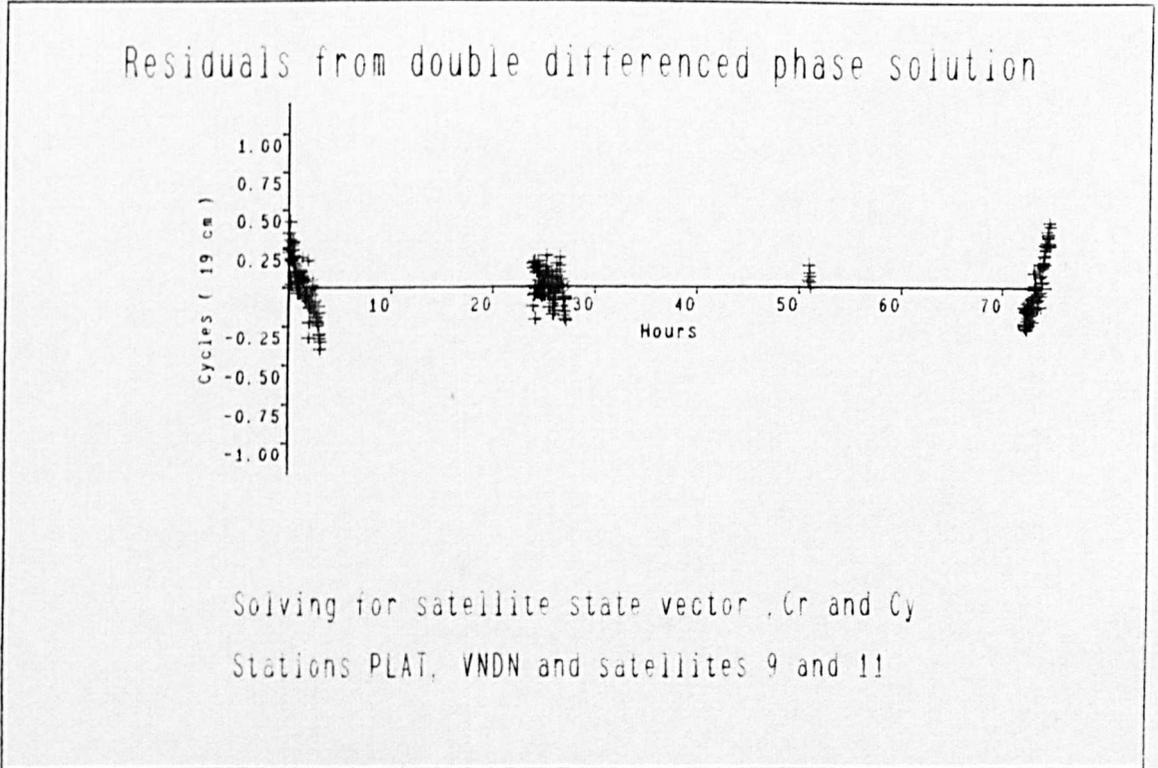
Figure 7.19: Double difference phase residuals from the four day solution (PLAT and VNDN) : eight parameters estimated per satellite

	Length (km)	WGS 84 minus GEM T1 solutions (mm)	ppm
ALGO - VNDN	3727	1	0.000
ALGO - WSFD	642	-2	0.003
PLAT - VNDN	1533	1	0.001
PLAT - WSFD	2752	-3	0.001
OVRO - VNDN	363	1	0.003
OVRO - WSFD	3929	-4	0.001
VNDN - WSFD	4228	-2	0.000

Table 7.14: Effect on the baseline length of using different geopotential models

7.3.6 The Effect of Errors in the Fiducial Site Coordinates

One of the single day solutions (day 4) was computed with a 10 cm bias added to the antenna height at the fiducial site of OVRO. The resulting estimates of the non fiducial site coordinates were compared with the original single day solution with the correct antenna height. The differences between the latitude, longitude and height of the two solutions for the non fiducial sites are given in table (7.15).

	Change in latitude (cm)	Change in longitude (cm)	Change in height (cm)
VNDN	1.3	5.1	10.2
WSFD	8.8	6.8	-8.8

Table 7.15: The effect of a 10 cm error in the fiducial site antenna height

The closest non fiducial site to OVRO is VNDN and predictably the height of this site increases by 10.2 cm, similar to the antenna height bias at OVRO. The height of the other non fiducial site WSFD decreases by 8.8 cm suggesting the network has been rotated about the fiducial sites. The horizontal coordinates of the two sites have also changed considerably, which may imply a distortion of the network. The magnitude of the change in the

horizontal coordinates is of a similar order to the antenna height bias, which means that any error in the antenna heights will not just affect the height components of the baselines, but it may well propagate into the determination of the baseline lengths.

7.4 Discussion of Results

All the solutions computed in this chapter used the data from CHUR in the adjustment. This site has not been occupied by VLBI or SLR equipment and the coordinates have only been established by previous GPS solutions. For this reason, no constraint has been placed on the coordinates of CHUR in the adjustment and no previous comparisons have been made with the GPS solutions.

A comparison of the coordinates of CHUR determined from the four single day solutions reveals some large differences in both the latitude and the longitude of up to half a meter. These differences were giving daily baseline repeatabilities of up to three parts in 10^7.

The fiducial sites (ALGO, OVRO and PLAT) lie very much in a line running east-west, whereas CHUR lies further to the north (figure 7.20). This geometrical configuration has been shown to give a poor estimation of the non fiducial receiver coordinates by other authors [Lichten et al, 1989]. A better estimation of the coordinates of CHUR would be expected by using another fiducial site located to the north of the three fiducial sites.

In separate solutions, each single day was computed without the data from CHUR. All the estimated GPS baseline vectors showed larger differences from the VLBI vectors, than the GPS solutions which contained the data from CHUR. This demonstrates the importance of using a well distributed tracking network to provide constraint for the orbit determination process ,

CHUR

△

ALGO

PLAT

OVRO
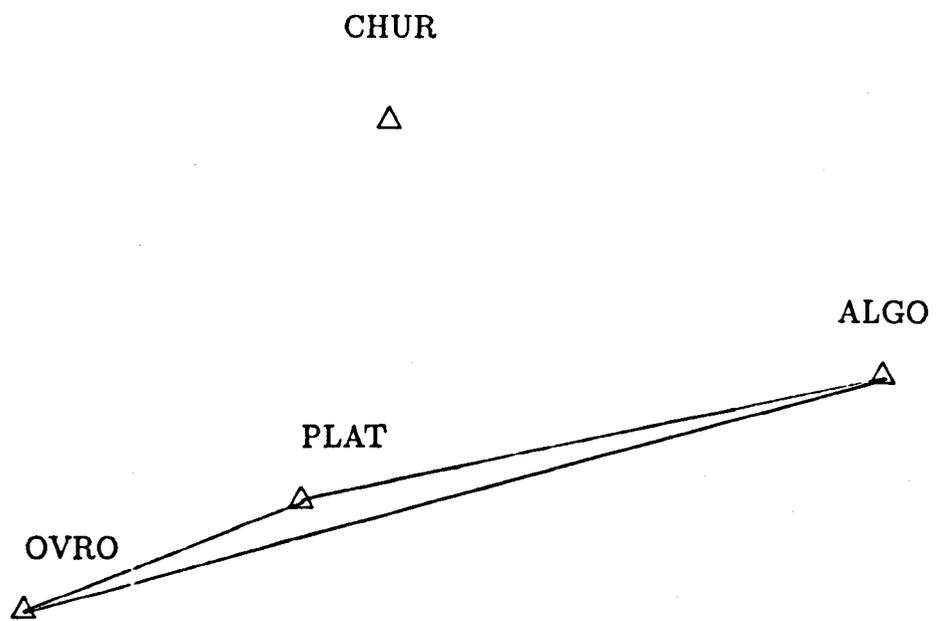
Figure 7.20: Location map of fiducial stations in North America

even if the coordinates of all the sites are not necessarily fixed.

One of the major error sources not investigated in these results is the effect of the troposphere. All the solutions were computed using the U.S. standard atmosphere model (section 2.5.2). This uses values of the Julian day number, height and latitude of the site to estimate the tropospheric delay (phase advance). There are two faults with this type of model,

1. Any variations in the state of the troposphere during the observation period will not be modelled, because a constant zenithal delay is computed for each site for the whole observing period.

2. The model does not account for any localised atmospheric conditions at each site. This will be negligible for small networks, but for the large network considered here, it is more likely to cause further error.

When computing a multi-day solution, the tropospheric model will assume a similar delay for each site, on each day of the observation campaign. Hence, any day to day atmospheric changes will be ignored, which may well contribute to the larger discrepancies seen in the four day solution when compared with the two and three day solutions.

It was noted previously that the determination of the east component of the baselines were generally worse than the north components. Investigations on the same data set [Dong and Bock, 1989] have shown that resolving the initial phase ambiguities to their *integer* values can significantly reduce the uncertainty in the east component of the baselines. The scheme used solves for the (L1 - L2)[3] *wide-lane* integer ambiguities using either the pseudoranges [Blewitt, 1989] or by using the approach of ionospheric constraints [Bender and Larden, 1985]. This work is outside the scope of this project, but it is being investigated by another research student at Nottingham.

The comparison of the NSWC precise ephemeris with the IESSG orbits has demonstrated the use of a regional tracking network for orbit deter-

---

[3]The L1 -L2 frequency is formed from the difference between the L1 and L2 frequencies. It has a wavelength of about 86 cm making the resolution of the phase integers much easier than the single frequency L1, which has a wavelength of about 19 cm.

mination over a particular region. These orbits will be more accurate for determining the coordinates of sites contained within or close to the fiducial network. A more global network would be expected to produce a more accurate global orbit, for use in determining the coordinates of sites away from the fiducial sites. This has been demonstrated with additional data from Europe used to supplement the North American fiducial network for baseline determination in South America [Lichten, 1989].

An estimation of the accuracy of the GPS orbits can be obtained from,

1. Orbit repeatability tests.

2. Orbit comparison with NSWC precise ephemeris.

3. Baseline comparison with VLBI.

4. Standard errors of the estimated satellite state vectors.

The orbit repeatability tests were carried out during the observing period of the tracking sites. Therefore, they only represent the repeatability of the orbits over the tracking network. The effect of any unmodelled satellite force model components or any errors in the satellite state vector will be magnified by the extrapolation process. Hence, the average repeatabilities of 1.7 m, 5.9 m and 6.4 m for the radial, along track and across track components represent a pessimistic estimate of the accuracy of the orbits over the region.

The comparison with the NSWC precise ephemeris showed agreements better than five metres for the period of observation, with differences up to three times this over the rest of the orbital arc. This an independent test and it may well be affected by the differences between the two coordinate references frames of the tracking sites which were used to determine the two different orbits.

The GPS derived baselines can be compared with the VLBI determined baselines as in independent check. However, other non-orbit error sources such as the troposphere will affect the baseline determinations, so the comparisons are only an indication of the orbital accuracy. The effect of orbital errors is more dominant on the longer baselines, hence a comparison

of the longer baselines will provide a better check on the orbital accuracy than the shorter baselines where residual tropospheric effects may dominate [Lichten et al, 1989]. In general the agreement between the GPS and VLBI baselines were better than one or two parts in 10^7 on the longer baselines. This approximates to an orbital error of between two and four metres using the simple relationship given in equation (2.57). This agrees with the estimates obtained from the orbit repeatability and the precise ephemeris comparison tests.

An indication of the precision of the orbit can also be obtained from the standard errors of the estimated satellite state vectors. The standard errors of the initial position vectors varied between 1.75 m and 4.26 m for the two day solution, to between 1.41 m and 3.53 m for the four day solution. These agree well with the estimates obtained above.

All the results in this chapter were obtained using less than three and a half hours of data on each day. With the use of a better distributed tracking network and the full GPS satellite constellation a further improvement to both the orbital accuracy and the baseline accuracy should be achievable.

Chapter 8.
Conclusions and Suggestions for Further Work

Conclusions and Suggestions for Further Work

8.1 Conclusions

1. The double difference phase observable can be used for regional GPS orbit determination, when using the fiducial network method. This has been demonstrated with the program **DDORB**, which has been developed for multiple day, multiple satellite and multiple receiver solutions, using the least squares method of adjustment.

2. The comparison of the regionally (North America) determined GPS orbits with the NSWC precise ephemeris, shows agreement better than five metres in all three components of the satellite's position. Larger differences (up to fifteen metres) are seen when the orbits are compared outside the satellite observation periods.

3. The root-mean-square (rms) repeatability of two independently determined, two day orbits is better than two metres in the radial direction and typically about six metres in the along track and across track direction. These comparisons are for orbits which have been extrapolated twenty four hours beyond the last observation.

4. The GPS satellite is particularly sensitive to errors in the solar radiation pressure model. Different lengths of orbital arc require different modelling strategies.

    (a) With the single day solutions, no estimates can be made for any solar radiation pressure coefficients. The six parameter satellite

state vector is sufficient to absorb any unmodelled satellite accelerations.

(b) For the two day solutions, the direct solar radiation pressure coefficient can be estimated for each satellite. The estimation of this parameter reduces the rms double difference phase residuals and also leads to a better determination of the baseline components between the ground sites.

(c) For the three day solutions, the y-bias acceleration can be estimated for each satellite, in addition to the direct solar radiation pressure coefficients. The estimation of the y-bias acceleration reduces the rms double difference phase residuals and gives a better determination of the baseline components between the ground stations.

(d) The four day solution also improves with the estimation of the y-bias acceleration. This again is reflected in the lower rms double difference phase residuals and the better determination of the baseline components.

5. The high altitude of the GPS satellite allows the high order terms of the earths geopotential model to be ignored and an expansion up to degree and order eight is suitable for the GPS satellites, for orbital arcs up to four days.

6. The use of a different geopotential model (and the implied change in GM) has only a small effect on the determination of the baselines with GPS.

7. A simpler alternative to integrating the GPS satellite force model for short spans of data, is to use an orbit relaxation technique. This can produce comparable results to the orbit integration technique, although the method relies very much upon the *quality* of the broadcast ephemeris.

8. The comparison of the GPS derived baseline components with the VLBI

192

determined baselines in North America, gives an agreement better than 1 or 2 parts in 10^7 in all three baseline components. This corresponds to an orbital accuracy of between two and four metres.

9. The accuracy of the fiducial site coordinates is fundamental to the fiducial network method for GPS orbit determination. Even small errors in measuring the antenna height at a fiducial site, will propagate into both the horizontal and vertical components of the non fiducial site coordinates.

10. The fiducial network method is suitable for determining the coordinates of the non fiducial sites, when they are located within or close to the fiducial network. The accuracy of the estimated non fiducial coordinates decreases, as the distance away from the fiducial network increases.

11. The geometry of the satellites and the tracking sites significantly affects the determination of the satellite orbits and the determination of the tracking site coordinates. The satellite constellation over North America provides a much better geometrical configuration, than the constellation over Europe, which results in a more reliable solution.

12. Multiple day GPS orbits are useful where there is a lack of tracking data from the fiducial sites. This was particularly noticeable in the tide gauge project, where single day solutions were not possible, but the estimation of the four day orbits made the determination of the tide gauge site coordinates possible.

8.2 Suggestions for Further Work

1. The resolution of the initial phase ambiguities into *integers* is necessary to improve the accuracy of both the orbit determination and the coordinate determination of the ground sites.

2. Further work is necessary on the modelling of the tropospheric delay in the phase observable. Methods such as estimating site dependent tropospheric delay parameters and time varying tropospheric delay parameters should be investigated.

3. Modifications are necessary to the GPS network adjustment programs (**PANIC** and **DDORB**) in order to maximise the amount of phase data that can be processed. The current generation of programs are relatively inflexible with the need to specify the baseline definitions from which to form the double differences.

4. The ROCK IV solar radiation pressure model should be tested in the GPS satellite force model. The possibility of introducing time varying solar radiation pressure coefficients should be investigated for longer orbital arcs, where the solar radiation pressure may not be constant.

5. The effect of the solid earth and ocean tides on the displacement of the GPS tracking sites should be investigated, to see if it significantly affects the results.

6. Further investigation is required into the detection and repair of cycle slips. The current methods employed, such as the visual inspection of the double difference phase residuals and fitting polynomial expressions to the phase data are very time consuming.

7. The orbit relaxation technique should be adapted for multiple day solutions. This could be achieved using a Helmert-Wolf blocking technique [Hill, 1989].

Appendix A.
Jobdecks for the GPS orbit determination programs

Jobdecks for the GPS orbit determination programs

The program *DDORB* is controlled from a jobdeck, which contains all the program options, the input files required and the output files required. The example below is of the type used for the three day solution using the GPS standard dataset described in chapter 7.

```
begin
stjnld(gindat.jnldd)
@ cf77(slr.ddorb,omf=omfddorb,LIST=NONE)
@  Input ephemeris data on channels 1 to 7(except chan. 5)
cnf(gps10cio,funit=1)
cnf(gps16cio,funit=2)
cnf(gps19cio,funit=3)
cnf(gps11cio,funit=4)
cnf(gps12cio,funit=6)
cnf(gps13cio,funit=7)
@  Input measurement files on channels 11 to 19
cnf(ngs004.ALGO456,funit=11)
cnf(ngs004.CHUR456,funit=12)
cnf(ngs004.VNDN456,funit=13)
cnf(ngs004.OVRO456,funit=14)
cnf(ngs004.PLAT456,funit=15)
cnf(ngs004.WSFD456,funit=16)
@  Input partial derivative files on channels 31 to 37
```

```
cnf(gpsl0parx,funit=31)
cnf(gpsl6parx,funit=32)
cnf(gpsl9parx,funit=33)
cnf(gpsl1parx,funit=34)
cnf(gpsl2parx,funit=35)
cnf(gpsl3parx,funit=36)
@ Input met data files on channels 41 to 49
@
@ NO MET DATA
@
@    Input chebyshev polynomial file
cnf(cheb86354p,funit=50)
@    Input satellite state vectors
cnf(ngs004.sv00456,funit=25)
cnf(ngs004.osv00456,access=w,funit=26)
@    Create output files
cnf(ngs004.odd456,access=w,funit=21,res=ignore)
cnf(ngs004.covarm,access=w,funit=22,res=ignore)
alb(omfddorb,access=e)
run(ddorb)
1    INPUT ANALYSIS INFORMATION
Z_____
2           : 1 = WGS 72 , 2 = WGS 84
0           : frequency  used.  1=L1  ,2=L2,   0=L1/L2
5           : Tropo. corrn, 0=NO  1=Hopf 2=Saast/Mar 3=Full Hopf
1           : Use of weight matrix 0=NO,1=YES      (4=Saast 5=Mag
4           : day number
1           : Output of residuals 0=NO  1=YES
Z_____
Z_____
2    INPUT SATELLITE INFORMATION
Z_____
```

```
6  2                  : Number of satellites
3 6 9 11 12 13        : PRN number of each satellite
11                    : Base satellite ID
1 1 1 1 1 1 1         : No. of ephemerides for each satellite
0 0 0 0 0 0 0         : 1 = satellite fixed, 0 = free
Z_____
Z
3  INPUT STATION INFORMATION
Z_____
6                     : Number of stations
1 0 0 1 1 0 0 0   : Station fixing choice
Z_____
   For each station write a block in the form
Station name
Receiver type
Approx X coordinate of station  (metres)
Approx Y coordinate of station  (metres)
Approx Z coordinate of station  (metres)
Antenna height(metres)
Z_____
ALGO
TI 4100
  918127.4990
-4346061.9153
 4561984.2599
1.399
Z_____
CHUR
TI 4100
 -236417.0093
-3307612.0551
 5430055.8889
```

```
      1.454

      Z_____     .

      VNDN

      TI 4100

      -2678071.7747

      -4525451.5663

       3597427.5067

      1.263

      Z_____

      OVRO

      TI 4100

      -2410422.5939

      -4477802.4623

       3838686.8365

      1.890

      Z_____

      PLAT

      TI 4100

      -1240708.2691

      -4720454.2018

       4094481.7816

      1.682

      Z_____

      WSFD

      TI 4100

       1492232.8794

      -4458091.7154

       4296045.9743

      0.000

      Z_____

      Z

      Z    Read baseline definitions(max NOSTNS-1)
```

```
Z_____
5 1
5 2
5 3
5 4
5 6
Z_____
3                 : IDATA 0=mag,1=can,2=nor,3=GSI
100               : accumulated solution mode
0                 : 0 = No integer fixing, 1 = Integer fixing
240.0             : integration step length
common start time of integration
32400.0
87,4              : year and day number for start of data
9                 : number of orbital parameters from ORBIT
8                 : number of orbital parameters solved for
0 0 0 0 0 0 0 0   : number of orbital parameters solved
3                 : number of days of tracking data
1                 : itimcor, 1 = auto.  (time correction)
end
```

Appendix B.
Definition of rotation matrices

APPENDIX B

Definition of rotation matrices

The rotation matrices $R1, R2, R3$ used in chapter 3 are defined as anti-clockwise rotations about the x, y and z axes respectively, for the angle θ. They are defined as [Moore, 1986],

$$R1(\theta) = \begin{bmatrix} 1 & 0 & 0 \\ 0 & \cos\theta & \sin\theta \\ 0 & -\sin\theta & \cos\theta \end{bmatrix} \tag{B.1}$$

$$R2(\theta) = \begin{bmatrix} \cos\theta & 0 & -\sin\theta \\ 0 & 1 & 0 \\ \sin\theta & 0 & \cos\theta \end{bmatrix} \tag{B.2}$$

$$R3(\theta) = \begin{bmatrix} \cos\theta & \sin\theta & 0 \\ -\sin\theta & \cos\theta & 0 \\ 0 & 0 & 1 \end{bmatrix} \tag{B.3}$$

Appendix C.
GINFEST GPS campaign results

APPENDIX C

GINFEST GPS campaign results

This appendix gives the full GINFEST solutions which were abbreviated in chapter 5 and the derivations of the receiver coordinates from the IESSG SLR solution.

Table (C.1) shows the IESSG SA-T coordinate set for the SLR facilities at the GINFEST sites. The coordinates were obtained from a short arc solution, which has been transformed onto a ten month long arc solution.

SLR site	x (m)	y (m)	z (m)
Grasse	4581690.988	556165.153	4389359.434
Graz	4194425.874	1162700.069	4647245.615
RGO	4033462.934	23668.925	4924305.704
Kootwijk	3899223.334	396749.554	5015074.038
Wettzell	4075529.209	931787.687	4801617.597

Table C.1: GINFEST SLR site coordinates : IESSG SA-T

Table (C.2) gives the IESSG SA-T coordinate set which have been transformed onto a WGS 84 coordinate set, using a seven parameter Helmert transformation. The following biases were found between the two coordinate sets, given with their standard errors.

$$dx \quad = \quad 0.857 \quad \pm \quad 0.470 \quad \text{metres}$$

$$dy \quad = \quad -0.386 \quad \pm \quad 0.446 \quad \text{metres}$$

$$dx \quad = \quad -1.046 \quad \pm \quad 0.431 \quad \text{metres}$$

$$x \text{ rot.} \quad = \quad -0.310 \quad \pm \quad 0.013 \quad \text{seconds}$$

$$y \text{ rot.} \quad = \quad -0.002 \quad \pm \quad 0.018 \quad \text{seconds}$$

$$z \text{ rot.} \quad = \quad -0.015 \quad \pm \quad 0.013 \quad \text{seconds}$$

$$\text{scale} \quad = \quad 0.004 \quad \pm \quad 0.052 \quad \text{ppm}$$

SLR site	x (m)	y (m)	z (m)
Grasse	4581691.874	556158.511	4389359.190
Graz	4194426.717	1162693.015	4647246.286
RGO	4033463.862	23661.438	4924304.669
Kootwijk	3899224.235	396741.923	5015073.565
Wettzell	4075530.071	931780.392	4801617.924

Table C.2: GINFEST SLR site coordinates : IESSG T-84

The WGS 84 coordinates of the SLR sites were then converted into WGS 72 coordinates, using the transformation parameters given in table (C.3) [D.O.D., 1986].

Transformation parameter	
ΔX	0.0000
ΔY	0.0000
ΔZ	-4.5000
x rot.	0.0000
y rot.	0.0000
z rot.	-0.5540
scale (ppm)	-0.2198

Table C.3: Transformation parameters between WGS 84 and WGS 72

Table (C.4) gives the eccentricity vectors between the SLR/VLBI sites and all the GPS antenna L1 phase centres for the GINFEST GPS campaign. There is some uncertainty in the eccentricity vector connecting Jodrell Bank. The eccentricities were obtained from various sources, including [Muller, 1988].

Site	Δx (m)	Δy (m)	Δz (m)
Grasse	20.586	-19.219	-23.514
Graz	-2.381	8.548	-1.128
RGO	-101.203	386.007	71.817
Kootwijk	-4.614	25.297	-0.986
Wettzell	22.551	44.407	-28.999
Zimmerwald	8.600	-0.142	-3.819
Onsala	53.327	-40.309	-42.745
Effelsberg	-4766.905	3769.375	3569.054
Westerbork	120.687	-611.337	-43.512
Jodrell Bank	107.371	84.346	-131.340

Table C.4: Eccentricity vectors for SLR/VLBI sites to GPS L1 phase centres for GINFEST GPS campaign

Table (C.5) gives the baseline differences between the solutions for days 322 and 324 when using the broadcast ephemeris.

Table (C.6) gives the baseline differences between the solutions for day 323 and day 324 when using the broadcast ephemeris.

Table (C.7) shows the baseline differences between the three day precise ephemeris solution and the precise ephemeris solution for day 322.

Table (C.8) shows the baseline differences between the three day precise ephemeris solution and the precise ephemeris solution for day 323.

Table (C.9) shows the baseline differences between the three day precise ephemeris solution and the precise ephemeris solution for day 324.

Tables (C.10), (C.11) and (C.12) show the baseline differences between the individual single day orbit determination solutions and the three day orbit determination solution. The single day solutions solve for the satellite state vector for each satellite, whereas the three day solution solves for the satellite state vector, direct solar radiation scaling coefficient and a y bias acceleration for each satellite.

		Length	Difference	ppm
		(km)	(cm)	
Kootwijk	- Grasse	939	-9.2	0.098
	- Graz	899	2.6	0.029
	- RGO	406	16.1	0.396
	- Effelsberg	195	0.3	0.015
	- Onsala	700	20.5	0.292
	- Westerbork	98	21.4	2.179
	- Jodrell Bank	560	-5.1	0.091
Grasse	- Graz	764	-4.3	0.056
	- RGO	932	-5.4	0.058
	- Effelsberg	757	-10.2	0.134
	- Onsala	1553	3.6	0.023
	- Westerbork	1017	6.1	0.060
	- Jodrell Bank	1251	3.5	0.028
Graz	- RGO	1182	14.5	0.123
	- Effelsberg	738	4.7	0.064
	- Onsala	1172	5.7	0.048
	- Westerbork	908	3.3	0.037
	- Jodrell Bank	1436	0.4	0.003
RGO	- Effelsberg	467	12.3	0.262
	- Onsala	1045	35.5	0.340
	- Westerbork	487	34.2	0.702
	- Jodrell Bank	319	11.8	0.369
continued on next page				

		Length (km)	Difference (cm)	ppm
Effelsberg	- Onsala	825	20.4	0.248
	- Westerbork	261	17.0	0.649
	- Jodrell Bank	701	-1.3	0.019
Onsala	- Westerbork	602	-1.7	0.028
	- Jodrell Bank	1011	-0.9	0.009
Westerbork	- Jodrell Bank	597	0.5	0.009
			rms = 13.6	

Table C.5: Comparison of baseline lengths for the broadcast ephemeris solution on day 322 with the day 324 solution

		Length (km)	Difference (cm)	ppm
Wettzell	- Kootwijk	602	0.5	0.008
	- Grasse	753	-7.6	0.101
	- Graz	302	-0.1	0.002
	- RGO	917	-10.4	0.113
	- Onsala	919	20.2	0.219
	- Jodrell Bank	1150	-12.5	0.108
Kootwijk	- Grasse	939	2.8	0.030
	- Graz	899	1.5	0.016
	- RGO	406	-8.9	0.216
	- Onsala	700	15.6	0.223
	- Jodrell Bank	560	-13.2	0.236
Grasse	- Graz	764	1.5	0.019
	- RGO	932	1.4	0.015
	- Onsala	1553	16.4	0.136
	- Jodrell Bank	1251	1.1	0.009
Graz	- RGO	1182	-6.3	0.053
	- Onsala	1172	10.2	0.087
	- Jodrell Bank	1436	-10.4	0.072
RGO	- Onsala	1045	3.9	0.038
	- Jodrell Bank	319	-2.2	0.068
Onsala	- Jodrell Bank	1011	-6.4	0.063
			rms = 9.3	

Table C.6: Comparison of baseline lengths for the broadcast ephemeris solution on day 323 with the day 324 solution

		Length (km)	Difference (cm)	ppm
Kootwijk	- Grasse	939	-13.1	0.139
	- Graz	899	1.7	0.012
	- RGO	406	-4.1	0.101
	- Effelsberg	195	-13.4	0.686
	- Onsala	700	20.2	0.288
	- Westerbork	98	13.7	1.399
	- Jodrell Bank	560	-41.4	0.739
Grasse	- Graz	764	-7.1	0.093
	- RGO	932	-2.7	0.029
	- Effelsberg	757	4.3	0.057
	- Onsala	1553	1.3	0.008
	- Westerbork	1017	-3.0	0.029
	- Jodrell Bank	1251	2.3	0.018
Graz	- RGO	1182	3.5	0.030
	- Effelsberg	738	2.2	0.030
	- Onsala	1172	7.3	0.062
	- Westerbork	908	2.0	0.021
	- Jodrell Bank	1436	-27.9	0.194
RGO	- Effelsberg	467	5.9	0.127
	- Onsala	1045	12.2	0.117
	- Westerbork	487	6.3	0.129
	- Jodrell Bank	319	8.1	0.254

		Length (km)	Difference (cm)	ppm
Effelsberg	- Onsala	825	-1.8	0.021
	- Westerbork	261	-7.0	0.268
	- Jodrell Bank	701	-28.9	0.413
Onsala	- Westerbork	602	6.1	0.102
	- Jodrell Bank	1011	-55.8	0.551
Westerbork	- Jodrell Bank	597	-45.1	0.755
			rms = 18.9	

Table C.7: Comparison of baseline lengths for the precise ephemeris solution on day 322 with the three day solution

		Length (km)	Difference (cm)	ppm
Wettzell	- Kootwijk	602	-4.8	0.079
	- Grasse	753	-6.2	0.082
	- Graz	302	-0.8	0.026
	- RGO	917	-6.5	0.070
	- Onsala	919	-0.6	0.006
	- Jodrell Bank	1150	-2.8	0.024
Kootwijk	- Grasse	939	6.4	0.068
	- Graz	899	-4.1	0.046
	- RGO	406	6.7	0.165
	- Onsala	700	-16.2	0.232
	- Jodrell Bank	560	5.4	0.096
Grasse	- Graz	764	-1.1	0.014
	- RGO	932	-0.8	0.009
	- Onsala	1553	-4.8	0.031
	- Jodrell Bank	1251	-3.3	0.026
Graz	- RGO	1182	-4.6	0.039
	- Onsala	1172	-5.3	0.043
	- Jodrell Bank	1436	-2.5	0.017
RGO	- Onsala	1045	-8.2	0.078
	- Jodrell Bank	319	-4.1	0.126
Onsala	- Jodrell Bank	1011	0.2	0.001
			rms = 5.7	

Table C.8: Comparison of baseline lengths for the precise ephemeris solution on day 323 with the three day solution

		Length (km)	Difference (cm)	ppm
Wettzell	- Kootwijk	602	0.8	0.014
	- Grasse	753	2.9	0.039
	- Graz	302	1.4	0.046
	- RGO	917	5.7	0.062
	- Effelsberg	455	-3.7	0.082
	- Onsala	919	-1.4	0.015
	- Westerbork	607	-0.4	0.006
	- Jodrell Bank	1150	12.1	0.105
Kootwijk	- Grasse	939	6.6	0.070
	- Graz	899	2.8	0.031
	- RGO	406	11.2	0.276
	- Effelsberg	195	-9.1	0.465
	- Onsala	700	20.2	0.288
	- Westerbork	98	-5.9	0.604
	- Jodrell Bank	560	15.0	0.268
Grasse	- Graz	764	0.4	0.006
	- RGO	932	0.0	0.000
	- Effelsberg	757	19.2	0.253
	- Onsala	1553	1.1	0.007
	- Westerbork	1017	1.2	0.012
	- Jodrell Bank	1251	-1.9	0.015
Graz	- RGO	1182	5.9	0.050
	- Effelsberg	738	0.5	0.007
	- Onsala	1172	3.2	0.028
	- Westerbork	908	1.6	0.017
	- Jodrell Bank	1436	12.6	0.087

		Length (km)	Difference (cm)	ppm
RGO	- Effelsberg	467	12.6	0.269
	- Onsala	1045	7.4	0.071
	- Westerbork	487	7.7	0.158
	- Jodrell Bank	319	-1.8	0.055
Effelsberg	- Onsala	825	-22.7	0.275
	- Westerbork	261	-17.8	0.680
	- Jodrell Bank	701	9.1	0.130
Onsala	- Westerbork	602	-1.7	0.028
	- Jodrell Bank	1011	23.2	0.229
Westerbork	- Jodrell Bank	597	17.2	0.288
			rms=9.7	

Table C.9: Comparison of baseline lengths for the precise ephemeris solution on day 324 with the three day solution

		Length (km)	Difference (cm)	ppm
Kootwijk	- Grasse	939	1.7	0.018
	- Graz	899	-2.9	0.032
	- RGO	406	-3.3	0.081
	- Effelsberg	195	-6.0	0.308
	- Onsala	700	1.8	0.026
	- Westerbork	98	14.2	1.449
	- Jodrell Bank	560	-22.4	0.400
Grasse	- Graz	764	33.2	0.435
	- Effelsberg	757	10.6	0.140
	- Westerbork	1017	12.0	0.118
	- Jodrell Bank	1251	-7.4	0.059
Graz	- RGO	1182	3.8	0.033
	- Effelsberg	738	1.8	0.024
	- Onsala	1172	-29.2	0.249
	- Westerbork	908	-6.6	0.073
	- Jodrell Bank	1436	-19.5	0.136
RGO	- Effelsberg	467	1.1	0.024
	- Westerbork	487	9.4	0.193
	- Jodrell Bank	319	-6.0	0.189
Effelsberg	- Onsala	825	-9.7	0.118
	- Westerbork	261	1.7	0.065
	- Jodrell Bank	701	-19.0	0.271
Onsala	- Westerbork	602	-12.6	0.209
	- Jodrell Bank	1011	-21.2	0.210
Westerbork	- Jodrell Bank	597	-16.8	0.281
			rms = 14.1	

Table C.10: Comparison of baseline lengths for the orbit determination solution on day 322 with the three day solution

		Length (km)	Difference (cm)	ppm
Wettzell	- Kootwijk	602	5.3	0.088
	- Grasse	753	-25.1	0.333
	- Graz	302	-0.3	0.010
	- RGO	917	-2.5	0.027
	- Onsala	919	23.1	0.251
	- Jodrell Bank	1150	-8.6	0.075
Kootwijk	- Grasse	939	-9.6	0.102
	- Graz	899	5.6	0.062
	- RGO	406	-7.6	0.187
	- Onsala	700	11.4	0.163
	- Jodrell Bank	560	4.5	0.080
Grasse	- Graz	764	-22.3	0.292
	- Jodrell Bank	1251	-0.8	0.006
Graz	- RGO	1182	-0.5	0.004
	- Onsala	1172	21.3	0.182
	- Jodrell Bank	1436	8.8	0.061
RGO	- Jodrell Bank	319	-2.6	0.082
Onsala	- Jodrell Bank	1011	12.0	0.119
			rms = 12.4	

Table C.11: Comparison of baseline lengths for the orbit determination solution on day 323 with the three day solution

		Length (km)	Difference (cm)	ppm
Wettzell	- Kootwijk	602	-0.2	0.003
	- Grasse	753	-17.1	0.227
	- Graz	302	-2.7	0.089
	- RGO	917	-1.0	0.011
	- Effelsberg	455	-4.4	0.096
	- Onsala	919	17.2	0.187
	- Westerbork	607	1.0	0.017
	- Jodrell Bank	1150	12.5	0.108
Kootwijk	- Grasse	939	-1.3	0.014
	- Graz	899	-2.0	0.022
	- RGO	406	5.0	0.123
	- Effelsberg	195	4.7	0.240
	- Onsala	700	-3.1	0.044
	- Westerbork	98	-1.0	0.100
	- Jodrell Bank	560	15.0	0.267
Grasse	- Graz	764	-21.8	0.285
	- Effelsberg	757	-7.1	0.094
	- Westerbork	1017	-3.0	0.029
	- Jodrell Bank	1251	7.5	0.060
Graz	- RGO	1182	-3.4	0.028
	- Effelsberg	738	-6.6	0.089
	- Onsala	1172	18.9	0.161
	- Westerbork	908	-1.1	0.012
	- Jodrell Bank	1436	10.1	0.070

		Length	Difference	ppm
		(km)	(cm)	
RGO	- Effelsberg	467	3.4	0.073
	- Westerbork	487	4.9	0.101
	- Jodrell Bank	319	8.1	0.255
Effelsberg	- Onsala	825	5.1	0.062
	- Westerbork	261	4.1	0.155
	- Jodrell Bank	701	15.3	0.218
Onsala	- Westerbork	602	-2.2	0.036
	- Jodrell Bank	1011	5.7	0.056
Westerbork	- Jodrell Bank	597	16.0	0.268
			rms=9.3	

Table C.12: Comparison of baseline lengths for the orbit determination solution on day 324 with the three day solution

SV 4 Coordinate Set for the North American Fiducial sites

The coordinate sets given refer to the GPS mark at each of the sites in the standard data set used in chapter 7. The coordinates are given in the SV 4 reference developed at the Massachussets Institute of Technology.

Site	x (m)	y (m)	z (m)
ALGO	918127.4990	-4346061.9153	4561984.2599
MOJA	-2356214.8002	-4646733.8012	3668460.5220
OVRO	-2410422.5939	-4477802.4623	3838686.8365
PLAT	-1240708.2691	-4720454.2018	4094481.7816
PVER	-2525452.9597	-4670035.4854	3522886.8679
VNDN	-2678071.7747	-4525451.5663	3597427.5067
WSFD	1492232.8794	-4458091.7154	4296045.9743

Table D.1: GPS standard data set coordinates : SV 4 reference frame

Site	Day 3	Day 4	Day 5	Day 6	Day 7
ALGO	1.399	1.399	1.399	1.399	1.399
MOJA	0.000	0.000	0.000	0.000	0.000
OVRO	1.387	1.890	1.890	1.890	1.890
PLAT	1.682	1.682	1.682	1.682	1.682
PVER	1.332	1.593	1.433	1.447	1.475
VNDN	1.264	1.263	1.260	1.260	1.260
WSFD	0.000	0.000	0.000	0.000	0.000

Table D.2: Antenna heights for the GPS standard data set

References

Agrotis, L.G. 1984. *The Determination of Satellite Orbits and the Global Positioning System*, Ph.D. Thesis, Nottingham University.

Aquino, M. 1989. *Improving GPS Positioning Accuracies by Orbit Relaxation*, M.Phil. Thesis in preparation, Nottingham University.

Ashkenazi, V. 1970. *Adjustment of Control Networks for Precise Engineering Surveys*, Chartered Surveyor, January 1970.

Ashkenazi, V. 1987. *To code or not to code : That is not the GPS question.*, Land and Mineral Surveyor

Ashkenazi, V., Gough, R.J. and Sykes, R.M. 1977. *Satellite-Doppler Positioning*, Seminar Notes, Nottingham University.

Ashkenazi, V., Agrotis, L.A. and Moore, T. 1984. *Determination of Satellite Orbits and the Analysis of LAGEOS Laser Range Observations*, Pres. Eighth UK Geophysical Assembly, Newcastle upon Tyne.

Ashkenazi, V. and Moore, T. 1986. *The Navigation of Navigation Satellites*, Journal of Navigation, Vol.3, No.3.

Ashkenazi, V., Hill, C.J. and Moore, T. 1987. *Long-arc and Short-arc Baseline Determination by Satellite Laser Ranging*, Pres. RETrig subcommission of IAG, Paris.

Ashkenazi, V., Boucher, C., Brouwer, F., Cambell, J., Hauck, H., Moore, T., Seeger, H. and Wakker, K. 1987. *GINFEST - A Space Geodetic Network in Europe*, Pres. XIX General Assembly of the IUGG, Vancouver, B.C.

Ashkenazi, V., Baker, T., Basker, G.A., Davison, M., Dodson, A.H., Hipkin, R. and Stewart, M. 1989. *The Determination of Mean Sea Level using GPS*, Pres. International Association of Geodesy, General Meeting, Edinburgh, Scotland.

Barber, G. 1989. *GPS: Overview and Status*, Lecture Notes, Seminar on the Global Positioning System, Nottingham University.

Basker, G.A. 1989. *The Determination of Mean Sea Level using GPS*, Ph.D. Thesis in preparation, Nottingham University.

Bender, P.L. and Larden, D.R. 1985. *GPS Carrier Phase Ambiguity Resolution Over Long Baselines*, Proceedings of the First International Symposium on Precise Positioning with the Global Positioning System, Rockville, Maryland.

Beutler,G., Gurtner,W., Bauerisma, I. and Rothacher, M. 1986. *Efficient Computation of the Inverse of the Covariance Matrix of Simultaneous GPS Carrier Phase Difference Observations*, Manuscripta Geodaetica, vol. 11, no. 4, pp249-255.

Beutler,G., Gurtner,W., Rothacher, M., Schildknecht, T. and Bauerisma, I. 1986. *Determination of GPS Orbits Using Double Difference Carrier Phase Observations from Regional Networks*, Proceedings of the Fourth International Geodetic Symposium on Satellite Positioning, Austin, Texas.

Beutler,G., Bauerisma,I., Gurtner,W., Rothacher,M., Schildknecht,T., and Geiger,A. 1987. *Atmospheric Refraction and Other Important Biases in GPS Carrier Phase Observables.*, Pres. XIX General Assembly IUGG, Vancouver, August 1987.

Blanchard, W. 1989. *Differential GPS*, Lecture Notes, Seminar on the Global Positioning System, Nottingham University.

Blewitt, G. 1989. *Carrier Phase Ambiguity Resolution for the Global Positioning System Applied to Geodetic Baselines up to 2000 km*, Submitted to the Journal of Geophysical Research, March 1989.

Boucher, C. et al 1986. *Proposal for a European Tracking Campaign of NAVSTAR GPS Satellites*, Pres. 62nd Meeting of the Study Group in Geodynamics, Louvain-la-neuve.

Boucher, C., Altamimi, Z. and Willis, P. 1988. *Relation between BTS-87, WGS-84 and GPS Activities*, Note Technique no. 10, Groupe de Recherches de Geodesie Spatiale, Institut Géographique National, Paris.

Colombo, O.L. 1986. *Ephemeris Errors in GPS Satellites*, Bulletin Géodésique, Vol. 68 no. 1.

Curley, R.A. 1988. *The Use of TI 4100 GPS Receivers and MAGNET Software to Determine Height Differences* , M.Sc. Thesis, Nottingham University.

de la Fuente, C. 1988. *High Accuracy Coordinate Determination using the Global Positioning System*, Ph.D. Thesis, Nottingham University.

Department of Defense 1986. *Supplement to Department of Defense World Geodetic System 1984 Technical Report: Part 1. Methods, Techniques and Data used in WGS84 Development*, Defense Mapping Agency.

Dodson, A.H. 1986. *Refraction and Propagation Delays in Space Geodesy*, Int. J. Remote Sensing, vol. 7, no. 4, pp515-524.

Dodson, A.H. 1989. *The Effects of Atmospheric Refraction on GPS Observables*, Seminar on the Global Positioning System, Nottingham University.

Dong, D. and Bock, Y. 1989. *Global Positioning System Network Analysis with Phase Ambiguity Resolution Applied to Crustal Deformation*

Studies in California, Journal of Geophysical Research, vol. 94, no. B4, April 1989.

Fliegel, H.F. et al 1985. *The GPS Radiation Force Model,* Proceedings of the First International Symposium on Precise Positioning with the Global Positioning System, Rockville, Maryland.

Fliegel, H.F. and Gallini, T.E. 1989. *Radiation Pressure Model for Block II GPS Satellites,* Proceedings of the Fifth International Geodetic Symposium on Satellite Positioning, Las Cruces, New Mexico.

Georgiadou,Y. and Kleusberg, A. 1987. *On the Effect of Ionospheric Delay on Geodetic Relative GPS Positioning,* Manuscripta Geodaetica (1988) 13: 1-8.

Goad, C.C. 1986. *Precise Positioning with the GPS,* Proceedings of the CERN Accelerator School for Particle Accelerators ,CERN ,Geneva, April 1986

Gouldman, M.W., Hermann, B.R. and Weedon, D.L. 1989. *Evaluation of GPS Production Ephemeris and Clock Quality ,* Proceedings of the Fifth International Geodetic Symposium on Satellite Positioning, Las Cruces, New Mexico.

Hill, C.J., 1989. *Satellite Laser Ranging and some Geophysical Applications,* Ph.D. Thesis, Nottingham University.

Hopfield,H.S., 1971. *Tropospheric Effect on Electromagnetically Measured Range: Prediction from Surface Weather Data,* Radio Science, Vol. 6 no. 3, pp357-367.

Kleusberg, A., Langley, R.B., Santerre, R., Vanicek, P., Wells, D.E. and Beutler, G. 1985 *Comparison of Survey Results from Different Types of GPS Receivers,* Proceedings of the First International Symposium on Precise Positioning with the Global Positioning System, Maryland, Rockville.

Landau, H. and Hein, G. 1986 *Preliminary Results of a Feasibility Study for a European GPS Tracking Network*, Proceedings of the Fourth International Geodetic Symposium on Satellite Positioning, Austin, Texas.

Lichten, S.M. and Border, J.S. 1987. *Strategies for High Precision Global Positioning System Orbit Determination*, Journal of Geophysical Research, Vol. 92, No. B12, November 10, 1988.

Lichten, S.M. 1989. *High Accuracy Global Positioning System Orbit Determination : Progress and Prospects*, Pres. International Association of Geodesy, General Meeting, Edinburgh, Scotland.

Lichten, S.M., Bertiger, W.I. and Lindqwister, U.J. 1989. *The Effect of Fiducial Network Strategy on High-Accuracy GPS Orbit and Baseline Determination*, Proceedings of the Fifth International Geodetic Symposium on Satellite Positioning, Las Cruces, New Mexico.

Marsh, J.G. et al 1988. *A New Gravitational Model for the Earth from Satellite Tracking Data : GEM-T1*, Journal of Geophysical Research, Vol. 93, No. B6, June 10, 1988.

Milliken, R.J. and Zoller, C.J. 1978. *Principal of Operation of NAVSTAR and System Characteristics*, Navigation, Journal of the Institute of Navigation, Vol. 25, No. 2.

Moore, T. 1986 *Satellite Laser Ranging and the Determination of Earth Rotation Parameters*, Ph.D. Thesis, Nottingham University.

Moore, T. and Ashkenazi, V. 1987. *Precise Orbit Determination at Nottingham*, Pres. AAS/AIAA Astrodynamics Specialist Conference, Kalispell, Montana.

Muller, A. 1988. *Station Eccentricities of European VLBI/LASER Sites*, Geodetic Institute, University of Bonn.

Nakiboglu, S.M., Krakiwsky, E.J., Schwarz, K.P., Buffet, B. and Wanless, B. 1985. *A Multi-station, Multi-pass approach to Global Positioning System Orbital Improvement and Precise Positioning*, Contract report submitted to Geodetic Survey of Canada.

O'Toole, J.W. 1976. *CELEST Computer Program for Computing Satellite Orbits*, NSWC/DL TR-3565.

Rizos, C. and Stolz, A. 1985. *Force Modelling for GPS Satellite Orbits*, Proceedings of the First International Symposium on Precise Positioning with the Global Positioning System, Maryland, Rockville.

Rizos, C., Govind, R. and Stolz, A. 1989 *The Australian GPS Orbit Determination Pilot Project : A Status Report*, Pres. International Association of Geodesy, General Meeting, Edinburgh, Scotland.

Rockwell International Corporation. 1981. *NAVSTAR GPS Space Segment/Navigation User Interfaces, (ICG-GPS-200)*, Rockwell International Corp., California 90241.

Saastamoinen, J. 1973. *Contributions to the Theory of Atmospheric Refraction. Part II: Refraction Corrections in Space Geodesy*, Bulletin Geodesique, no. 107.

Sims, M.L. 1985 *Phase Centre Variations in the Geodetic TI 4100 GPS Receiver Systems Conical Spiral Antenna*, Proceedings of the First International Symposium on Precise Positioning with the Global Positioning System, Maryland, Rockville.

Spencer, A.J.M. et al 1977. *Engineering Mathematics Vol. 2*, Van Nostrand Reinhold.

Spilker, J.J. 1978. *Signal Structure and Performance Characteristics*, Navigation, Journal of the Institute of Navigation, Vol. 25, No. 2.

Varnum, F. and Chaffee, J. 1982. *Data Processing at the Global Positioning System Master Control Station*, Proceedings of the Third International Symposium on Satellite Doppler Positioning, Las Cruces, New Mexico.

224

Wells, D.E (editor). 1986. *Guide to GPS Positioning*, Canadian GPS Associates.

Yau, J. 1986. *Relative Geodetic Positioning using GPS Interferometry*, Ph.D. Thesis, Nottingham University.